VOL. 10 NO. 3 SEPTEMBER 1965
PUBLISHED MONTHLY

Journal of

# ELECTROANALYTICAL CHEMISTRY

*International Journal Dealing with all Aspects of Electroanalytical Chemistry, Including Fundamental Electrochemistry*



E L S E V I E R

# GENERAL INFORMATION

See also Suggestions and Instructions to Authors which will be sent free, on request to the Publishers.

*Types of contributions*

(a) Original research work not previously published in other periodicals.
(b) Reviews on recent developments in various fields.
(c) Short communications.
(d) Bibliographical notes and book reviews.

*Languages*

Papers will be published in English, French or German.

*Submission of papers*

Papers should be sent to one of the following Editors:

Professor J. O'M. BOCKRIS, John Harrison Laboratory of Chemistry, University of Pennsylvania, Philadelphia 4, Pa., U.S.A.
Dr. R. PARSONS, Department of Chemistry, The University, Bristol 8, England.
Professor C. N. REILLEY, Department of Chemistry, University of North Carolina, Chapel Hill N.C., U.S.A.

Authors should preferably submit two copies in double-spaced typing on pages of uniform size. Legends for figures should be typed on a separate page. The figures should be in a form suitable for reproduction, drawn in Indian ink on drawing paper or tracing paper, with lettering etc. in thin pencil. The sheets of drawing or tracing paper should preferably be of the same dimensions as those on which the article is typed. Photographs should be submitted as clear black and white prints on glossy paper.
All references should be given at the end of the paper. They should be numbered and the numbers should appear in the text at the appropriate places.
A summary of 50 to 200 words should be included.

*Reprints*

Twenty-five reprints will be supplied free of charge. Additional reprints can be ordered at quoted prices. They must be ordered on order forms which are sent together with the proofs.

*Publication*

The *Journal of Electroanalytical Chemistry* appears monthly and has six issues per volume and two volumes per year.

Subscription price: £ 12.12.0 or $ 35.00 or Dfl. 126.00 per year; £ 6.6.0 or $ 17.50 or Dfl. 63.00 per volume.
Additional cost for copies by air mail available on request.
For advertising rates apply to the publishers.

*Subscriptions*

Subscriptions should be sent to:

ELSEVIER PUBLISHING COMPANY, P.O. Box 211, Amsterdam, The Netherlands.

# SUMMARIES OF PAPERS PUBLISHED IN JOURNAL OF ELECTROANALYTICAL CHEMISTRY

Vol. 10, No. 3, September 1965

## ELECTRODE KINETICS AT OPEN CIRCUIT AT THE STREAMING MERCURY ELECTRODE

### II. EXPERIMENTAL RESULTS

The shift of potential at open circuit of a streaming mercury electrode (S.M.E.) was determined and analyzed for control by diffusion or charge transfer and for mixed control by diffusion and charge transfer. The following systems were investigated: Hg(I) in 1 *M* perchloric acid, Cr(III)/Cr(II) in 1 *M* potassium chloride and V(III)/V(II) in 1 *M* perchloric acid. The charging current of the S.M.E. was also investigated and observations were made on the discharge of H(I) and Hg(II) with mixed control by diffusion and migration.

V. S. Srinivasan, G. Torsi and P. Delahay,
*J. Electroanal. Chem.*, 10 (1965) 165–175

## THEORY OF STAIRCASE VOLTAMMETRY

The theoretical relationships for voltammetry with a staircase potential function are developed for a reversible electrode reaction and are shown to be in accord with experiment. Current–potential curves are calculated and tabulated.

J. H. Christie and P. J. Lingane,
*J. Electroanal. Chem.*, 10 (1965) 176–182

## DISTORTION OF LINEAR-SWEEP POLAROGRAMS BY OHMIC DROP

An exact computation of reversible linear-sweep polarograms at a plane electrode distorted by ohmic drop is presented. It follows from these calculations that ohmic drop causes a decrease of the peak current, a shift of even the corrected peak potential, and a considerable increase of the width of the peak, suggesting non-reversible behaviour.

It is deduced that for quantitative studies of electrode processes, the use of a mercury-drop electrode (or other micro-electrodes of similar geometry) in conjunction with linear-sweep voltammetry should be avoided (even when using a three-electrode potentiostat) when the ohmic drop in the solution exceeds about $20/n$ mV.

W. T. de Vries and E. van Dalen,
*J. Electroanal. Chem.*, 10 (1965) 183–190

## ANODIC PROPERTIES OF PLATINUM–CHROMIUM ALLOYS IN SULPHURIC ACID SOLUTION

Hydrogen adsorption and the formation and reduction of oxygen layers were investigated on four Pt–Cr alloys in $N$ $H_2SO_4$ at 30° in the potential region between hydrogen and oxygen evolution. Periodic voltammetric current–potential curves measured at 3 mV/sec give evidence of two different oxidation states of the passive layer on the part of the surface with the electrochemical behavior of chromium. The presence of platinum atoms on the surface may be detected by their influence on the ohmic and capacitive component of the interfacial impedance between 100 c/s and 10 kc/s for the alloys with chromium contents above 11 atomic %.

M. W. BREITER,
*J. Electroanal. Chem.*, 10 (1965) 191–198

## THE STRUCTURE OF THE SEMICONDUCTOR–ELECTROLYTE INTERFACE

Generalizations are probably unjustifiable at the present stage, but a number of interesting features seem to be well established.

Both zinc oxide and germanium, and to a lesser extent silicon, have been found to behave consistently with the simple physical model of a system with properties dominated by the semiconductor space-charge layer. Germanium shows complicated time effects whereas zinc oxide does not.

The effect of hydrogen ion on $\varphi_s - \varphi^s$ (the p.d. between a point just inside the semiconductor surface and the bulk of the solution) is very marked in all cases. The absence of a discreteness of charge effect on germanium suggests a rapid exchange of charge between bound hydroxyl groups and hydrogen ion in solution. This further suggests that $\varphi_1 - \varphi^s$ may be independent of polarization at constant pH.

On germanium electrodes, variations in $\varphi_s - \varphi^s$ due to changes in crystal orientation, ionic strength and concentration of halide ion have been observed. Since polarization of the electrode also produces variations in $\varphi_s - \varphi^s$, it is frequently advantageous to work under conditions where the effect due to polarization is minimized, *i.e.*, by making comparisons at constant current.

P. J. BODDY,
*J. Electroanal. Chem.*, 10 (1965) 199–244

## THE IMPEDANCE OF THE QUINHYDRONE ELECTRODE

*(Short Communication)*

J. R. GALLI AND R. PARSONS,
*J. Electroanal. Chem.*, 10 (1965) 245–248

## CHARACTERISTICS OF GLOW-DISCHARGE ELECTROLYSIS IN AQUEOUS, NON-AQUEOUS AND MOLTEN SYSTEMS

*(Short Communication)*

B. S. R. SASTRY,
*J. Electroanal. Chem.*, 10 (1965) 248–250

# ELECTRODE KINETICS AT OPEN CIRCUIT AT THE STREAMING MERCURY ELECTRODE

## II. EXPERIMENTAL RESULTS

V. S. SRINIVASAN, G. TORSI* AND P. DELAHAY**
*Coates Chemical Laboratory, Louisiana State University, Baton Rouge, Louisiana 70803 (U.S.A.)*
(Received March 16th, 1965)

The analysis of the previous paper[1] will be examined experimentally for the following cases: double-layer charging current in 0.01 and 1 *M* perchloric acid; diffusion control for discharge of mercurous ion in 1 *M* perchloric acid; charge transfer control for the Cr(III)/Cr(II) system in 1 *M* potassium chloride; mixed control for V(III)/V(II) in 1 *M* perchloric acid. The influence of migration in a dilute supporting electrolyte will also be examined for the discharge of Hg(I) and Hg(II).

## EXPERIMENTAL

### *Solutions*

All chemicals were of analytical reagent-grade. Solutions were prepared with water which had been distilled twice with potassium-permanganate.

Solutions of Hg(I) were prepared from a stock solution of mercurous nitrate (approximately 0.1 *M*) in 1 *M* perchloric acid. This stock solution was analyzed by electrogravimetry.

Solutions of V(III) and V(II) were prepared as follows:
A known volume of 0.1 *M* vanadyl sulfate in 1 *M* perchloric acid was reduced by electrolysis under nitrogen, using a mercury pool as cathode and a platinum electrode, in a separate compartment, as anode. The solution was transferred to the cell fitted with the streaming mercury electrode (S.M.E.) under nitrogen, and the V(III)/V(II) ratio was determined by polarography.

A stock solution of Cr(III) was prepared by reduction of a known amount of potassium dichromate by hydrogen peroxide in hydrochloric acid. The solution was boiled for 2 h to eliminate the excess hydrogen peroxide. A known volume of this solution was reduced by shaking the solution with zinc amalgam for 2 min in a separatory funnel. The amalgam was removed, and the solution was transferred under nitrogen to the cell fitted with the S.M.E. The desired Cr(III)/Cr(II) ratio was obtained by aeration with polarographic monitoring.

---

* On leave from the University of Bari, Italy.
** Address after August, 1965: Department of Chemistry, New York University, Washington Square, New York, N.Y. 10003.

*Cell and streaming mercury electrode*

The S.M.E. was a modified form of the cell designed by HEYROVSKÝ AND FORJET[2]. Variation of the solution level in the main compartment was avoided by connecting the side-arm, in which the mercury jet emerged, to the main compartment by a 7-mm diameter tube. The bottom of the side-arm was connected to a horizontal S-shaped capillary tube. Mercury, that collected at the bend, sealed the cell. The rate of flow of mercury of the S.M.E. was determined by collecting mercury that overflowed from the S-tube.

The mercury jet was obtained by forcing mercury under constant pressure through a precision (tolerance, 0.0002 in) capillary* (0.00625 and 0.0075 cm radius, 2 cm-long) attached to a glass tube (7 mm diameter). The latter was bent in a V-shape, the capillary turning upward with an angle of approximately 30 degrees to the vertical. The length of the jet was computed from this angle, as measured by projection on paper, and from the difference in the levels between the tip of the capillary and the tip of the cone of solution adhering to the mercury jet just above the solution level. The latter was measured by a cathetometer to better than 0.1 mm. Optical distortion caused by the meniscus at the wall of the cell was avoided by coating the inside of the cell with silicone.

*Measurements*

The potential of the S.M.E. was measured against a mercury pool in the main compartment of the cell by means of either the Hewlett-Packard high impedance microvoltmeter, model 425-A, or the Keithley electrometer, model 600-A. All experiments were conducted at room temperature, *i.e.*, 24°.

All polarographic recordings were carried out with a Sargent polarograph, model XV, with model A ohmic drop compensator. This compensator was quite essential in capacity current measurements with the S.M.E. because of the relatively high ohmic drop, especially in dilute solutions.

## DESCRIPTION AND DISCUSSION OF RESULTS

*Capacity current*

Some results on the capacity current are given in Fig. 1 and are compared with GRAHAME's data in Fig. 2. The integral capacity was computed from eqn. (2) in Part I[1] from the slope of the lines in Fig. 1. It was observed that the capacity current was essentially independent of the length of the mercury column, as predicted by eqn. (2). The capacities calculated from the S.M.E. measurements are slightly smaller than the integral capacities computed from GRAHAME's data on differential capacities. The capacity current between $E-E_z=\pm 0.1$ V was too small in S.M.E. measurements, and calculation of the integral capacity was uncertain. At least two causes of error affected these results: the faradaic current for impurities (especially residual oxygen) added algebraically to the capacity current; and the varying meniscus effect as the mercury jet emerged from solution, interfered. The latter effect was studied in detail by WEAVER AND PARRY[4] and need not be discussed here. At any rate, it appears from the results of Fig. 2 that eqn. (2), Part I, is *reasonably* obeyed, and that this equation may serve as a basis for the treatment of Part I.

* Obtained from Wilmad Glass Co., Buena, New Jersey.

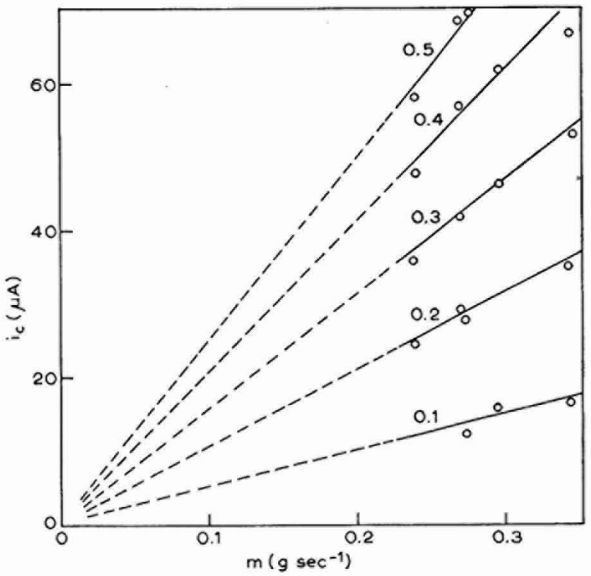


Fig. 1. Capacity current at constant potential against the rate of flow of mercury in 0.01 *M* $HClO_4$ for different values of $E-E_z$ (V).

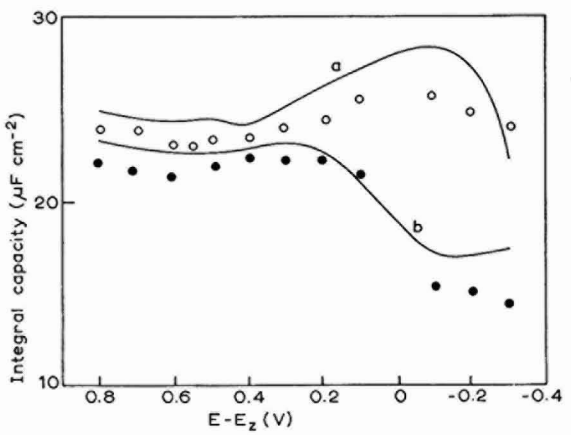


Fig. 2. Comparison of integral capacities deduced from S.M.E. measurements with values deduced from GRAHAME's differential capacity measurements. GRAHAME: (a), 1 *M*; (b), 0.01 *M*. S.M.E.: (○), 1 *M*; (●), 0.01 *M*.

*Diffusion control: discharge of Hg(I)*

The validity of the treatment in Part I for diffusion control was verified for the discharge of Hg(I) in perchloric acid medium. This process is indeed diffusion-controlled for the conditions prevailing at the S.M.E. Equations (6) and (11) of Part I are for Hg(I) discharge with diffusion control:

$$\frac{E-E_z}{1-\exp\,(nF/RT)\eta} = \frac{2\,nF\gamma\,\delta^{\frac{1}{3}}}{c}\,C_0{}^0 D_0{}^{\frac{2}{3}}\left(\frac{l}{m}\right)^{\frac{1}{3}} \quad \text{(any } \eta\text{)} \qquad (1)$$

$$-\frac{1}{\eta} = 2\frac{(nF)^2}{RT}\frac{r\delta^{\frac{1}{2}}}{c(E-E_z)}Co^0Do^{\frac{1}{2}}\left(\frac{l}{m}\right)^{\frac{1}{2}} \quad (|\eta| \leqslant 5\,\text{mV}) \tag{2}$$

Some data for large overvoltages are listed in Table 1 and results are plotted in Figs. 3 and 4.

TABLE 1

DATA FOR Hg(I) IN 1 *M* PERCHLORIC ACID FOR LARGE OVERVOLTAGES*

| *Hg(I) Concn.* *(mmoles $l^{-1}$)* | *m* *($gsec^{-1}$)* | *l* *(cm)* | $-\eta$ *(mV)* |
|---|---|---|---|
| 1.03 | 0.44 | 1.19 | 5.65 |
| 1.03 | 0.40 | 0.72 | 7.45 |
| 1.03 | 0.51 | 0.72 | 8.70 |
| 1.03 | 0.54 | 0.72 | 9.55 |
| 0.52 | 0.37 | 1.08 | 13.5 |
| 0.52 | 0.48 | 1.08 | 17.3 |
| 0.52 | 0.42 | 0.63 | 26.5 |
| 0.52 | 0.48 | 0.63 | 31 |
| 0.52 | 0.59 | 0.63 | 58 |
| 0.26 | 0.39 | 1.19 | 88 |
| 0.26 | 0.49 | 1.19 | 153 |
| 0.26 | 0.38 | 0.71 | 288 |
| 0.26 | 0.47 | 0.71 | 342 |

* $r = 0.0075$ cm.

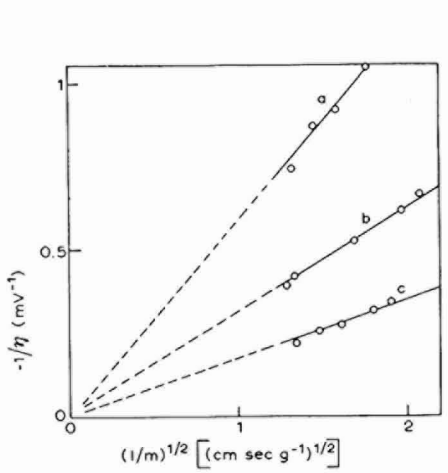


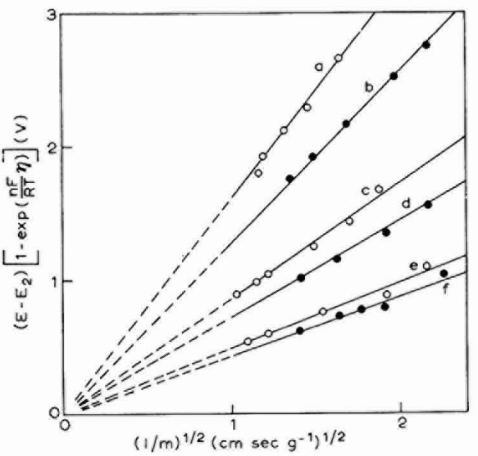


Fig. 3. Plot corresponding to eqn. (2) for low overvoltages (< 5 mV) for Hg(I), at different concns., in 1 *M* $HClO_4$: (a), 10 m*M*; (b), 5 m*M*; (c), 2.5 m*M*.

Fig. 4. Plot corresponding to eqn. (1) for any overvoltage for Hg(I), at different concns., in 1 *M* $HClO_4$ and for two capillaries: (○), $r = 0.0075$ cm; (●), $r = 0.00625$ cm. Concns. of Hg(I): $1.03 \times 10^{-3}$ *M* (a and b); $5.15 \times 10^{-4}$ *M* (c and d); $2.57 \times 10^{-4}$ *M* (e and f).

It follows from eqns. (1) and (2) that the plots of Figs. 3 and 4, for a given concentration of Hg(I), ought to be linear and intersect the origin, if the integral capacity were constant in the interval of potential between $\eta = 0$ and the maximum overvoltage.

SLUYTERS-REHBACH AND SLUYTERS recently noted[5] that the *differential* capacity of the double layer for the Hg(I)–Hg interface in perchloric acid varies very rapidly with potential in the region corresponding to the equilibrium potential for the Hg(I)–Hg reaction. Variations of the *integral* capacity with potential are less rapid than those of the differential capacity but the effect cannot be overlooked. Variations of $c$ and $E$ also account for the lack of proportionality between the slope of the lines in Figs. 3 and 4 and the Hg(I) concentration. Thus, $c$ increases when $E$ becomes more positive, *i.e.*, when the concentration of Hg(I) increases. Hence, the ratio of the slope of the lines in Fig. 3 to the concentration of Hg(I) decreases with increasing concentration of Hg(I).

The integral capacity, $c$, was computed from the slope of the lines in Figs. 3 and 4 and similar data on the doubtful assumption that such plots are linear (see above). Results, calculated for $D = 9.2 \times 10^{-6}$ cm$^2$ sec$^{-1}$ (see ref. 6), are shown in Fig. 5 and are compared with the integral capacities deduced from the data of

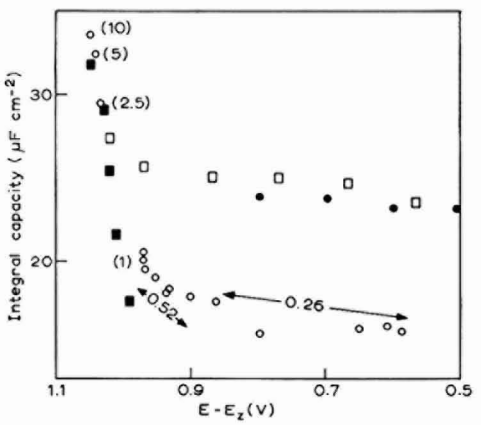


Fig. 5. Integral capacity against potential for Hg(I)/Hg in 1 $M$ $HClO_4$. Potentials referred to the point of zero charge of 1 $M$ $HClO_4$. (○), capacities calculated from data in this work; (●), GRAHAME; (■), KOENIG *et al.*; (□), SLUYTERS-REHBACH AND SLUYTERS. Concn. Hg(I) (mmoles/l) is indicated for each point or group of points for this work.

GRAHAME[3] (differential capacities), SLUYTERS-REHBACH AND SLUYTERS[5] (differential capacities) and KOENIG *et al.*[7] (charge). The agreement is good for the more concentrated solutions (low overvoltages) but is very poor otherwise. This is to be expected, as indicated above.

*Charge transfer control: the Cr(III)/Cr(II) system*

The apparent standard rate constant $k_a^0$ value [eqn.(15), Part I] for the Cr(III)/Cr(II) couple in 1 $M$ potassium chloride, as determined by RANDLES AND SOMERTON[8] is $1.0 \times 10^{-5}$ cm sec$^{-1}$ at 20°. This system therefore was selected to verify the treatment of Part I for control by charge transfer.

Equation (10), Part I, for control by charge transfer and for any overvoltage can be rewritten as

$$\eta = \frac{RT}{\alpha nF} \ln \frac{\pi r^2 \delta I_a^0}{c} + \frac{RT}{\alpha nF} \ln \frac{[1 - e^{(nF/RT)\eta}]\left(\frac{l}{m}\right)}{E - E_z} \qquad (3)$$

Hence, a plot of $\eta$ against the second logarithmic term on the right-hand is linear provided $c$ is constant over the interval of potentials being considered. The slope of this line yields $\alpha$ and the intercept yields $I_a{}^0$. Results in Fig. 6 indicate that eqn. (3) is verified. Values of $\alpha$ determined from these and similar results are listed in Table 2. Determination of $I_a{}^0$ was not attempted from Fig. 6 because of a long extrapolation and the uncertainty on the value of $E - E_z$.

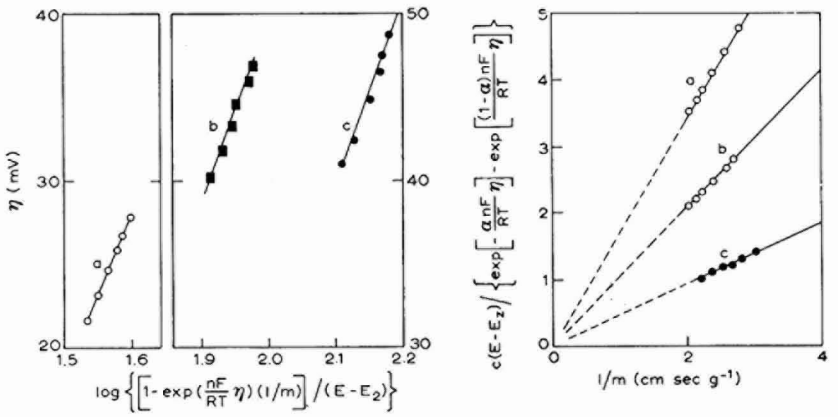


Fig. 6. Plot corresponding to eqn. (3) for different ratios of Cr(III)/Cr(II): (a) 0.53; (b), 0.43; (c), 0.083; in 1 $M$ KCl. Total Cr concn.: (○), 0.1 $M$; (■, ●), 0.04 $M$. The scale on the right-hand side corresponds to the ratio 0.083.

Fig. 7. Plot corresponding to eqn. (10), Part I, for different ratios of Cr(III)/Cr(II): (a), 0.53; (b), 4.55; (c), 8.35. Total Cr concn.: (○), 0.1 $M$; (●), 0.04 $M$.

TABLE 2

VALUES OF $\alpha$ AND $k_a{}^0$ FOR Cr(III)/Cr(II) IN 1 $M$ POTASSIUM CHLORIDE

| *Total Cr concn.: (mole $l^{-1}$)* | *Cr(III)/(Cr(II)* | $\alpha$ | $k_a{}^0$ *($10^{-4}$ cm $sec^{-1}$)* |
|---|---|---|---|
| 0.1 | 0.22 | 0.50 | 0.95 |
| 0.1 | 0.53 | 0.64 | 1.4 |
| 0.1 | 3.25 | 0.78 | 2.2 |
| 0.1 | 4.55 | 0.50 | 1.6 |
| 0.1 | 5.90 | 0.78 | 1.8 |
| 0.04 | 0.083 | 0.59 | 2.1 |
| 0.04 | 0.24 | 0.54 | 1.7 |
| 0.04 | 0.43 | 0.57 | 1.8 |
| 0.04 | 0.77 | 0.58 | 1.7 |
| 0.04 | 1.3 | 0.51 | 1.9 |
| 0.04 | 2.04 | 0.60 | 2.2 |
| 0.04 | 3.58 | 0.66 | 2.0 |
| 0.04 | 8.35 | 0.79 | 2.3 |

It is noted that $\alpha$ varies markedly in Table 2 and possibly tends to increase with the ratio Cr(III)/Cr(II). The trend, if any, may not merely reflect experimental errors and possibly indicates a complexity of the reaction mechanism or of the chemistry of the system. SLOTTER[9], who analyzed current–potential curves for the

S.M.E. for the Cr(III)/Cr(II) system in various electrolytes, commented on the possibility of kinetic complexity. He reported values of $\alpha$ ranging from approximately 0.6–0.7 in perchlorate medium of varying concentration, but he did not give data for potassium chloride.

RANDLES AND SOMERTON[8] did not determine $\alpha$ since their faradaic impedance measurements were carried out purposely for Cr(III)/Cr(II) = 1. Since the Cr(III)/Cr(II) system is probably more complex than initially suspected, eqn. (3) should really not be applicable. It turns out that linear plots are obtained in Fig. 6 but that the resulting value of $\alpha$ is not constant.

The parameters $I_a^0$ and $k_a^0$ were determined for whatever they are worth from the plot of Fig. 7 and similar plots for other data. This plot is directly based on eqn. (10), Part I. The plots are linear and intersect the origin, as expected from eqn. (10), Part I; their slope yields immediately $I_a^0$ and, consequently, $k_a^0$. The resulting values of $k_a^0$ for the mean value of $\alpha = 0.61$ are listed in Table 2. The integral capacity, $c$, was computed from the differential capacity of GRAHAME AND PARSONS[10*] for 1 $M$ potassium chloride. No attempt was made to correct the values of these authors for the presence of Cr(II) and Cr(III), and the capacities are therefore somewhat approximate. No definite trend in the values of $k_a^0$ in Table 1 can be discerned. It may be noted that values are larger than those reported by RANDLES AND SOMERTON by more than one order of magnitude. Unravelling of the kinetics of this system seems in order and *the foregoing results are very tentative.*

*Mixed control by diffusion and charge transfer: the V(III)/V(II)*

The kinetics parameters for V(III)/V(II) in 1 $M$ perchloric acid are, at 20°, $k_a^0 = 3.2 \times 10^{-3}$ cm sec$^{-1}$ and $\alpha = 0.52$ according to JOSHI, MEHL AND PARSONS[11]. RANDLES AND SOMERTON[8] reported $k_a^0 = 4.0 \times 10^{-3}$ cm sec$^{-1}$ at 20° but did not determine $\alpha$. RANDLES later obtained values of $\alpha$ varying from 0.50–0.57 by the analysis of polarographic waves[14]. This system was selected for the verification of treatment of mixed control by diffusion and charge transfer. Measurements were carried out for the ratio V(III)/V(II) = 5:1, 1:1 and 1:5.

The general eqn. (6) of Part I was applied for large overvoltages, and $I_a^0$ and $\alpha$ were computed as follows: the value of $\lambda$ was deduced by application of eqn. (6), Part I, from the experimental values of $\eta$, $(l/m)^{\frac{1}{2}}$ and other parameters in this equation. A plot was prepared of the quantity

$$\ln \lambda \frac{nF}{\pi r \delta^{\frac{1}{2}}} \frac{1}{(C_O^0 D_O^{\frac{1}{2}})^{-1} + \exp[(nF/RT)\eta]/C_R^0 D_R^{\frac{1}{2}}} \frac{1}{(l/m)^{\frac{1}{2}}}$$

against $\eta$ (Fig. 8) by using[12] $D_{V(II)} = 8.12 \times 10^{-6}$ cm$^2$ sec$^{-1}$ and $D_{V(III)} = 5.38 \times 10^{-6}$ cm$^2$ sec$^{-1}$. Points were scattered, but the line drawn in Fig. 8, which corresponds to $\alpha = 0.53$ and $I_a^0 = 1.1 \times 10^{-3}$ A cm$^{-2}$ ($k_a^0 = 4.4 \times 10^{-3}$ cm sec$^{-1}$), is in good agreement with the data obtained by analysis of data for small overvoltages.

Analysis of small-overvoltage data by eqns. (11) and (12) of Part I was more successful. The value of $\lambda$ satisfying eqn. (11) was computed from experimental values of $\eta$ and $(l/m)$, and the $I_a^0$ was computed from eqn. (12), Part I. Integral capacities were those determined for 1 $M$ perchloric acid (see Fig. 2). Some results

* Complete data are not given in ref. 10, but were kindly supplied by Dr. R. PARSONS.

TABLE 3

DATA FOR V(III)/V(II) IN 1 *M* PERCHLORIC ACID*

| $m$ ($g sec^{-1}$) | $l$ ($cm$) | $l/m$ ($cm\ sec\ g^{-1}$) | $-\eta$ ($mV$) | $\lambda$ |
|---|---|---|---|---|
| 0.255 | 0.696 | 2.73 | 2.45 | 0.53 |
| 0.277 | 0.466 | 1.68 | 3.50 | 0.46 |
| 0.267 | 0.366 | 1.37 | 4.20 | 0.41 |
| 0.306 | 0.388 | 1.27 | 4.50 | 0.39 |
| 0.295 | 0.278 | 0.94 | 6.00 | 0.33 |

* V(III)/V(II) = 1:1; V(III) + V(II) = 30.9 mmole $l^{-1}$; $r$ = 0.00625 cm.

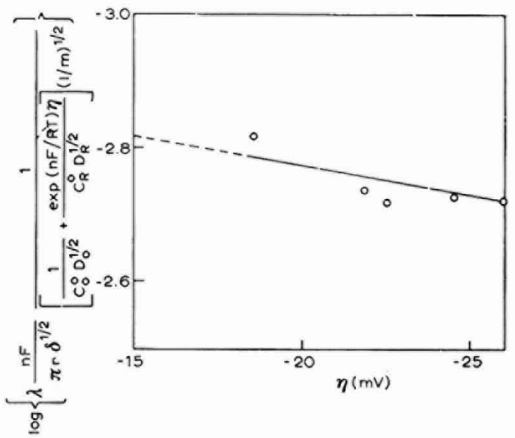


Fig. 8. Plot for the determination of $\alpha$ and $I_a^0$ for large overvoltages for the V(III)/V(II) couple in 1 *M* $HClO_4$. V(III)/V(II) = 1, V(III) + V(II) = 5.16 mmoles/l.

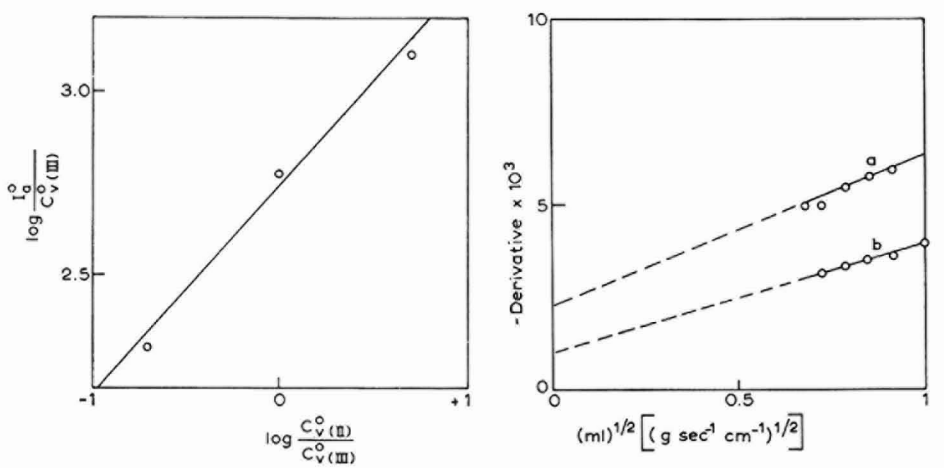


Fig. 9. Results for V(III)/V(II) in 1 *M* $HClO_4$ from small-overvoltage analysis. Total concn. V(III) + V(II), 30.9 mmoles/l.

Fig. 10. Plot for derivative analysis of data for V(III)/V(II) in 1 *M* $HClO_4$. V(III)/V(II) = 1:1. Total concn. V(III) + V(II): (a), 20.7; (b), 30.9 mmoles/l.

are listed in Table 3. Results are plotted in Fig. 9. One deduces $\alpha = 0.56$ and $k_a^0 = 5.7 \times 10^{-3}$ cm sec$^{-1}$, in fairly good agreement with the literature values quoted above.

An alternative method of analysis of small-overvoltage data which does not require values of $c$ and $E_z$ was also applied. It follows from eqn. (11), Part I, that a plot of the derivative $\mathrm{d}(l/m)^{1/2}/\mathrm{d}(1/\eta)$ against $(m/l)^{1/2}$ is linear (Fig. 10). The intercept and slope are, respectively

$$-\frac{RT}{2(nF)^2}\left(\frac{1}{C_O^0 D_O^{\frac{1}{2}}}+\frac{1}{C_R^0 D_R^{\frac{1}{2}}}\right)\frac{c(E-E_z)}{r\delta^{\frac{1}{2}}}$$

$$-\frac{RT}{nF}\frac{c(E-E_z)}{2\pi r^2\delta}\frac{1}{I_a^0}$$

The ratio of the slope to the intercept is thus

$$\frac{nF}{\pi r\delta^{\frac{1}{2}}}\frac{1}{(C_O^0 D_O^{\frac{1}{2}})^{-1}+(C_R^0 D_R^{\frac{1}{2}})^{-1}}\frac{1}{I_a^0}$$

The quantities, $c$ and $E_z$, need not be known in this method, and the analysis is simplified. Values of $k_a^0$ calculated by this method were $9.5 \times 10^{-3}$ and $5.9 \times 10^{-3}$ cm sec$^{-1}$, respectively, for the 20.7 and 30.9 mmoles l$^{-1}$ V(III) + V(II) solutions. The agreement with the data cited above is good, but it must be noted that a rather long extrapolation, with its attending uncertainty, is involved in Fig. 10. Moreover, determination of the first derivative, as required by this method, is somewhat uncertain.

*Control by diffusion and migration: discharge of Hg(I) and Hg(II) in sodium fluoride*

The effect of migration was examined without complication by charge-transfer kinetics, *i.e.*, for the discharge of Hg(I) and Hg(II) in sodium fluoride of varying concentration. Complexation of Hg(I) and Hg(II) with fluoride is quite negligible[13]. Results for Hg(II) discharge are plotted in Fig. 11, which was prepared

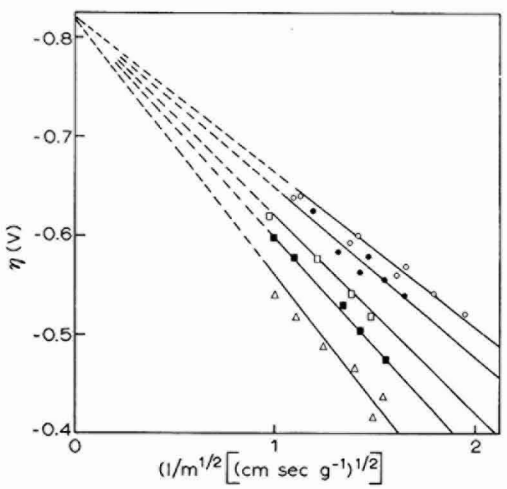


Fig. 11. Plot of potential against $(l/m)^{\frac{1}{2}}$ for $2.2 \times 10^{-4}$ $M$ Hg(II) in NaF at the following molar concns.: (○), 0; (●), 0.003; (□), 0.01; (■), 0.03; (△), 0.1.

by noting that for large cathodic overvoltages and diffusion control, eqn. (6), Part I, reduces to

$$\eta + E_e - E_z = \frac{2\,nFr\delta^{\frac{1}{3}}C_O^0 D_O^{\frac{2}{3}}}{c}\left(\frac{l}{m}\right)^{\frac{1}{3}} \qquad (4)$$

This equation applies to diffusion control, but can presumably be applied, *as a crude approximation*, to mixed control by diffusion and migration provided the diffusion coefficient is replaced by some apparent value. Such an approach has been followed in polarography and chronopotentiometry but it is well known that a more sophisticated treatment is in order. We shall not go into this matter, and we shall

TABLE 4

"APPARENT" DIFFUSION COEFFICIENTS DEDUCED FROM EQN. (4)*

| *NaF concn.* *(mole $l^{-1}$)* | *Apparent diffusion coeff.* *($10^{-6}$ $cm^2$ $sec^{-1}$)* | |
|---|---|---|
| | *Hg(I)* | *Hg(II)* |
| 0 | 0.6 | 1.2 |
| 0.003 | — | 1.8 |
| 0.01 | 2.3 | 4.0 |
| 0.03 | — | 5.8 |
| 0.05 | 7.4 | — |
| 0.1 | — | 9.6 |

* Concns.: $2.1 \times 10^{-4}$ *M* for Hg(I) and $2.2 \times 10^{-4}$ *M* for Hg(II)

limit ourselves to pointing out that $E$ seems to vary linearly with $(l/m)^{1/2}$ as predicted from eqn. (4) for the discharge of both Hg(II) (Fig. 11) and Hg(I). It is also noted that all lines on such plots converge on a single point, as one would expect for negligible complexation with fluoride. Values of the *apparent* diffusion coefficients deduced from eqn. (4) are listed in Table 4.

## CONCLUSION

The analysis worked out in Part I is verified experimentally for control by diffusion or charge transfer and for mixed control by diffusion and charge transfer. Application to kinetics appears to be feasible and may be considered, especially in conjunction with the more classical analysis of current–potential current with the S.M.E. (*cf.*, *e.g.*, SLOTTER[9]). Extension to media of low conductivity may be considered, but the difficulties mentioned in the conclusion of Part I ought to be investigated before any conclusion can be reached on this point.

## ACKNOWLEDGEMENT

Support of the National Science Foundation (V.S.S., G.T. and P.D.) and the Office of Naval Research (P.D.) is gladly acknowledged.

## SUMMARY

The shift of potential at open circuit of a streaming mercury electrode (S.M.E.)

was determined and analyzed for control by diffusion or charge transfer and for mixed control by diffusion and charge transfer. The following systems were investigated: Hg(I) in 1 *M* perchloric acid, Cr(III)/Cr(II) in 1 *M* potassium chloride and V(III)/V(II) in 1 *M* perchloric acid. The charging current of the S.M.E. was also investigated and observations were made on the discharge of Hg(I) and Hg(II) with mixed control by diffusion and migration.

## REFERENCES


1 P. DELAHAY, *J. Electroanal. Chem.*, 10 (1965) 1.
2 J. HEYROVSKÝ AND J. FORJET, *Z. Physik. Chem.*, 193 (1943) 83.
3 D. C. GRAHAME, *Chem. Rev.*, 41 (1947) 441.
4 J. R. WEAVER AND R. W. PARRY, *J. Am. Chem. Soc.*, 76 (1954) 6258; 78 (1956) 5542.
5 M. SLUYTERS-REHBACH AND J. H. SLUYTERS, *Rec. Trav. Chim.*, 83 (1964) 217, 967.
6 I. M. KOLTHOFF AND C. S. MILLER, *J. Am. Chem. Soc.*, 63 (1941) 2732.
7 F. O. KOENIG, H. C. WOHLERS AND D. BANDINI, paper presented at the Moscow C.I.T.C.E. meeting, 1963.
8 J. E. B. RANDLES AND E. W. SOMERTON, *Trans. Faraday Soc.*, 48 (1952) 937.
9 R. A. SLOTTER, *Kinetic Studies at the Streaming Mercury Electrode*, dissertation, University of Michigan, 1960; microfilm Mic 60-2568, University Microfilms, Inc., Ann Arbor, Michigan.
10 D. C. GRAHAME AND R. PARSONS, *J. Am. Chem. Soc.*, 83 (1961) 1291.
11 K. M. JOSHI, W. MEHL AND R. PARSONS, *Transactions of the Symposium on Electrode Processes*, edited by E. YEAGER, Wiley, New York, 1961, pp. 249–263.
12 J. J. LINGANE AND L. MEITES, *J. Am. Chem. Soc.*, 70 (1948) 2525.
13 J. BJERRUM, G. SCHWARZENBACH AND L. G. SILLÉN, *Stability Constants*, Vol. 2, The Chemical Society, London, 1958, p. 91.
14 J. E. B. RANDLES, *Can. J. Chem.*, 37 (1959) 238.

# THEORY OF STAIRCASE VOLTAMMETRY

JOSEPH H. CHRISTIE AND PETER JAMES LINGANE
*Division of Chemistry and Chemical Engineering,* California Institute of Technology, Pasadena, California (U.S.A.)*
(Received March 29th, 1965)

## INTRODUCTION

When the potential of an electrode is changed abruptly from $E_j$ to $E_{j+1}$, the double layer charges rapidly and the current flowing at any time after about 100 $\mu$sec is purely faradaic. BARKER[1] has suggested that this fact be exploited in a technique which has come to be known as voltammetry with a staircase potential function, or simply, staircase voltammetry. If the current flowing at the end of each time interval is plotted as a function of potential, curves similar to linear sweep $I-E$ curves are obtained. However, unlike linear sweep voltammetry, effects of the double-layer charging current have been largely eliminated. Staircase voltammetry has been studied experimentally by MANN[2,3] and by NIGMATULLIN AND VYASELEV[4]. The latter have presented the theory for small values of the potential step interval and have shown that this case coincides with linear sweep voltammetry. The present work considers the general theory for reversible electrode reactions, without restriction on the magnitude of the potential step.

## THEORY

The treatment given here for staircase voltammetry is similar to that given by MATSUDA AND AYABE[5] for linear sweep voltammetry, and neglects double-layer charging. Consider a single reversible reaction

$$O + n\,e \rightleftharpoons R$$

For semi-infinite linear diffusion we have

$$\frac{\partial C_O}{\partial t} = D_O \frac{\partial^2 C_O}{\partial x^2}\,;\quad \frac{\partial C_R}{\partial t} = D_R \frac{\partial^2 C_R}{\partial x^2}\,;\quad x \geqslant 0 \tag{1}$$

with the initial and boundary conditions

$$\begin{aligned} &x \geqslant 0,\ t=0 && C_O = {}^*C_O,\ C_R = 0 \\ &x \to \infty,\ t \geqslant 0 && C_O \to {}^*C_O,\ C_R \to 0 \\ &x=0,\ t>0 && D_O \frac{\partial C_O}{\partial x} = -D_R \frac{\partial C_R}{\partial x} = \frac{I}{nf} \end{aligned} \tag{2}$$

where $I$ is the current density.

* Contribution No. 3226 from the Gates and Crellin Laboratories of Chemistry.

The solutions to this set of equations are[5],

$$C_O(0, t) = \frac{-1}{nF\sqrt{D_O\pi}} \int_0^t \frac{I(\theta)}{\sqrt{t-\theta}}\, d\theta + {}^*C_O \tag{3}$$

$$C_R(0, t) = \frac{1}{nF\sqrt{D_R\pi}} \int_0^t \frac{I(\theta)}{\sqrt{t-\theta}}\, d\theta \tag{4}$$

Since we have assumed reversibility, the Nernst equation is obeyed at the surface of the electrode.

$$C_O(0, t) = C_R(0, t)\sqrt{\frac{D_R}{D_O}} \exp\left[\frac{nF}{RT}(E-E_{\frac{1}{2}})\right] \tag{5}$$

where $E_{\frac{1}{2}}$ is the reversible half-wave potential.
Eliminating $C_O(0, t)$ and $C_R(0, t)$ between eqns. (3), (4) and (5), we have

$$\frac{1}{\sqrt{\pi}} \int_0^t \frac{I(\theta)}{\sqrt{t-\theta}}\, d\theta = nF\sqrt{D_O}\, {}^*C_O \left\{1 + \exp\left[\frac{nF}{RT}(E-E_{\frac{1}{2}})\right]\right\}^{-1} \tag{6}$$

The applied potential function is of the form

$$\begin{aligned} &E \geqslant E_i \qquad t < 0 \\ &E = E_i + j\Delta E \quad j\tau \leqslant t < (j+1)\tau, \end{aligned} \tag{7}$$

where $I = 0$ for $E \geqslant E_i$, (*cf.* Fig. 1). Equation (6) is satisfied by

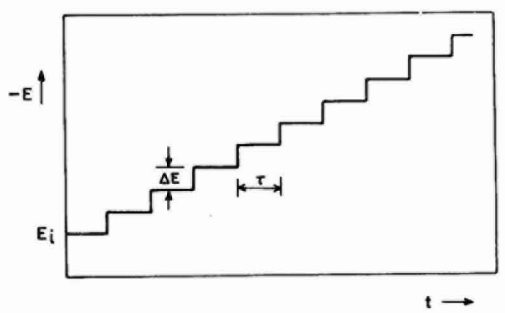


Fig. 1. Staircase potential function.

$$I = \frac{nF\,{}^*C_O\sqrt{D_O}}{\sqrt{\pi}} \left\{ \frac{\varepsilon_0}{1+\varepsilon_0} \frac{1}{\sqrt{t}} + \left[\frac{1}{1+\varepsilon_0} - \frac{1}{1+\varepsilon_1}\right] \frac{1}{\sqrt{t-\tau}} + \ldots \right.$$
$$\left. + \left[\frac{1}{1+\varepsilon_{j-1}} - \frac{1}{1+\varepsilon_j}\right] \frac{1}{\sqrt{t-(j)\tau}} \right\} \tag{8}$$

where

$$j\tau \leqslant t < (j+1)\tau$$
$$\varepsilon_j = \exp\left[-\frac{nF}{RT}(E_i + j\Delta E - E_{\frac{1}{2}})\right]; \quad j = 0, 1, 2, \ldots \tag{9}$$

We are primarily interested in the current at the end of each time interval. If

we substitute $t=j\tau$ into eqn. (8), we obtain upon rearrangement,

$$I(j\tau) = \frac{nF^*C_O D_O^{\frac{1}{2}}}{\tau^{\frac{1}{2}}} \psi_s(j, \Delta E)$$

where

$$\psi_s(j, \Delta E) = \frac{1}{\sqrt{\pi}} \left\{ \frac{1}{\sqrt{j}} + \frac{1}{1+\varepsilon_0} \left[ \frac{1}{\sqrt{j-1}} - \frac{1}{\sqrt{j}} \right] + \frac{1}{1+\varepsilon_1} \left[ \frac{1}{\sqrt{j-2}} - \frac{1}{\sqrt{j-1}} \right] + \cdots \right.$$
$$\left. + \frac{1}{1+\varepsilon_{j-2}} \left[ 1 - \frac{1}{\sqrt{2}} \right] - \frac{1}{1+\varepsilon_{j-1}} \right\} . \qquad (11)$$

If we take the limit $\Delta E \to 0$ subject to the condition that the "sweep rate", $\Delta E/\tau$, remain constant, the current becomes identical to the linear sweep current [*cf.* eqns. (17) and (18), ref. (5)], as we would expect.

## RESULTS AND DISCUSSION

$\psi_s$ was evaluated as a function of $(nF/RT)\,(E-E_{\frac{1}{4}})$ for several values of $(nF/RT)\Delta E$. These are tabulated in Table 1 and representative curves are presented in Fig. 2. It should be emphasized that the curves shown in Fig. 2 are envelopes of a discontinuous function. Each point is plotted individually for the larger potential steps.

TABLE 1

$\sqrt{\pi}\psi_s$ CALCULATED FROM EQN. (11) FOR VARIOUS VALUES OF $(nF/RT)\Delta E$

| $-\frac{nF}{RT}(E-E_{\frac{1}{4}})$ \ $\frac{nF}{RT}\Delta E$ | −1.0 | −0.8 | −0.6 | −0.4 | −0.2 | −0.08 | −0.04 |
|---|---|---|---|---|---|---|---|
| −7.0 | 0.0009 | 0.0009 | 0.0009 | 0.0009 | | | |
| −6.6 | | | | 0.0011 | 0.0009 | 0.0006 | 0.0005 |
| −6.4 | | | 0.0014 | | | | |
| −6.2 | | 0.0018 | | 0.0015 | 0.0012 | 0.0009 | 0.0007 |
| −6.0 | 0.0022 | | | | | | |
| −5.8 | | | 0.0024 | 0.0022 | 0.0018 | 0.0013 | 0.0009 |
| −5.4 | | 0.0038 | | 0.0032 | 0.0026 | 0.0018 | 0.0014 |
| −5.2 | | | 0.0043 | | | | |
| −5.0 | 0.0059 | | | 0.0047 | 0.0038 | 0.0027 | 0.0020 |
| −4.6 | | 0.0083 | 0.0078 | 0.0070 | 0.0056 | 0.0040 | 0.0030 |
| −4.2 | | | | 0.0103 | 0.0083 | 0.0059 | 0.0045 |
| −4.0 | 0.0156 | | 0.0140 | | | | |
| −3.8 | | 0.0182 | | 0.0153 | 0.0123 | 0.0087 | 0.0066 |
| −3.4 | | | 0.0251 | 0.0225 | 0.0181 | 0.0129 | 0.0097 |
| −3.0 | 0.0411 | 0.0392 | | 0.0329 | 0.0264 | 0.0188 | 0.0141 |
| −2.8 | | | 0.0443 | | | | |
| −2.6 | | | | 0.0478 | 0.0383 | 0.0272 | 0.0204 |
| −2.2 | | 0.0819 | 0.0765 | 0.0685 | 0.0548 | 0.0388 | 0.0292 |
| −2.0 | 0.1023 | | | | | | |
| −1.8 | | | | 0.0964 | 0.0770 | 0.0545 | 0.0408 |
| −1.6 | | | 0.1272 | | | | |
| −1.4 | | 0.1600 | | 0.1327 | 0.1056 | 0.0744 | 0.0557 |
| −1.0 | 0.2260 | | 0.1994 | 0.1772 | 0.1403 | 0.0984 | 0.0734 |

TABLE 1 (continued)

| $-\frac{nF}{RT}(E-E_i)$ \ $\frac{nF}{RT}\Delta E$ | −1.0 | −0.8 | −0.6 | −0.4 | −0.2 | −0.08 | −0.04 |
|---|---|---|---|---|---|---|---|
| −0.6 | | 0.2780 | | 0.2277 | 0.1792 | 0.1250 | 0.0930 |
| −0.4 | | | 0.2878 | | | | |
| −0.2 | | | | 0.2800 | 0.2188 | 0.1515 | 0.1122 |
| 0 | 0.4008 | | | | | | |
| 0.2 | | 0.4088 | 0.3751 | 0.3282 | 0.2543 | 0.1746 | 0.1288 |
| 0.6 | | | | 0.3668 | 0.2815 | 0.1916 | 0.1405 |
| 0.8 | | | 0.4401 | | | | |
| 1.0 | 0.5370 | 0.5006 | | 0.3922 | 0.2982 | 0.2010 | 0.1467 |
| 1.4 | | | 0.4713 | 0.4041 | 0.3042 | 0.2032 | 0.1475 |
| 1.8 | | 0.5287 | | 0.4044 | 0.3017 | 0.1998 | 0.1444 |
| 2.0 | 0.5721 | | 0.4724 | | | | |
| 2.2 | | | | 0.3963 | 0.2933 | 0.1927 | 0.1387 |
| 2.6 | | 0.5108 | 0.4546 | 0.3829 | 0.2814 | 0.1836 | 0.1317 |
| 3.0 | 0.5402 | | | 0.3670 | 0.2680 | 0.1739 | 0.1244 |
| 3.2 | | | 0.4285 | | | | |
| 3.4 | | 0.4743 | | 0.3503 | 0.2545 | 0.1644 | 0.1173 |
| 3.8 | | | 0.4009 | 0.3338 | 0.2415 | 0.1554 | 0.1107 |
| 4.0 | 0.4900 | | | | | | |
| 4.2 | | 0.4357 | | 0.3183 | 0.2295 | 0.1473 | 0.1048 |
| 4.4 | | | 0.3749 | | | | |
| 4.6 | | | | 0.3040 | 0.2186 | 0.1399 | 0.0994 |
| 5.0 | 0.4434 | 0.4012 | 0.3517 | 0.2910 | 0.2088 | 0.1334 | 0.0947 |
| 5.4 | | | | 0.2792 | 0.2000 | 0.1276 | 0.0905 |
| 5.6 | | | 0.3316 | | | | |
| 5.8 | | 0.3722 | | 0.2686 | 0.1921 | 0.1224 | 0.0868 |
| 6.0 | 0.4052 | | | | | | |
| 6.2 | | | 0.3142 | 0.2590 | 0.1850 | 0.1178 | 0.0835 |
| 6.6 | | 0.3481 | | 0.2503 | 0.1786 | 0.1137 | 0.0805 |
| 6.8 | | | 0.2992 | | | | |
| 7.0 | 0.3746 | | | 0.2425 | 0.1729 | 0.1099 | 0.0779 |
| 7.4 | | 0.3280 | 0.2861 | 0.2353 | 0.1677 | 0.1066 | 0.0755 |
| 7.8 | | | | 0.2288 | 0.1629 | 0.1035 | 0.0733 |
| 8.0 | 0.3499 | | 0.2746 | | | | |
| 8.2 | | 0.3110 | | 0.2227 | 0.1586 | 0.1007 | 0.0713 |
| 8.6 | | | 0.2644 | 0.2172 | 0.1545 | 0.0981 | 0.0695 |
| 9.0 | 0.3296 | 0.2965 | | 0.2120 | 0.1508 | 0.0957 | 0.0678 |
| 9.2 | | | 0.2553 | | | | |
| 9.4 | | | | 0.2073 | 0.1474 | 0.0935 | 0.0662 |
| 9.8 | | 0.2838 | 0.2471 | 0.2028 | 0.1442 | 0.0915 | 0.0648 |
| 10.0 | 0.3126 | | | | | | |
| 10.2 | | | | 0.1986 | 0.1412 | 0.0896 | 0.0634 |
| 10.4 | | | 0.2397 | | | | |
| 10.6 | | 0.2728 | | 0.1947 | 0.1384 | 0.0878 | 0.0621 |
| 11.0 | 0.2980 | | 0.2329 | 0.1910 | 0.1357 | 0.0861 | 0.0609 |
| 11.4 | | 0.2629 | | 0.1876 | 0.1332 | 0.0845 | 0.0598 |
| 11.6 | | | 0.2267 | | | | |
| 11.8 | | | | 0.1843 | 0.1309 | 0.0830 | 0.0587 |
| 12.0 | 0.2853 | | | | | | |
| 12.2 | | 0.2541 | 0.2210 | 0.1812 | 0.1286 | 0.0816 | 0.0577 |
| 12.6 | | | | 0.1782 | 0.1265 | 0.0802 | 0.0568 |
| 12.8 | | | 0.2157 | | | | |
| 13.0 | 0.2742 | 0.2462 | | 0.1754 | 0.1245 | 0.0789 | 0.0559 |

The maximum value of $\psi_s$ is observed to decrease with decreasing potential step in a manner analogous to the decrease in the maximum current with decreasing sweep rate observed in linear sweep voltammetry. The current in staircase voltammetry is parametrically dependent on both $\Delta E$ and $\tau$. Therefore, displaying $\psi_s$ at decreasing values of the potential step interval is equivalent to displaying the current at decreasing values of the "sweep rate", $\Delta E/\tau$.

Referring to eqn. (10), we observe that the current is linear in $1/\tau^{\frac{1}{2}}$. In Fig. 3, the maximum current is plotted *vs.* $[(nF/RT)(\Delta E)]^{\frac{1}{2}}$ and the current for a linear

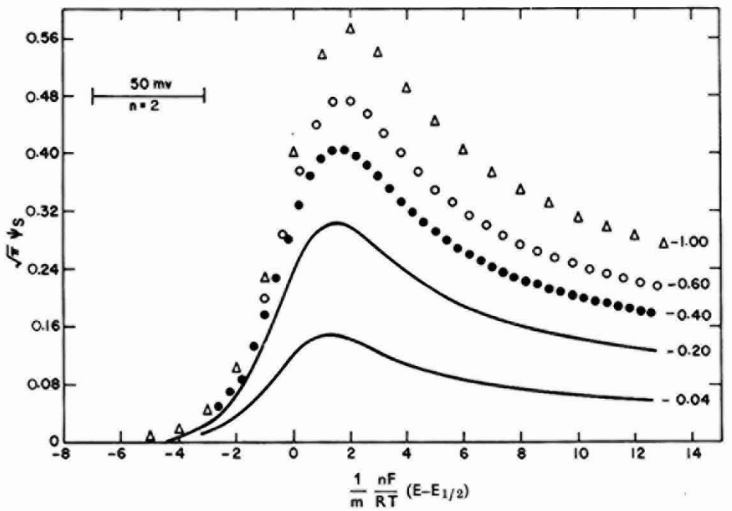


Fig. 2. Current–potential functions calculated from eqn. (11). Number shown is the value of $(nF/RT)\Delta E$ used in calculating that curve (1.0 = 12.8 mV for $n = 2$ at 298°K). The peak current for linear sweep voltammetry occurs at $(nF/RT)(E-E_{\frac{1}{4}}) = +1.11$.

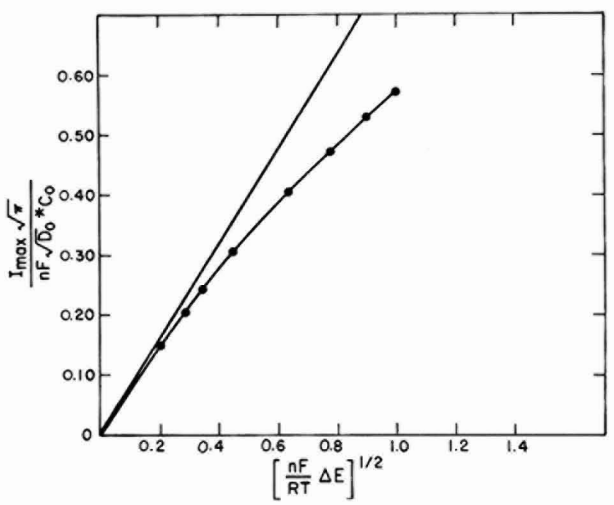


Fig. 3. Maximum current as a function of the potential step interval for constant $\tau$. The straight line corresponds to a linear potential sweep.

potential sweep is plotted in similar units for comparison. The maximum currents deviate strongly from linear sweep case at high values of $(\Delta E)^{\frac{1}{2}}$. This is in accord with the experimental observations of MANN, *cf.* Fig. 4 in ref. (3).

The "sweep rate", $\Delta E/\tau$, can be varied by varying $\Delta E$, $\tau$, or both. As observed above, the "peak" currents vary linearly with $1/\tau^{\frac{1}{2}}$ [eqn. (10)] and approximately linearly with $(\Delta E)^{\frac{1}{2}}$ (Fig. 3). Both $\Delta E$ and $\tau$ can only be varied within certain limits. The minimum value of $\tau$ must be larger than the time constant for double-layer charging. The maximum value of $\tau$ is fixed by the requirement that the diffusion remain linear. On the other hand, $\Delta E$ must always be large compared with the noise in the potential control circuit. For very large steps, the current envelope is poorly defined although MANN[3] appears to have employed steps as large as 40 mV successfully.

The disadvantage in varying the "sweep rate" by varying $\Delta E$ is that the "peak" potential appears to shift slightly as the step interval is varied, *cf.* Fig. 2. This means that in analytical applications the potential at which the current is measured must vary and perhaps more importantly that the shift might be confused with or mask the effects of electrode irreversibility. It should be remembered that the "peak" potential is a fiction since the current function is discontinuous and the "peak" current is constrained to occur at an integral number of potential steps from $E_i$.

It is evident from the foregoing that the most convenient analytical scheme would be to use a large constant potential step and to vary $\tau$ in the calibration procedure. In this way, the largest values of the current compatible with a convenient current envelope are obtained, and the "peak" potential is constant.

In his original paper[2], MANN states that he was unable to observe oxygen reduction using this technique. Experiments in this laboratory show that in fact the waves MANN attributes to "absorption and desorption phenomena" are due to the two-step reduction of dissolved oxygen and that these waves disappear if the solution is deaerated. In addition, the first wave observed by MANN in KCl supporting electrolyte is undoubtedly due to the reduction of calomel since the wave is not present in the perchlorate supporting electrolyte[2].

The work of MANN has shown that staircase voltammetry has distinct analytical applications. It appears that staircase voltammetry can be extended to other cases where linear sweep voltammetry has been employed; *e.g.*, stripping analysis, the study of irreversible reactions, and the study of coupled solution reactions by cyclic voltammetry.

ACKNOWLEDGEMENT

We thank Professor F. C. ANSON for helpful discussion. This work was supported in part by predoctoral fellowships from North American Aviation, Inc. (JHC), and from the U.S. Public Health Service, Division of General Medical Sciences (PJL), and by the U.S. Army Research Office (Durham).

SUMMARY

The theoretical relationships for voltammetry with a staircase potential

function are developed for a reversible electrode reaction and are shown to be in accord with experiment. Current–potential curves are calculated and tabulated.

REFERENCES

1 G. C. BARKER, *Advances in Polarography*, edited by I. S. LONGMUIR, Pergamon Press, New York, 1960, p. 144.
2 C. K. MANN, *Anal. Chem.*, 33 (1961) 1484.
3 C. K. MANN, *ibid.*, 37 (1965) 326.
4 R. SH. NIGMATULLIN AND M. R. VYASELEV, *Zh. Analit. Khim.*, 19 (1964) 545.
5 H. MATSUDA AND Y. AYABE, *Z. Elektrochem.*, 59 (1955) 494.

# DISTORTION OF LINEAR-SWEEP POLAROGRAMS BY OHMIC DROP

W. T. DE VRIES AND E. VAN DALEN
*Department of Chemistry, The Free University, Amsterdam (The Netherlands)*
(Received April 15th, 1965)

## INTRODUCTION

The theory of linear-sweep voltammetry assumes the working electrode (WE) potential $E(t)$ to be a linear function of time $t$:

$$E(t) = E_i - vt,$$

where $E_i$ is the initial potential and $v$ the sweep rate (a reduction process is thus

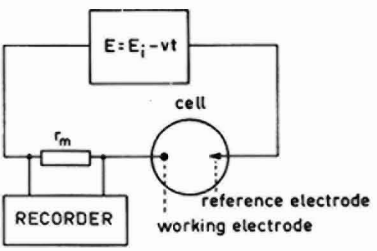


Fig. 1. Simple circuit for linear-sweep voltammetry.

assumed). When, however, a simple circuit like that in Fig. 1 is used, the WE potential is

$$E(t) = E_i - vt + (nFAq(t) + i_c)(r_m + r_{cell}),$$

where $q(t)$ denotes the flux of oxidized and reduced substances at the electrode surface, defined to have a positive value, $n$ is the number of electrons occurring in the electron-transfer reaction equation, $F$ is the Faraday, $A$ the electrode area, $r_m$ and $r_{cell}$ the values of the current-measuring resistor and the a.c. resistance of the cell, respectively, and $i_c$ the capacity current due to the charging of the double layer.

DELAHAY AND STIEHL[1,2] have estimated the influence of the ohmic drop on the peak height of the linear-sweep polarogram (LSP), neglecting the capacity current. Their treatment is approximate and gives no information about other effects on the form of the LSP and its position on the potential axis.

Linear-sweep voltammetry finds increasing use for elucidation of the nature of electrode reactions. Unlike in purely analytical applications, the peak current is not the only important property, but the dependence of the (half-) peak potential and the width (*e.g.*, the width at half height) on the sweep rate are equally important. We therefore tried to find an exact computation of LSP's distorted by ohmic drop.

Our treatment also neglects the capacity current and thus the expression for the WE potential becomes:

$$E(t) = E_i - vt + nFA\Omega q(t), \tag{1}$$

where $\Omega$ is the sum of all resistances which contribute to the ohmic drop, and is assumed to be constant.

The influence of the capacity current will be discussed qualitatively in a following section.

## THE INTEGRAL EQUATION; GENERAL PROPERTIES OF DISTORTED LSP's

The diffusion equations and initial and boundary conditions for the reversible reduction of an oxidized species, $O$, to a reduced species, $R$, at a plane electrode are summarized elsewhere[3,4]. Using DELAHAY's notation the boundary condition obtained by applying the Nernst equation must be written as:

$$C_O(0, t) = \theta C_R(0, t)\varepsilon(t); \tag{2}$$

$$\varepsilon(t) = \exp\left[-\sigma t + \frac{n^2F^2}{RT} A\Omega q(t)\right]; \tag{3}$$

$$\sigma = (nF/RT)v.$$

The following integral equation for the flux $q(t)$ is easily derived[4]:

$$\int_0^t \frac{q(\lambda)}{\sqrt{t-\lambda}}\,d\lambda = \frac{C^0\sqrt{\pi D_O}\,(1-\varepsilon(t))}{\gamma\theta\varepsilon(t)+1}, \tag{4}$$

where $C^0$ is the initial concentration of $O$, $D_O$ and $D_R$ are the diffusion coefficients of $O$ and $R$, and $\gamma = (D_O/D_R)^{\frac{1}{2}}$. Following the treatment of NICHOLSON AND SHAIN[4] the integral equation is transformed by the substitutions

$$\xi = \lambda/\sigma;$$

$$q(t) = C^0\sqrt{D_O\sigma}\;P'(\sigma t), \tag{5}$$

which result in:

$$\int_0^{\sigma t} \frac{P'(\xi)}{\sqrt{\sigma t-\xi}}\,d\xi = \frac{\sqrt{\pi}\,(1-\varepsilon(\sigma t))}{\gamma\theta\varepsilon(\sigma t)+1}; \tag{6}$$

$$\varepsilon(\sigma t) = \exp\left[-\sigma t + \frac{n^2F^2}{RT} A\Omega C^0\sqrt{D_O\sigma}\;P'(\sigma t)\right]. \tag{7}$$

If $\Omega = 0$ (absence of ohmic drop) eqn. (6) describes the well-known Ševčik–Randles $P$-function multiplied by a factor $(1 + 1/\gamma\theta)$, which is very nearly unity. But if $\Omega$ differs from zero, eqn. (6) describes a distorted $P'$-function characterized by the parameters $\gamma\theta$ and $(n^2FA\Omega C^0(D_O\sigma)^{\frac{1}{2}})$. A LSP is almost independent of $\gamma\theta$[5], and the distorted $P'$-function can thus be characterized by the value of

$$n^2FA\Omega C^0\sqrt{D_O\sigma}\;P'_{MAX} = n(i_P'\Omega),$$

*i.e.*, $n$ times the maximal value of the appearing ohmic drop. It is rather obvious, however, that the ratio $P'_{MAX}/P_{MAX}$ is a single-valued function of $n(i_P'\Omega)$ and therefore the distorted $P'$-function is also wholly determined by $n$ times *expected* maximal

ohmic drop, *i.e.*, $n$ times the product of resistance and peak current which would appear in the absence of ohmic drop.

## CALCULATION OF DISTORTED $P'$-FUNCTIONS

Some general properties of distorted LSP's having been established, the principles of the numerical calculations will now be explained.

By applying HUBER's method for numerically solving integral equations[6] the following formula results:

$$P_j' = \frac{3}{4}\sqrt{\frac{\pi}{\delta}}\,\frac{(1-\varepsilon(j\delta))}{\gamma\theta\varepsilon(j\delta)+1} - S\,,$$

with

$$S = \sum_{k=1}^{j-1}(P_k'-P_{k-1}')\,\{(j-k+1)^{\frac{1}{2}}-(j-k)^{\frac{1}{2}}\}-P_{j-1}'\,;$$

$$\varepsilon(j\delta) = \exp\left[-j\delta + \frac{n^2F^2}{RT}A\Omega C^0\sqrt{D_0\sigma}\;P_j'\right],$$

and where $\delta$ is the width of the intervals into which the $\sigma t$-axis is divided, and $P_j'$ is the value of $P'(\sigma t)$ at $\sigma t = j\delta$.

Equation (8) can be written symbolically as

$$P_j' = \Phi(P_j') - S\,,$$

where $S$ is independent of $P_j'$, and this form suggests that under certain conditions eqn. (8) can be solved by the process of iteration: on substituting a suitably chosen value $P_{j,0}'$ into the right-hand side of eqn. (8) a new value, $P_{j,1}'$, is found:

$$P_{j,1}' = \Phi(P_{j,0}') - S\,,$$

and repeating the process:

$$P_{j,2}' = \Phi(P_{j,1}') - S\,.$$

It can be proved[7] that the series $P_{j,0}'$, $P_{j,1}'$, $P_{j,2}'$, ... converges to the limit, $P_j'$, when the condition

$$\left|\frac{\mathrm{d}\Phi(P_j')}{\mathrm{d}P_j'}\right| < 1$$

is fulfilled. Differentiating the right-hand side of eqn. (8) with respect to $P_j'$ one finds for the first derivative $D^1$:

$$D^1 = \frac{\mathrm{d}\Phi(P_j')}{\mathrm{d}P_j'} = -\frac{3}{4}g\sqrt{\frac{\pi}{\delta}}\,\frac{(1+\gamma\theta)\varepsilon(j\delta)}{(\gamma\theta\varepsilon(j\delta)+1)^2}\,,$$

where

$$g = \frac{n^2F^2}{RT}A\Omega C^0\sqrt{D_0\sigma}\,.$$

The first derivative is always negative and has a maximum in absolute value for $\varepsilon(j\delta) = 1/\gamma\theta$:

$$|D^1|_{MAX} = \frac{3}{16} g \sqrt{\frac{\pi}{\delta}} \left( \frac{1}{\gamma\theta} + 1 \right).$$

The effect of these results on the numerical calculations can be summarized as follows. If $|D^1|_{MAX} < 1$, the whole LSP can be computed by the process of iteration. If this is not the case, $D^1$ should be estimated and iteration is still possible if its absolute value is smaller than 1. If iteration is impossible another way of computing $P_j'$ must be used; this will be explained below. A consequence of the principle of this method is that its use is more advantageous than iteration if $|D^1| > 0.5$.

By using the fact that $D^1$ is always negative, it can be proved (using the mean value theorem of the differential calculus) that on substitution of a value $(P_j' + P)$ into the right-hand side of eqn. (8), which value is thus too large by the positive amount $p$, a new value $\Pi_j' < P_j'$ is found and substitution of the value $(P_j' - p)$ yields a value $\Pi_j' > P_j'$.

Let $P_{j,L}'$ and $P_{j,R}'$ be the left- and right-hand side end-points, respectively, of an interval containing the unknown value, $P_j'$, which must be found. By substituting the values of these end-points into eqn. (8) new values, $\Pi_{j,L}'$ and $\Pi_{j,R}'$, are found for which $\Pi_{j,L}' > P_j' > P_{j,L}'$, and $\Pi_{j,R}' < P_j' < P_{j,R}'$. The mid-point of the interval under consideration is $P_{j,M} = (P_{j,L}' + P_{j,R}')/2$, and substitution of this value into eqn. (8) yields $\Pi_{j,M}'$. If $\Pi_{j,M}' > P_{j,M}'$ then the desired value, $P_j'$, lies in the right-hand-side half of the interval, and in the other case, in the other half. Having thus located $P_j'$ in a half-interval, we can divide this into two parts and apply the same reasoning again to select the $P_j'$-containing quarter-interval. Repeating this process we can find $P_j'$ to any desired degree of accuracy.

An ALGOL-60 program for a digital electronic computer based on these principles has been written and the calculations of the $P'$-functions have been performed for a temperature of 25°, an initial potential of $E_{\frac{1}{2}} + 151.4/n$ mV, and with an accuracy of the $P'_{MAX}$-values of better than 0.5%.

## RESULTS, DISCUSSION, AND CONCLUSIONS

### (a) *Results of the calculations*

Figure 2 shows the undistorted $P$-function and some $P'$-functions distorted by ohmic drop, which are characterized by $n$ times expected and appearing ohmic drop. The $P'$-functions have been plotted against $E(t)$, the corrected electrode potential, according to eqn. (1). A reduction process is assumed here, but adaptation of the results to oxidation processes is readily made by reversing the signs of $n(E - E_{\frac{1}{2}})$ and $n(E_P - E_{\frac{1}{2}})$. It can be seen that the reversible LSP is shifted towards more negative potentials, resulting in a more negative peak potential. It can also be inferred that the tail of the peak becomes higher with increasing ohmic drop; this is not surprising, as beyond the maximum of the LSP the real sweep rate is higher than in the absence of ohmic drop. This effect, coupled with the decrease in peak height, causes a considerable increase in the width of the peak.

These effects are more clearly demonstrated in Figs. 3, 4, and 5, which show $P_{MAX}'/P_{MAX} = P_{MAX}'/0.4463$, $n(E_P - E_{\frac{1}{2}})$, and $b_{\frac{1}{2}}$ (the width at half height) as functions of $n$ times expected and appearing ohmic drop. An expected ohmic drop of 100 mV for a two-electron electrode reaction causes a decrease of the peak current by

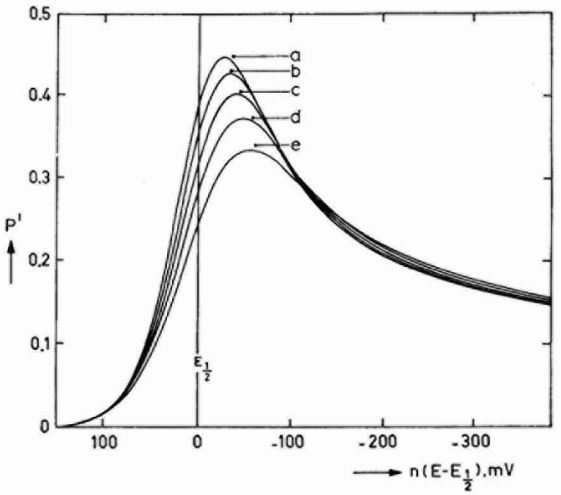


Fig. 2. Undistorted $P$-function and distorted $P'$-functions, plotted *vs.* corrected electrode potential. Numbers denote $n$ times expected maximal ohmic drop; corresponding numbers in parentheses denote $n$ times appearing ohmic drop. (a), 0(0); (b), 20(19); (c), 50(45); (d), 100(84); (e), 200(150).

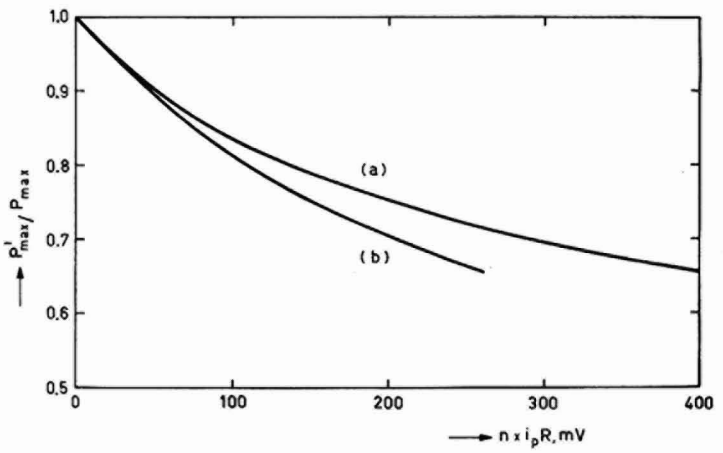


Fig. 3. Ratio $P_{MAX}'/P_{MAX}$ plotted *vs.* (a), $n$ times expected maximal ohmic drop; (b), $n$ times appearing maximal ohmic drop.

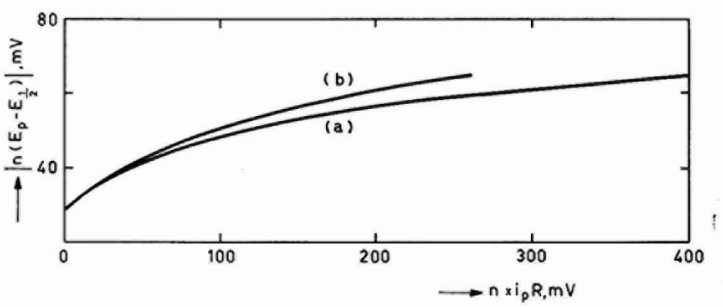


Fig. 4. Corrected peak potential as function of expected and appearing maximal ohmic drop.

a factor 0.75, a shift of the peak from −14.3 to −28.1 mV, and an increase in the width at half height from 102 to 178 mV.

It is thus apparent that a reversible LSP is deformed to a considerable extent by ohmic drop, and simulates non-reversible behaviour as manifested by shifting and broadening of the peak.

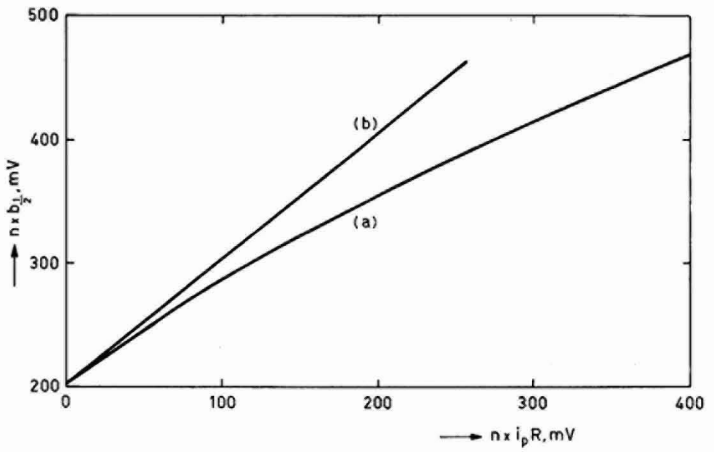


Fig. 5. Width at half height as function of expected and appearing maximal ohmic drop.

(*b*) *Influence of the capacity current*

The above results were obtained neglecting the capacity current, $i_c$. A simple calculation, assuming a (rather high) sweep rate of 100 V/sec, an average double-layer capacity of 50 $\mu$F/cm$^2$, and a spherical electrode radius of 0.05 cm, gives a value of 0.15 mV/Ω for $i_c$. Owing to the non-linearity of the WE potential sweep (caused by ohmic drop in the presence of reacting substance) and because of the non-constancy of the double-layer capacity this figure is only approximate, and certainly not a constant. Under the same conditions, a mercury-pool electrode with an area of 5 cm$^2$ gives an $i_c$ of 25 mV/Ω. It is thus evident, especially in the case of a mercury-pool electrode, that the capacity current can cause an appreciable deviation from linearity of the WE potential sweep.

It is possible to calculate exactly the influence of the capacity current, caused by a non-constant double-layer capacity, in the presence of a reacting substance. However, from the discussion to follow it will appear that these calculations would be of relatively little use, and therefore we have not yet attempted this.

(*c*) *Elimination of ohmic drop*

It can be ascertained from the figures that a maximal ohmic drop of about $20/n$ mV causes a discernible deviation from simple reversible behaviour when registration of the LSP is moderately accurate.

It has been demonstrated that linear-sweep voltammetry is a powerful and versatile technique for investigating electrode reactions[8], but our calculations demonstrate that it is necessary to choose the experimental conditions carefully so as to reduce ohmic drop, and failure to keep it below about $20/n$ mV will make it very

laborious to obtain accurate values for electrode reaction parameters in quantitative studies of electrode reactions.

Elimination of ohmic drop by the use of operational amplifier instrumentation[8] is relatively easy when using a mercury-pool or a platinum-foil electrode. The high value of the double-layer charging current at high sweep rates, however, necessitates a careful positioning of the reference electrode tip relative to the WE, irrespective of the value of the faradaic current caused by the electrode reaction.

It is sometimes believed that ohmic drop can always be effectively eliminated by using a three-electrode potentiostat. However, SCHAAP AND MCKINNEY[9] and others have pointed out that this is not generally true, and that working electrode geometry can prevent elimination of ohmic drop. It is especially difficult to eliminate ohmic drop occurring in the solution when using a hanging mercury-drop electrode or a dropping-mercury electrode. For this reason the use of a mercury-drop electrode (or other micro-electrodes of similar geometry) should be avoided in the linear-sweep voltammetry technique if the appearing ohmic drop in the solution is more than about $20/n$ mV.

ACKNOWLEDGEMENTS

The authors are grateful to Dr. J. A. ZONNEVELD of the Mathematical Centre, Amsterdam, for making available the X1 for the numerical calculations, and to Z.W.O. for financial support of part of this work.

SUMMARY

An exact computation of reversible linear-sweep polarograms at a plane electrode distorted by ohmic drop is presented. It follows from these calculations that ohmic drop causes a decrease of the peak current, a shift of even the corrected peak potential, and a considerable increase of the width of the peak, suggesting non-reversible behaviour.

It is deduced that for quantitative studies of electrode processes, the use of a mercury-drop electrode (or other micro-electrodes of similar geometry) in conjunction with linear-sweep voltammetry should be avoided (even when using a three-electrode potentiostat) when the ohmic drop in the solution exceeds about $20/n$ mV.

NOTE ADDED IN PROOF

Recently NICHOLSON published some calculations on the same problem (*Anal. Chem.*, 37 (1965) 667), and his results, although not so extensive as ours, were the same. His numerical calculations were carried out by using the Newton–Rhapson iteration method, and this method is more rapid than the bisection method used in our calculations; with the Newton–Rhapson method the convergence improves during the calculation of subsequent approximations.

It should be remarked that HUBER's method for solving numerically Volterra integral equations is to be preferred to the approach used by NICHOLSON, as the approximation embodied in Huber's method is more refined; this enables the use of larger values of $\delta$, which reduces the computation time considerably.

REFERENCES

1 P. DELAHAY, *New Instrumental Methods in Electrochemistry*, Interscience Publishers, Inc., New York, 1954, p. 132.
2 P. DELAHAY AND G. L. STIEHL, *J. Phys. Colloid Chem.*, 55 (1951) 570.
3 Ref. 1, p. 116.
4 R. S. NICHOLSON AND I. SHAIN, *Anal. Chem.*, 36 (1964) 707.
5 W. H. REINMUTH, *J. Am. Chem. Soc.*, 79 (1957) 6358.
6 W. T. DE VRIES, *J. Electroanal. Chem.*, 9 (1965) 448.
7 J. B. SCARBOROUGH, *Numerical Mathematical Analysis*, Oxford University Press, London, 1930, pp. 184–187.
8 R. S. NICHOLSON AND I. SHAIN, *Anal. Chem.*, 37 (1965) 178, 190.
9 W. B. SCHAAP AND P. S. MCKINNEY, *Anal. Chem.*, 36 (1964) 1251.

# ANODIC PROPERTIES OF PLATINUM–CHROMIUM ALLOYS IN SULFURIC ACID SOLUTION

M. W. BREITER
*General Electric Research Laboratory, Schenectady, New York (U.S.A.)*
(Received April 2nd, 1965)

## INTRODUCTION

The electrochemical study of alloys of metals of the platinum group with other metals promises new insight into the question of why platinum metals are better catalysts for many heterogeneous reactions than other metals. The recent review[1] on electrochemistry and the structure of solid surfaces by PARSONS shows the necessity for experimental work on this subject.

Results on hydrogen adsorption and on the formation and reduction of oxygen layers for four Pt–Cr alloys in $N$ $H_2SO_4$ at 30° are reported in this paper. The techniques of measuring periodic current–potential curves ($I-U$ curves) potentiostatically and of voltammetry with superimposed a.c. voltage, were used at small sweep rates. Information on changes of the composition of oxygen layers are mainly obtained from the $I-U$ curves. The impedance measurements allow the presence of platinum atoms to be detected on the surface of Pt–Cr alloys with chromium contents of 30 atomic % (and larger) by their influence on the capacitive component in the potential range where hydrogen atoms are adsorbed.

Pure chromium is active[2,3] in sulfuric acid solutions at potentials negative to that of the hydrogen electrode in the same solution. The passive region where chromium dissolves as $Cr^{3+}$ at a small rate of $10^{-7}$ A/cm$^2$ extends to about +1.05 V. At more anodic potentials than 1.05 V, chromium goes into solution as chromate[2,3]. The measurements on Pt–Cr alloys were made in the potential region +0.05 to +1.5 V for chromium contents up to 52 atomic % and from +0.05 to +1.3 V for the 75 atomic % Cr alloy. Thus the rate of dissolution as $Cr^{3+}$ could be kept negligible with respect to the other reactions which occur in the potential range studied. Voltammetric $I-U$ curves were taken on smooth platinum at the end of the measurements on Pt–Cr alloys in the same solution to see if any influence of chromate could be detected. It is well-known that chromate is reduced[4] on platinum at potentials positive to the hydrogen electrode. Inhibiting layers are formed[4] in different potential regions. A noticeable effect of the nature described was not found. This means that the bulk concentration of chromate remained negligibly small under the conditions chosen.

## EXPERIMENTAL

The measurements were carried out in a Pyrex-glass vessel of conventional

design. The vessel was thermostatted at 30°±0.5°. The solution was prepared from doubly-distilled water and A.R.-grade sulfuric acid. Voltammetric $I-U$ curves on a smooth platinum-wire electrode at 3 and 30 mV/sec did not show at 30° the additional peaks that are characteristic[5] for impurities. The solution was saturated with purified helium before the measurements; during the measurements it was quiescent. The solution was replaced by a fresh one at the end of the runs on each of the alloys. The electrode potential is referred to a hydrogen electrode in $N$ $H_2SO_4$. The current densities were computed on the basis of the geometric surface area.

The assembly described recently[6] was used (with one modification) for taking the $I-U$ curves and the capacitive or ohmic components of the interfacial impedance in an equivalent series circuit of capacitor, $C_s$, and resistor, $R_s$. The zero-stability of the resolved component indicator had to be improved for the measurements at a slow sweep rate of 3 mV/sec. This was achieved by placing a General Radio type 578 shielded transformer between each of the outputs of the two Tektronix amplifiers and the inputs of the resolved component indicator (Fig. 1, in ref. 6) and by changing the resistors of the indicator (Fig. 2 in ref. 6) to $R_1=R_3=3$ kΩ, $R_2=2.75$ kΩ, $R_4=500$-Ω taper, $R_5=100$-kΩ potentiometer. By putting a 10 μF capacitor across the output, the Hewlett Packard 412A d.c. vacuum tube voltmeter between the output of the

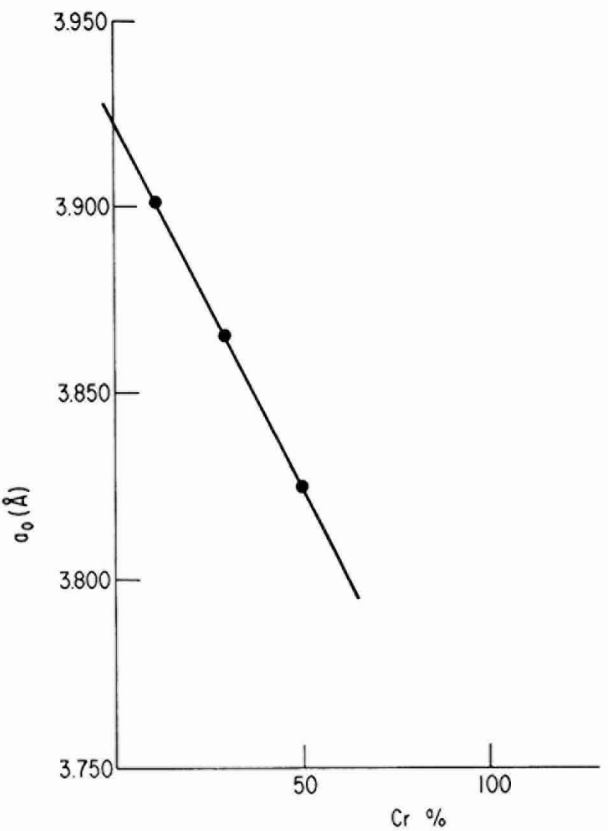


Fig. 1. Lattice parameter as a function of composition in atomic %.

indicator and the recorder (Fig. 1 in ref. 6) could be eliminated. The Varian F80 X-Y recorder allowed a good resolution of the $I-U$ curves, $1/\omega C_s-U$ curves, and $R_s-U$ curves.

## PREPARATION AND COMPOSITION OF ELECTRODES

The Pt–Cr alloys (10, 30, 52, 75 atomic % Cr or 3, 10, 20, 44.49 weight % Cr) were supplied by Englehard Co. They had irregular shapes with the exception of the 10 atomic % alloy which was in the form of a foil. The alloys were annealed at 1400° in argon for 1 h. A mirror-like surface was produced by polishing mechanically. X-ray diffraction patterns were taken from the ground surface of the specimen. The Debye–Scherrer patterns yielded lines characteristic of Pt–Cr solid solution with weak superlattice reflections for the 10, 30, and 52 atomic % Cr alloys. A face-centered cubic-type pattern was obtained. The crystallite size could not be determined exactly, but from visual observation of the lines it is greater than 3000 Å. The plot of the lattice parameter $a_o$ *vs.* the composition in atomic per-cent in Fig. 1, is linear for the first three alloys, as expected for solid solutions. The intersection of the straight line with the ordinate yields the lattice parameter of platinum. Thus the parameters of the alloys fall on a line not far from the straight line predicted by VEGARD's law[7]. The diffractometer trace of the 75 atomic % Cr alloy contained lines characteristic of $PtCr_3$, along with a very weak trace of $PtCr_2$.

The simplest and most effective method for studying electrochemical reactions on the ground surface alone, was to cover the other surfaces and the platinum leads (which were spot-welded to the back of the brittle alloys) with red stopoff lacquer. It was found, by tests with platinum electrodes which were partially covered with red lacquer, that the resulting contamination of the solution was negligible if the lacquer had dried for at least 1 h in air before the electrode was used in $N$ $H_2SO_4$ at 30°. If the time of drying is too short, some acetone does not evaporate from the lacquer and dissolves in the electrolyte. Anodic waves, which are probably caused by the oxidation of acetone, were observed on platinum in voltammetric $I-U$ curves at 30 mV/sec, in this case.

## RESULTS

It was observed that the shape of the $I-U$ curves became better developed during the initial cycles, at 30 mV/sec, on the alloys. After about 20 cycles the shape remained the same. A similar behavior which, however, involves fewer cycles, was found on pure platinum[5,8]. The nature of the change during the initial cycles cannot yet be elucidated; it may result from the gradual removal of impurities from the surface of the alloys. It may require about 20 cycles before the composition of the chromium oxide which was formed during the exposure to air is changed into that of the passive layer in $N$ $H_2SO_4$. After 20 cycles the current density at a given potential increased slowly with the number of cycles, probably because of a slow increase of the surface roughness. The main measurements at 3 mV/sec were taken after each alloy had been cycled about 30 times at 30 mV/sec.

Figure 2 represents $I-U$ curves at 3 mV/sec for the four alloys. A curve on pure platinum is not shown since it looks very like the curve (a) of the 10 atomic % Cr

alloy. The similarity between the $I-U$ curve on platinum and that on the alloys disappears for alloys of larger chromium content.

The $1/\omega C_s-U$ curves at 1 kc/sec for the alloys are plotted in Fig. 3. Since the impedance is largely capacitive between 100 c/s and 10 kc/sec, the capacitive component will be mainly discussed. The amplitude of the a.c. signal was smaller than 3 $mV_{eff}$. The sweep rate was 3 mV/sec. Arrows indicate the direction of the sweep.

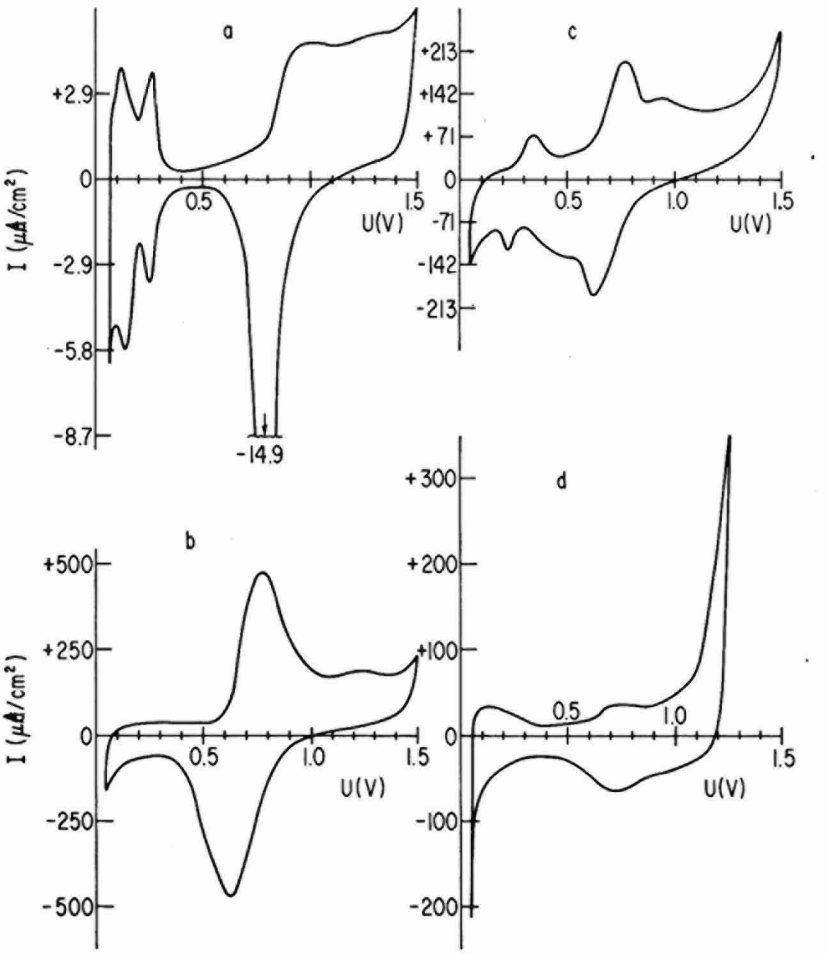


Fig. 2. Potentiostatic current–potential curves on platinum–chromium alloys in $N$ $H_2SO_4$ at 3 mV/sec: (a), 10 atomic %; (c), 52 atomic %; (b), 30 atomic %; (d), 75 atomic %.

The $R_s-U$ curves and the $1/\omega C_s-U$ curves on platinum and on the 75 atomic % Cr alloy are compared at 10 kc/sec in Fig. 4. A compensation for the ohmic voltage drop that is located in the electrolyte between the test electrode and the reference electrode was not applied. The determination of the $IR_{El}$-drop, the correctness of which was checked previously[9], is demonstrated for platinum in Fig. 4(a). The sweep rate was 3 mV/sec. The sweep direction is given by arrows.

DISCUSSION

The $I-U$ curve in Fig. 2(a) of the 10 atomic % Cr alloy has a similar shape to the curve on platinum. There are three characteristic regions: region of hydrogen adsorption, double-layer region, region of the oxygen layer. Two large peaks exist in the hydrogen region corresponding to weakly- and strongly-bonded hydrogen atoms.

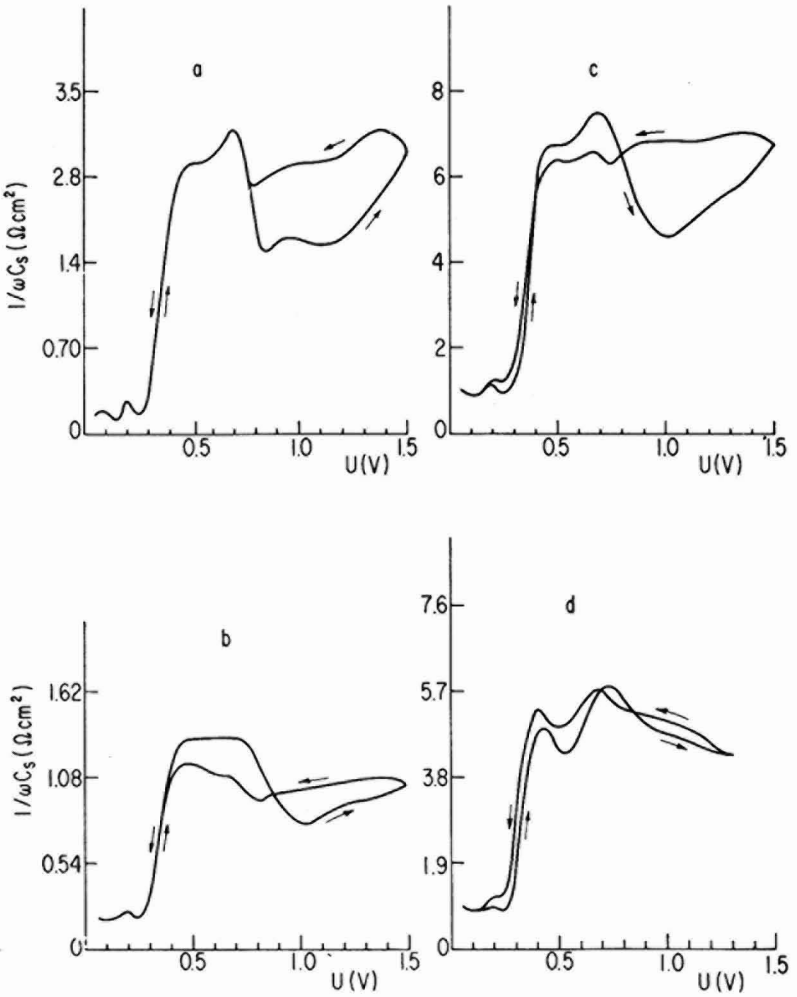


Fig. 3. Capacitive components of the alloys as a function of potential. Sweep rate: 3 mV/sec; frequency: 1 kc/sec: (a), 10 atomic %; (c), 52 atomic %; (b), 30 atomic %; (d), 75 atomic %.

The peak of the weakly-bonded hydrogen is larger during the cathodic than during the anodic sweep. This effect[10], which becomes more pronounced at smaller sweep rates, is attributed to a larger extent of the competitive $H_2$-evolution during the cathodic than during the anodic sweep. Stirring with an inert gas increases the effect

as may be expected for a diffusion-controlled process of $H_2$-evolution. It may be concluded from the evidence in Fig. 2 that hydrogen adsorption on the platinum atoms is not influenced much by the presence of chromium up to at least 10 atomic %. The chromium is in the passive state; otherwise the observed currents should be larger because of chromium dissolution.

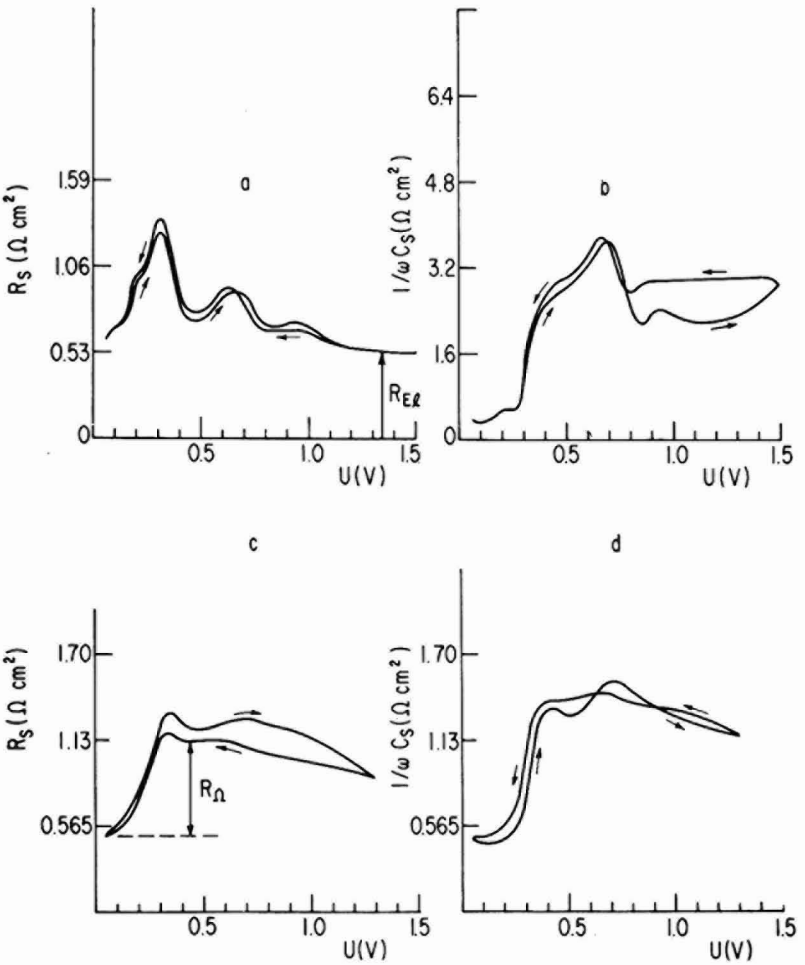


Fig. 4. Capacitive components (b and d) and ohmic components (a and c) as a function of potential. Sweep rate: 3 mV/sec; frequency: 10 kc/sec: (a and b), Pt; (c and d), 75 atomic %.

The amount of electricity which is used for the formation of the oxygen layer of the 10 atomic % Cr alloy between 0.6 and 1.5 V is noticeably larger than the amount during its reduction between 1.1 and 0.5 V. Further experimental evidence is required for a satisfactory interpretation of this effect which was also observed on platinum at comparable rates[11] when taking anodic and cathodic charging curves at small current densities.

On the other three alloys, the current densities in the so-called hydrogen region are too large to be able to attribute them to the formation or removal of a layer of adsorbed hydrogen atoms. Other reactions occur with a large rate and obscure the partial currents due to the Volmer reaction. It is not possible on the basis of the $I-U$ curves (b), (c), and (d) in Fig. 2 to detect the presence of platinum atoms by their electrochemical behavior in the hydrogen region. The waves in these $I-U$ curves are attributed to changes in the composition of the passive layer on the chromium. It is suggested that the oxidation of chromium to CrOOH occurs during the anodic sweep between 0.05 and 0.50 V. Then CrOOH is oxidized further between 0.5 and 1.2 V. Chromate goes into solution above 1.1 V in the case of curves (c) and (d). During the cathodic sweep, the higher oxide is reduced to CrOOH between 1.2 and 0.5 V and CrOOH is reduced to chromium between 0.5 and 0.05 V. The reaction between 0.5 and 1.2 V is less irreversible on the 75 atomic % Cr alloy. This may be due to the transition from a solid solution of chromium in platinum to the compound $PtCr_3$. The interpretations on the passive layer are tentative. Similar phenomena were observed[12] during the voltammetric oxidation of nickel single crystals.

The remarkable feature of the $1/\omega C_s-U$ curves in Fig. 3 is their similarity in the potential range 0.05–0.4 V. It is concluded that the similarity results from the occurrence of the Volmer reaction on platinum atoms of the surface. The Volmer reaction is considerably less hindered than the formation and reduction of CrOOH, thus it determines the impedance. The correctness of this conclusion is evident for the 10 atomic % Cr alloy from a comparison of the $I-U$ curve with the $1/\omega C_s-U$ curve in the hydrogen region. The two minima[13] of the $1/\omega C_s-U$ curves in Fig. 3 demonstrate the presence of strongly- and weakly-bonded hydrogen atoms for the alloys studied. A larger resolution than the one used during the impedance measurements of Fig. 3 led to more pronounced minima and verified the shape of the $1/\omega C_s-U$ curves in the hydrogen region.

The double-layer region and the oxygen region are well distinguished[6] in the $1/\omega C_s-U$ curves at 1 kc/sec on platinum. This distinction becomes less pronounced with increasing chromium content in Fig. 3. The hysteresis between the anodic and cathodic sweep of the $1/\omega C_s-U$ curves above 0.3 V is correlated to the irreversibility of the reactions discussed which change the composition of the passive layer. This is shown by a comparison of the $1/\omega C_s-U$ curves in Fig. 3 with the respective $I-U$ curves in Fig. 2. The fine structure of the $1/\omega C_s-U$ curves reflects the appearance of waves in the $I-U$ curves. The values of $I$ in Fig. 2 and of $1/\omega C_s$ in Fig. 3 at a given potential, indicate that the 30 atomic % Cr alloy has a larger roughness factor than the 52 and 75 atomic % Cr alloys. Therefore, a comparison of the capacities, say at 0.5 V, will not lead to a method of determining the chromium content of the alloys.

Figure 4 represents the results of the measurements on platinum and on the 75 atomic % Cr alloy at 10 kc/sec. The preceding discussion of the $1/\omega C_s-U$ curve at 1 kc/sec can be applied to the curves in Fig. 4. The fine structure of the $R_s-U$ curve on platinum changes strongly when chromium is present. $R_s$ in curve (c) has values which do not vary much with potential between 0.4 and 1.0 V. This suggests the presence of an ohmic resistance $R_\Omega$ in the passive layer. An average value of 0.5 $\Omega$-cm$^2$ can be estimated for this resistance as indicated in Fig. 4(c). The value of $R_\Omega$ increases with the chromium content.

ACKNOWLEDGEMENTS

The author gratefully acknowledges the X-ray diffraction analysis by the Metallographic Laboratory, GE Research Laboratory, and the supply of the alloys by General Electric's DECO, Lynn, Mass.

SUMMARY

Hydrogen adsorption and the formation and reduction of oxygen layers were investigated on four Pt–Cr alloys in $N$ $H_2SO_4$ at 30° in the potential region between hydrogen and oxygen evolution. Periodic voltammetric current–potential curves measured at 3 mV/sec give evidence of two different oxidation states of the passive layer on the part of the surface with the electrochemical behavior of chromium. The presence of platinum atoms on the surface may be detected by their influence on the ohmic and capacitive component of the interfacial impedance between 100 c/s and 10 kc/s for the alloys with chromium contents above 11 atomic %.

REFERENCES

1 R. PARSONS, Lecture at the International Conference on Physics and Chemistry of Solid Surfaces, Brown University, 1964; *Surface Sci.*, 2 (1964) 418.
2 Y. M. KOLOTYRKIN, *Z. Elektrochem.*, 62 (1958) 664.
3 TH. HEUMANN AND H. S. PANESAR, *J. Electrochem. Soc.*, 110 (1963) 628.
4 D. REINKOWSKI AND C. A. KNORR, *Z. Electrochem.*, 58 (1954) 709.
5 M. W. BREITER, *J. Electroanal. Chem.*, 8 (1964) 230.
6 M. W. BREITER, *J. Electroanal. Chem.*, 7 (1964) 38.
7 L. VEGARD, *Z. Physik.*, 5 (1921) 17; *Z. Krist.*, 67 (1928) 239.
8 W. G. FRENCH AND T. KUWANA, *J. Phys. Chem.*, 68 (1964) 1279.
9 M. W. BREITER, *J. Phys. Chem.*, 68 (1964) 2254.
10 F. G. WILL AND C. A. KNORR, *Z. Elektrochem.*, 64 (1960) 258.
11 K. J. VETTER AND D. BERNDT, *Z. Elektrochem.*, 62 (1958) 378.
12 J. L. WEININGER AND M. W. BREITER, *J. Electrochem. Soc.*, 110 (1963) 484.
13 M. W. BREITER, *J. Phys. Chem.*, 68 (1964) 2249.

REVIEW

# THE STRUCTURE OF THE SEMICONDUCTOR–ELECTROLYTE INTERFACE

P. J. BODDY
*Bell Telephone Laboratories, Incorporated, Murray Hill, New Jersey (U.S.A.)*
(Received April 22nd, 1965)

## INDEX

SYMBOLS

| | |
|---|---|
| $a_i$ | Relative activity of species $i$. |
| Å | Ångstrom unit. |
| $b$ | Mobility ratio $\left(=\frac{\mu_p}{\mu_n}\right)$. |
| $C_{\text{Gouy}}$ | Gouy-layer capacitance. |
| $C_{\text{Helmholtz}}$ | Helmholtz-layer capacitance. |
| $C_{\text{Meas.}}$ | Measured value of capacitance. |
| $C_{\text{s.c.}}$ | Semiconductor space-charge capacitance. |
| $C_{\text{s.s.}}$ | Surface state capacitance. |
| $d$ | Distance of closest approach between a semiconductor surface and free charges in another phase. |
| $D_p$ | Diffusion constant for holes in eqn. (68). |
| $e$ | Elementary charge. |
| $E_c$ | Energy of edge of conduction band. |
| $E_F$ | Energy of Fermi level. |
| $E_{i,b}$ | Energy of intrinsic level in the bulk. |
| $E_{i,s}$ | Energy of intrinsic level at the surface. |
| $E_t$ | Energy of discrete surface state. |
| $E_v$ | Energy of edge of valence band. |
| $E_{\text{vacuum}}$ | Energy of an electron in vacuum just outside a surface. |
| $f$ | Occupancy factor for an energy level according to Fermi–Dirac statistics. |
| $g$ | Total degeneracy of a surface state in eqn. (22). |
| $g_{\text{ion}}$, $g_{\text{dipole}}$ | Contributions to the inner p.d. between two phases due to effects of space-charge formation and oriented dipoles, respectively. |
| $\Delta G$ | Change in surface conductance. |
| $\mathscr{H}$ | P.d. across $d$ due to charge separation. |
| $i$ | Current density. |
| $i_s$ | Saturation current density. |
| $k$ | Boltzmann's constant. |
| $L$ | Light intensity. |
| $\mathscr{L}$ | Debye length $\left(=\left(\frac{\varepsilon kT}{8\pi n_i e^2}\right)^{\frac{1}{2}}\right)$. |
| $n$ | Electron concentration; or as subscript, of electrons. |
| $n_o$ | Bulk electron concentration. |
| $n_i$ | Intrinsic electron concentration $(=p_i)$. |
| $p$ | Hole concentration; or as subscript, of holes. |
| $p_o$ | Bulk hole concentration. |
| $q$ | Charge density. |
| $s$ | Surface recombination velocity. |
| $T$ | Temperature. |
| $u_b$ | $e\varphi_b^*/kT$. |
| $u_s$ | $e\varphi_s^*/kT$. |
| $U$ | Electrode potential. |
| $Y$ | $e(\varphi_s-\varphi_b)/kT$, $e\psi_s/kT$. |
| $\Gamma$ | Surface excess. |

| | |
|---|---|
| $\delta$ | Change in some quantity. |
| ${}^{\alpha}\Delta^{\beta}$ | Value of a quantity in phase $\beta$ minus the value in phase $\alpha$. |
| $\varepsilon$ | Relative dielectric constant. |
| $\eta$ | Overvoltage. |
| $\lambda$ | $p_o/n_i$ or $n_i/n_o$. |
| $\mu_p$ ($\mu_n$) | Mobility of holes (electrons). |
| $\mu_i^{\alpha}$ | Chemical potential of species $i$ in phase $\alpha$. |
| $\bar{\mu}_i^{\alpha}$ | Electrochemical potential of species $i$ in phase $\alpha$. |
| $\mu_i^{o,\alpha}$, $\bar{\mu}_i^{o,\alpha}$ | Standard values of $\mu_i^{\alpha}$ and $\bar{\mu}_i^{\alpha}$. |
| $\tau$ | Minority carrier lifetime in eqn. (68). |
| $\varphi^{\alpha}$ | Inner potential of phase $\alpha$ (electrochemical system). |
| $\varphi_b$ | Inner potential in the bulk of a semiconductor. |
| $\varphi_m$ | Inner potential just inside the surface of a metal. |
| $\varphi_s$ | Inner potential just inside the surface of a semiconductor. |
| $\varphi_1$ | Inner potential at the inner Helmholtz plane. |
| $\varphi_2$ | Inner potential at the outer Helmholtz plane. |
| $\varphi^s$ | Inner potential in the bulk of a solution. |
| $\varphi_b^*$ | $-(kT/e) \ln \lambda$ |
| $\varphi_s^*$ | $\psi_s-(kT/e) \ln \lambda$ } Physical system. |
| $\chi^{\alpha}$ | Surface potential of phase $\alpha$. |
| $\psi^{\alpha}$ | Outer potential of phase $\alpha$. |
| $\psi_o$ | Electrostatic potential in the bulk of a semiconductor. } Physical system |
| $\psi_s$ | Electrostatic potential just inside the surface of a semiconductor. } Physical system |

## INTRODUCTION

Recent work on the properties of semiconductor electrodes has led to a considerable amount of new information regarding the properties of the double-layer region which will be summarized in this review. The content has been deliberately limited to structural properties and a number of otherwise excellent papers dealing with semiconductor–electrolyte interfaces have not been considered since they do not relate to this particular aspect of the problem. On the other hand some relevant, but previously unpublished, data are included.

Semiconductors cover a wide range of non-metallic crystals ranging from the purely covalent, as in the lighter Group IV-A elements, to compounds of quite high ionicity exemplified by the oxides of Group II metals, and hence one anticipates that behavior not found with metallic electrodes will be observed and should contribute particularly to the understanding of the electrochemistry of non-metallic materials. Although a variety of semiconductor electrodes has been investigated it appears at present that germanium constitutes the closest approach to an ideal experimental system in the same sense that mercury does in the case of metal electrodes.

In the past, information on the double-layer structure and electrochemical behavior of non-metallic materials has usually been deduced from observations of electrokinetic phenomena and their variation with environment. At the present time, measurements of the distribution of charge and potential across the semiconductor–electrolyte interface are providing more detailed information for specific crystallographic faces of single crystal electrodes.

## I. GENERAL CONSIDERATIONS

In this section we will introduce the necessary nomenclature and discuss a few important questions of principle. The theory of semiconductor electrodes has been discussed a number of times recently[1-6] and it would serve no useful purpose to add a further general discussion of the same material. For electrochemically-oriented readers unfamiliar with the semiconductor field, ref. 1 is recommended as the easiest to follow since it contains a minimum of symbolism while ref. 3 is recommended as being both comprehensive and relatively up-to-date. Experimental aspects have also been reviewed[7,8]. In the following, a knowledge of the elementary properties of semiconductors is assumed. However, since the distribution of potential is of particular importance to the material covered in this review, it will be treated in some detail. The important topic of electrode kinetics will not be touched upon except in passing; the present state of knowledge in this subject has been fully covered recently[3,7].

There are differences in the notation used in electrochemistry and physics to describe semiconductor surfaces and both are encountered in the literature of semiconductor electrochemistry. Since this review is addressed to electrochemists, their notation will generally be used. However, the two systems will be compared since it is difficult to follow the literature without also being familiar with the physical notation.

### (i) *Isolated semiconductor surface*

Figure 1 represents the surface of an *n*-type semiconductor to which a field is applied by means of a negatively-charged metal electrode close to the surface on which is induced an equal positive charge. Because of the typically low densities of electrons and holes and the moderate values of dielectric constant, semiconductors can support space-charge regions of considerable extent near their surfaces. The deep penetration of this space-charge (*e.g.*, several thousand Å in intrinsic germanium) permits quite a large, and variable, potential difference (p.d.) within the semicon-

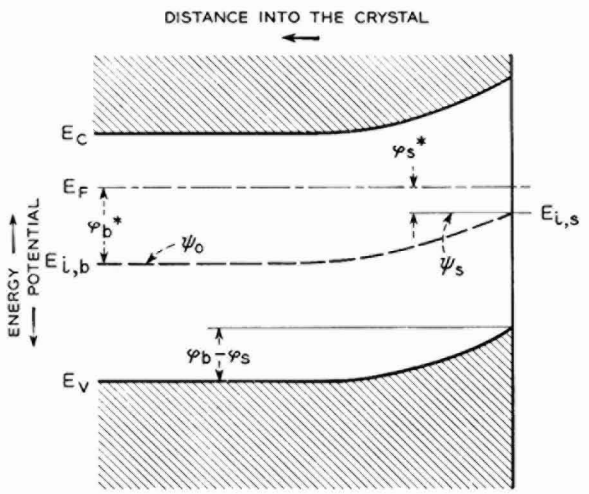


Fig. 1. Energy band diagram for a semiconductor surface; surface states are assumed to be absent.

ductor. This p.d. is commonly represented by a bending of the energy bands and written in electrochemical notation as the inner p.d. between points in the neutral bulk and just inside the surface, $\varphi_b - \varphi_s$, where the inner potential of a phase $\alpha$ is defined in electrochemistry as the sum of the outer potential ($\psi^\alpha$) due to free charge on the phase, and the surface potential ($\chi^\alpha$) due to dipoles at the surface of the phase[9].

$$\varphi^\alpha = \psi^\alpha + \chi^\alpha \tag{1}$$

For further discussion of this equation, refs. 6 and 9 may be consulted. $\varphi$ cannot be determined except by calculation since it contains $\chi$ which is not experimentally measurable. The difference $\varphi_b - \varphi_s$ within a homogeneous phase, however, may be measured in several ways which will be discussed in a later section. Since $\varphi$ contains the unknown quantity $\chi$, neither $\varphi_b$ nor $\varphi_s$ can be individually located on Fig. 1. As drawn, the bands are said to be "bent up", which corresponds to a positive space-charge, and $\varphi_b - \varphi_s$ is a positive quantity.

There are several physical methods of describing this same situation. The simplest considers the difference in electrostatic potential between points in the bulk and just inside the surface (symbolized by $\psi_o$ and $\psi_s$). In this case, $\psi$ is the electrostatic potential, arbitrarily taken as zero at the intrinsic level $E_{i,b}$ in Fig. 1, and is *not* the same as $\psi$ in eqn. (1).

For the p.d. across the space-charge layer we have

$$\psi_o - \psi_s = \varphi_b - \varphi_s \tag{2}$$

But since $\psi_o$ is defined as zero

$$-\psi_s = \varphi_b - \varphi_s \tag{3}$$

*i.e.*, $\psi_s$, the symbol often used in physics to denote the p.d. across the space-charge layer, is negative for a positive space-charge. The symbol $Y$ is used to denote the same p.d. in units of $kT/e$

$$Y = \frac{e\psi_s}{kT} \tag{4}$$

The symbols $\varphi_b$ and $\varphi_s$ are frequently encountered in the physical literature but are defined differently from the identical electrochemical symbols and hence can become a source of confusion. In this case, the zero of electrostatic potential is taken as $E_{i,b}$, the Fermi level in the bulk of the intrinsic semiconductor. This is very close to being the middle of the energy gap, differing from it by a generally small amount depending on the relative effective masses of holes and electrons. The symbol $E_i$ is preferred to $E_F{}^{in}$, which is sometimes used, to emphasize that this energy level differs from a real Fermi level in that it does not remain horizontal across a diagram like Fig. 1 for a semiconductor in equilibrium, but follows the bending of the bands, remaining at the same (approximately mid-gap) position throughout. Since in the case of internal p.d.'s within the semiconductor, $E_i$ is a function of position, it will be labelled $E_{i,b}$ and $E_{i,s}$ for bulk and surface values.

In order to distinguish them we will mark the physical symbols with an asterisk, thus: $\varphi_b{}^*$ and $\varphi_s{}^*$. This is simply for convenience and is not an accepted convention. The definitions of these quantities are

$$e\varphi_b{}^* = E_F - E_{i,b} \tag{5}$$

$$e\varphi_s{}^* = E_F - E_{i,s} \tag{6}$$

From eqn. (5) it can be seen that $\varphi_b{}^*$ is a measure of the position of the bulk

Fermi level and is zero for an intrinsic semiconductor while $\varphi_s^*$ is the sum of the position of the bulk Fermi level and the bending of the bands. The difference between the $\psi$- and $\varphi^*$-symbolism should be noted. The latter is generally more useful, since it often eliminates from consideration the effect on equilibrium properties of differences in bulk Fermi level in variously doped electrodes.

It should be clear that

$$\varphi_b^* - \varphi_s^* = -\psi_s \tag{7}$$

$$= \varphi_b - \varphi_s \tag{8}$$

and also, by definition, we have

$$u_b = \frac{e\varphi_b^*}{kT} \tag{9}$$

$$u_s = \frac{e\varphi_s^*}{kT} \tag{10}$$

and hence from eqns. (4) and (7)

$$u_b - u_s = -Y \tag{11}$$

The quantities $\psi_s$, $\varphi_s$, $Y$ and $u_s$ have each been called the "surface potential" at one time or another in the literature and are not to be confused with $\chi$ in eqn. (1). In fact, $\chi$ is used in semiconductor surface physics for the "electron affinity" ($\chi = E_{\text{vacuum}} - E_c$). It is, therefore, obvious that considerable caution should be exercised in deciding exactly what a particular author intends by his symbols.

$\varphi_b^*$ is related to the bulk electron concentration by

$$\varphi_b^* = \frac{kT}{e} \ln\left(\frac{n_o}{n_i}\right) \tag{12}$$

but since at equilibrium

$$p_o n_o = n_i^2 \tag{13}$$

then

$$\varphi_b^* = -\frac{kT}{e} \ln\left(\frac{p_o}{n_i}\right) \tag{14}$$

$(p_o/n_i)$ is given the symbol $\lambda$ and is often a useful quantity in calculating properties of the space-charge layer. It may be determined from the specific conductivity and type of the sample. The relationship for germanium at 15° and 25° is shown in Fig. 2.

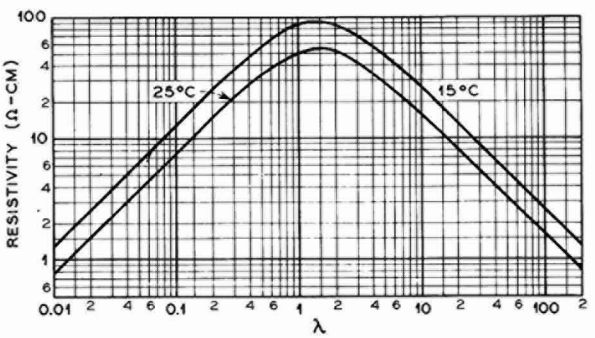


Fig. 2. $\lambda$ *vs.* resistivity for Ge at 15° and 25°.

Since

$$\varphi_b^* = -\frac{kT}{e}\ln\lambda \tag{15}$$

then from eqn. (7)

$$\varphi_s^* = \psi_s - \frac{kT}{e}\ln\lambda \tag{16}$$

and correspondingly from eqns. (4) and (10)

$$u_s = Y - \ln\lambda \tag{17}$$

In Fig. 1, the charges in the semiconductor space-charge region and on the metal plate are equal and opposite. In the non-degenerate case the charge in the space-charge layer is related to $\varphi_b - \varphi_s$ by

$$q_{sc} = \pm en_i\mathscr{L}\{\lambda[\exp(e(\varphi_b-\varphi_s)/kT)-1]+\lambda^{-1}[\exp(-e(\varphi_b-\varphi_s)/kT)-1] + (\lambda-\lambda^{-1})[-e(\varphi_b-\varphi_s)/kT]\}^{\frac{1}{2}} \tag{18}$$

taking the appropriate sign of the root.

The p.d. ($\mathscr{H}$) across the vacuum gap ($d$) separating the two electrodes is given by

$$\mathscr{H} = \frac{4\pi q_{sc} ed}{\varepsilon} \tag{19}$$

where

$$q_{sc} = -q_m \tag{20}$$

When eqns. (18) and (19) are solved for $\varphi_b - \varphi_s$ and $\mathscr{H}$, it is found for the case of intrinsic germanium that if $d \lesssim 10^{-7}$ cm, then

$$(\varphi_b - \varphi_s) \gg \mathscr{H} \tag{21}$$

This indicates that practically all of the p.d. due to *free* charge on the semiconductor appears across its own space-charge region provided $\varphi_b - \varphi_s$ is not large enough to cause degeneracy at the surface. Specific examples are calculated by DEWALD[1] and by GREEN[10].

*(ii) Effect of surface states*

Considerable complications are introduced by the presence of surface states. These may be defined as energy levels for holes or electrons, different from those present in the bulk and localized at the surface of the crystal. The fractional occupation, $f$, of the levels is determined by their energy relative to the Fermi level at the surface, according to the Fermi–Dirac distribution law. Assuming a single donor energy level, $E_t$,

$$f = (1+g^{-1}\exp\{(E_t-E_F)/kT\})^{-1} \tag{22}$$

where $g$ is the degeneracy of the state through spin and other causes[11]. When the energy of a state is more than a few $kT$ from the Fermi level, it is for all practical purposes completely occupied or completely unoccupied as the case may be and is ineffective in-so-far as *changes* in the potential distribution are concerned. When the Fermi level moves close to or crosses the energy of the state because of a change in $\varphi_b - \varphi_s$, charge of the appropriate sign is either trapped or released. The result is a relatively rapid change in the surface charge for a small change in $\varphi_b - \varphi_s$. The importance of surface states in this instance is that when they carry a net charge this can cause a consider-

able p.d. due to charge separation across the Helmholtz region (more specifically defined in I (iii)).

Since the total charge on the semiconductor is equal and opposite to the charge on the metal plate,

$$q_{sc}+q_{ss}=-q_m \tag{23}$$

It is evident that the p.d. across the vacuum gap is now given by

$$\mathscr{H} = \frac{4\pi(q_{sc}+q_{ss})ed}{\varepsilon} \tag{24}$$

and that depending on $q_{ss}/q_{sc}$, the other terms being constant, $\mathscr{H}$ may be relatively quite large with respect to $\varphi_b-\varphi_s$. In particular when

$$q_{sc}=0 \tag{25}$$

*i.e.*, no free charge on the electrode, and

$$q_{ss}\neq 0 \tag{26}$$

*i.e.*, some considerable charge in surface states, then $\varphi_b-\varphi_b$ is equal to zero and all the p.d. due to charge separation across the interface occurs in the vacuum gap.

When there is a change in the magnitude of this charge two cases may be considered.

(*a*) $E_t$ *distant from* $E_F$. As discussed above, due to charged surface states, $\mathscr{H}$ may be large compared with $\varphi_b-\varphi_s$ but since a change in $\varphi_b-\varphi_s$ does not cause a perceptible change in occupancy of the states

$$\delta q_{sc} = -\delta q_m \tag{27}$$

and

$$\delta(\varphi_b-\varphi_s) \gg \delta\mathscr{H} \tag{28}$$

*i.e.*, the *change* in p.d. is almost entirely due to $\delta(\varphi_b-\varphi_s)$, as is true also in the absence of surface states.

(*b*) $E_t$ *close to* $E_F$. Once again $\mathscr{H}$ may or may not be large compared with $\varphi_b-\varphi_s$ but now

$$\delta q_{sc}+\delta q_{ss} = -\delta q_m \tag{29}$$

and if

$$|\delta q_{ss}| \gg \delta q_{sc} \tag{30}$$

then it is also possible that $\delta\mathscr{H}$ is greater than or comparable with $\delta(\varphi_b-\varphi_s)$.

(*iii*) *Model of the interface*

The preliminary model will be based largely on our present knowledge of the structure of the interface at metal electrodes. In Fig. 3, the vertical lines represent the surface, *i.e.*, the outer layer of germanium atoms, the inner Helmholtz plane (ihp) and the outer Helmholtz plane (ohp). The ohp is assumed to be analogous to that at metal electrodes and represents simply the distance of closest approach of the nuclei of free ions. Since this plane is only a few Å from the surface, the potential distribution in a system in which all excess charge in the solution resides at the ohp will resemble that described above for the case of a metal electrode separated from the surface by a small vacuum gap. In the absence of changes in dipole layers, or considerable charging of surface states, polarization of the system will appear almost entirely across the semiconductor space-charge layer (assuming the ionic strength is sufficiently great

that the space-charge layer in the solution may be neglected), *i.e.*,

$$\delta(\varphi_b - \varphi_s) \gg \delta(\varphi_s - \varphi^s) \tag{31}$$

If sizable densities ($N_t > \sim 10^{12}$ cm$^{-2}$) of surface states are present near the Fermi level, eqn. (31) may no longer hold.

The ihp also has a similar significance to that at metal electrodes and represents the plane containing nuclei of ions which are "specifically adsorbed" or in some other

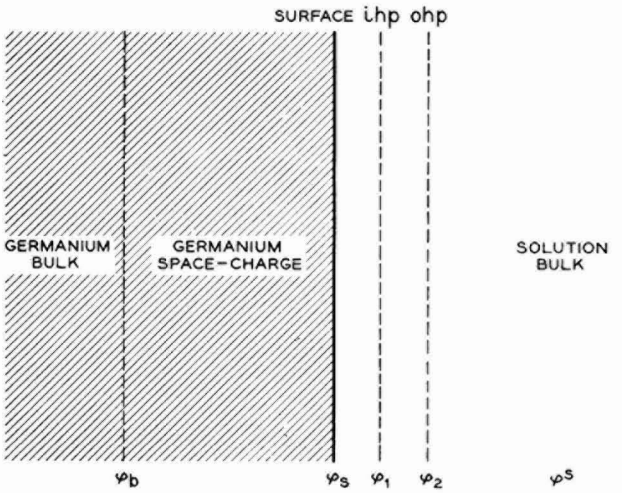


Fig. 3. Model of semiconductor–electrolyte interface.

way strongly bound so as to be closer to the surface than the ions at the ohp. Justification for the inclusion of this plane except by analogy with metal electrodes, will be deferred until consideration of the experimental data.

The usual difficulty of distinguishing between the averaged macro-potential, $\varphi$, of a plane of ions and the periodic micro-potential actually experienced by charged particles, applies here just as at metal electrodes. However, in subsequent discussion it will be assumed, as usual, that the concept of macro-potential is a sufficiently good approximation. HARTEN[4] discusses this problem very clearly.

*(iv) Reversible processes at semiconductor electrodes*

Consider a semiconductor electrode at which a reversible process is occurring denoted by

$$X^{n+} + e \rightleftarrows X^{(n-1)+} \tag{32}$$

The electrode potential is the sum of the inner p.d.'s across all the interfaces in the circuit,

metal | semiconductor | solution | reference electrode | metal

$$U = \Sigma \Delta\varphi \tag{33}$$

Considering now the effect of changing the Fermi level in the bulk of the semiconductor, it is obvious that only the interfaces (metal/s.c.) and (s.c./solution) are affected.

At (metal/s.c.), equilibrium exists between the bulk phases, *i.e.*,

$$\bar{\mu}_e{}^m = \bar{\mu}_e{}^{\text{s.c.}} \tag{34}$$

and since

$$\bar{\mu}_i = \mu_i{}^o + kT \ln a_i + z_i e\varphi \tag{35}$$

and

$$\mu_i = \mu_i{}^o + kT \ln a_i \tag{36}$$

then

$$\mu_e{}^{o,\text{s.c.}} + kT \ln a_e{}^{\text{s.c.}} - e\varphi_{\text{s.c.}} = \mu_e{}^m - e\varphi_m \tag{37}$$

whence, writing $\varphi_m - \varphi_{\text{s.c.}}$ as ${}^{\text{s.c.}}\Delta^m\varphi$,

$${}^{\text{s.c.}}\Delta^m\varphi = \text{const.} + \frac{\mu_e{}^m}{e} - \frac{kT}{e} \ln a_e{}^{\text{s.c.}} \tag{38}$$

At (s.c./solution), considering again the equilibrium between the bulk phases,

$$\bar{\mu}_{X^{n+}} + \bar{\mu}_e{}^{\text{s.c.}} = \bar{\mu}_{X^{(n-1)+}} \tag{39}$$

and therefore

$$\mu^o_{X^{n+}} + kT \ln a_{X^{n+}} + \mu_e{}^{o,\text{s.c.}} + kT \ln a_e{}^{\text{s.c.}} - e\varphi_{\text{s.c.}} = \mu^o_{X^{(n-1)+}} + kT \ln a_{X^{(n-1)+}} - e\varphi_{\text{soln.}} \tag{40}$$

Hence

$${}^{\text{soln.}}\Delta^{\text{s.c.}}\varphi = \text{const.} + \frac{kT}{e} \ln \frac{a_{X^{n+}} \cdot a_e{}^{\text{s.c.}}}{a_{X^{(n-1)+}}} \tag{41}$$

and considering the case where $a_{X^{(n+)}}$ and $a_{X^{(n-1)+}}$ remain constant

$${}^{\text{soln.}}\Delta^{\text{s.c.}}\varphi = \text{const.} + \frac{kT}{e} \ln a_e{}^{\text{s.c.}} \tag{42}$$

Then from eqns. (38) and (42)

$${}^{\text{soln.}}\Delta^m\varphi = \text{const.} + \frac{\mu_e{}^m}{e} \tag{43}$$

By considering the whole cell it can easily be shown (*e.g.* ref. 2) that $\mu_e{}^m/e$ is cancelled out by an equal term arising in the similar metal contact between the reference electrode and the voltmeter. The final conclusion is that ${}^{\text{soln.}}\Delta^m\varphi$ is independent of $a_e{}^{\text{s.c.}}$, and since the other interfaces are not affected by the semiconductor properties, then the equilibrium electrode potential is also independent of $a_e{}^{\text{s.c.}}$, *i.e.*, Fermi level. Equations (38) and (42) show that this is so because changes in $a_e{}^{\text{s.c.}}$ produce equal and opposite changes in inner p.d. at the metal–semiconductor and semiconductor–solution interfaces. It is the behavior of this latter p.d. under a variety of circumstances which will be of most interest to us in this review.

(v) *Effect of Fermi level on the inner p.d.*

Although the equilibrium electrode potential is independent of Fermi level, the inner p.d. *does* vary as indicated by eqn. (42). The relative activity of electrons in the bulk, $a_e{}^{\text{s.c.}}$, can be taken as $n_o/n_i$ in view of the small concentrations involved

(the standard state is that of the intrinsic semiconductor at 25°), and since

$$\frac{n_i}{n_o} = \lambda \tag{44}$$

then

$$\ln a_e^{\text{s.c.}} = -\ln \lambda \tag{45}$$

and from eqns. (42) and (45), for a fixed composition of the solution,

$${}^{\text{soln.}}\Delta^{\text{s.c.}}\varphi + \frac{kT}{e}\ln\lambda = \text{const.} \tag{46}$$

Dividing the inner p.d. into parts representing charge separation and dipolar layers we have

$${}^{\text{soln.}}\Delta^{\text{s.c.}}\varphi = {}^{\text{soln.}}g_{\text{ion}}^{\text{s.c.}} + {}^{\text{soln.}}g_{\text{dipole}}^{\text{s.c.}} \tag{47}$$

and obviously also

$$\delta({}^{\text{soln.}}\Delta^{\text{s.c.}}\varphi) = \delta({}^{\text{soln.}}g_{\text{ion}}^{\text{s.c.}}) + \delta({}^{\text{soln.}}g_{\text{dipole}}^{\text{s.c.}}) \tag{48}$$

Equation (47) is discussed more fully in ref. 9. A separation in this form is necessary since eqn. (1) is inappropriate for phases in contact due to the existence of image forces. It is emphasized that eqn. (47) is simply a convenient definition, not an operation that we will attempt to carry out. For our purposes, eqn. (48) is of particular importance since *changes* in inner p.d. can be measured.

Since only minute changes in chemical composition are required to shift the bulk Fermi level by significant amounts, we will assume that as a result of such a change

$$\delta({}^{\text{soln.}}g_{\text{dipole}}^{\text{s.c.}}) = 0 \tag{49}$$

so that from eqns. (48) and (49)

$$\delta({}^{\text{soln.}}\Delta^{\text{s.c.}}\varphi) = \delta({}^{\text{soln.}}g_{\text{ion}}^{\text{s.c.}}) \tag{50}$$

The inner p.d. is distributed across three regions, the space-charge layers in the semiconductor and the solution, and the region which lies between the planes of closest approach of free charge carriers in the two phases, *i.e.*,

$${}^{\text{soln.}}\Delta^{\text{s.c.}}\varphi = (\varphi_b - \varphi_s) + (\varphi_s - \varphi_2) + (\varphi_2 - \varphi^s) \tag{51}$$

In the absence of charged surface states or other bound charge either on the surface or in the ihp, we have from the inequality (21)

$$\delta^{\text{soln.}}g_{\text{ion}}^{\text{s.c.}} \approx \delta(\varphi_b - \varphi_s) \tag{52}$$

provided the ionic strength is sufficient that

$$\varphi_b - \varphi_s \gg \varphi_2 - \varphi^s \tag{53}$$

When charged surface states are present, but removed from the Fermi level, then by considering the inequality (28) it may be seen that

$$\delta({}^{\text{soln.}}g_{\text{ion}}^{\text{s.c.}}) \approx \delta(\varphi_b - \varphi_s) \tag{54}$$

again provided the ionic strength is sufficient that

$$\delta(\varphi_b - \varphi_s) \gg \delta(\varphi_2 - \varphi^s) \,. \tag{55}$$

Hence from eqns. (50) and (54)

$$\delta({}^{\text{soln.}}\Delta^{\text{s.c.}}\varphi) \approx \delta(\varphi_b - \varphi_s) \tag{56}$$

and from eqn. (46)

$$\delta({}^{\text{soln.}}\Delta^{\text{s.c.}}\varphi) = -\delta\left(\frac{kT}{e}\ln\lambda\right) . \tag{57}$$

For changes in bulk Fermi level only, we have from eqns. (56) and (57)

$$\delta\left\{(\varphi_b - \varphi_s) + \frac{kT}{e}\ln\lambda\right\} \approx 0 \tag{58}$$

which from eqns. (3) and (16) is also equivalent to

$$\delta\varphi_s^* \approx 0 \tag{59}$$

The conclusion is, that for a particular semiconductor under a given electrochemical equilibrium the value of $(\varphi_b - \varphi_s) + (kT/e)\ln\lambda$ is approximately constant and independent of the bulk Fermi level even though surface states are present (but distant from the Fermi level). It is assumed that one specific crystal face is involved throughout, otherwise the dipole term may not be constant and eqn. (49) is invalidated.

(*vi*) *Effect of polarization on the inner p.d.*

For polarization of the semiconductor–electrolyte interface

$$\delta U = \delta^{\text{soln.}}\Delta^{\text{s.c.}}\varphi \tag{60}$$

since the semiconductor–metal interface is not affected. Hence from eqn. (51)

$$\delta U = \delta(\varphi_b - \varphi_s) + \delta(\varphi_s - \varphi^s) \tag{61}$$

It will be assumed once again that there are no surface states close to the Fermi level, and no other source of change in the density of *bound* charge.

Case (a)

$$\delta({}^{\text{soln.}}g^{\text{s.c.}}_{\text{dipole}}) = 0 \tag{49}$$

Hence from eqns. (48), (49), (54) and (60)

$$\delta U \approx \delta(\varphi_b - \varphi_s) \tag{62}$$

*i.e.*, the polarization appears almost entirely across the space-charge layer.

Case (b)

$$\delta({}^{\text{soln.}}g^{\text{s.c.}}_{\text{dipole}}) \neq 0 \tag{63}$$

Hence from eqns. (48), (54) and (60)

$$\delta({}^{\text{soln.}}g^{\text{s.c.}}_{\text{dipole}}) \approx \delta U - \delta(\varphi_b - \varphi_s) \tag{64}$$

The terms on the right-hand-side of eqn. (64) are experimentally measurable.

*(vii) Distinction between free and bound charge*

It will be convenient for some purposes further to divide ${}^{\text{soln.}}g_{\text{ion}}^{\text{s.c.}}$ (as defined in eqn. (47)) thus:

$$ {}^{\text{soln.}}g_{\text{ion}}^{\text{s.c.}} = {}^{\text{soln.}}g_{\text{ion,free}}^{\text{s.c.}} + {}^{\text{soln.}}g_{\text{ion,bound}}^{\text{s.c.}} \tag{65}$$

where ${}^{\text{soln.}}g_{\text{ion, free}}^{\text{s.c}}$ is that part of ${}^{\text{soln.}}\Delta^{\text{s.c.}}\varphi$ due to charge in the semiconductor space-charge layer and may generally be approximated, for not too dilute electrolytes, by $\varphi_b - \varphi_s$. The second term of the right-hand-side of eqn. (65) is that part of ${}^{\text{soln.}}\Delta^{\text{s.c.}}\varphi$ arising from bound charge associated with the semiconductor surface. This may be due to charged surface states or ionized surface groups. In these cases there may be charge separation between the semiconductor surface and the solution and it would seem illogical to include them in ${}^{\text{soln.}}g_{\text{dipole}}^{\text{s.c.}}$. Since these cases of charge separation can be distinguished from the effect of space-charge on the electrode, we believe the distinction in eqn. (65) to be warranted.

As we have already discussed, the contribution by ${}^{\text{soln.}}g_{\text{ion,free}}^{\text{s.c.}}$ to $\varphi_s - \varphi^s$ is negligible, and hence any changes in $\varphi_s - \varphi^s$ which are due to charge separation rather than dipole layers must be ascribed to $\delta^{\text{soln.}}g_{\text{ion,bound}}^{\text{s.c.}}$. When the distinction is made it becomes necessary to modify any equations that we have previously derived by substituting $(\delta^{\text{soln.}}g_{\text{ion,bound}}^{\text{s.c.}} + \delta^{\text{soln.}}g_{\text{dipole}}^{\text{s.c.}})$ for $\delta^{\text{soln.}}g_{\text{dipole}}^{\text{s.c.}}$. We avoided this problem earlier by requiring that there should be no change in the density of bound charges.

The separation in eqn. (65) should be useful since, in principle, the distinction can be made although it has not yet been done experimentally. What is needed is a means of measuring the space-charge p.d. in the solution at $\varphi_b - \varphi_s = 0$. Approximations to this quantity may be arrived at from electrokinetic phenomena such as streaming potential or electro-osmosis. A few such measurements have been made.

SPARNAAY[12] measured electro-osmosis through germanium powder and concluded that a positive space-charge existed in the aqueous solution due to ionization of an acidic group attached to the surface. This conclusion is in accord with measurements of potential distribution at germanium electrodes as a function of hydrogen-ion concentration[13–15].

ERIKSEN AND CAINES[16] measured streaming potential for germanium powder in contact with water, acetone, methanol and nitrobenzene. Surprisingly, in all cases a negative space-charge was found in the liquid.

What is particularly needed is some method of determining the space-charge p.d. in solutions adjacent to single crystal surfaces. Failing this, the measurement of zeta-potential would be a useful first step. There is no fundamental reason why this could not be done although experimentally it may be very difficult. Successful experiments along these lines would help to resolve a number of current problems, particularly on germanium electrodes where related measurements are somewhat more advanced than on other semiconductors.

*(viii) Faradaic processes*

Polarized semiconductor electrodes behave in a variety of ways. Zinc oxide may be subjected to considerable anodic and cathodic polarization in neutral solution with negligible current flow (c.d. $< 10^{-9}$ A cm$^{-2}$). This property permits the study of the interface at (or close to) thermodynamic equilibrium. If larger crystals of better

controlled impurity content were available, zinc oxide would probably be the most important semiconductor electrode because it approximates to ideally polarizable behavior in appropriate solutions.

The germanium–electrolyte interface passes current fairly readily in either direction (anodic dissolution, cathodic hydrogen evolution) but may be polarized about 300 mV at an anodic current density of $\sim 10^{-4}$ A cm$^{-2}$. The cathodic polarization is of similar magnitude, but of less interest since in this region surface states appear and changes in lifetime of the bulk material occur (due to diffusion of hydrogen atoms) which complicate measurements[48,49]. Anodic dissolution, on the other hand, has the useful effect of renewing the surface, since the usual product at moderate current densities ($GeO_2$ or germanate ion) is moderately soluble in aqueous solutions and hence does not accumulate. Galvanostatic rather than potentiostatic techniques are frequently used since passivation does not occur at low c.d. in aqueous solutions.

Silicon is subject to the formation of thick oxide films which passivate the surface, although this can be avoided to some extent with electrolytes containing fluoride ion[17]. The presence of the oxide film is a disadvantage to impedance measurements but makes surface conductance measurements somewhat easier than on germanium.

The polarization behavior of gallium arsenide has been described[18] but although this material looks quite promising, attempts to measure details of the potential distribution do not seem to have been made.

*(ix) The Helmholtz region*

The eventual aim is to understand the details of the distribution of charge and potential across the interface at all frequencies and the relation of this to the electrode kinetics. The problems are somewhat complex and at the present stage it seems more reasonable to try to understand the simpler features of the structure of the Helmholtz layer and to determine the principal factors, both chemical and physical, involved in its behavior.

One important source of information is the variation of $\varphi_s - \varphi^s$. Hence the measurement of changes in the space-charge p.d. is of primary importance since a difference between change in electrode potential and change in space-charge p.d. must signify that a significant change in $\varphi_s - \varphi^s$ has occurred as given by eqn. (61). In actual fact it is possible to determine $\varphi_b - \varphi_s$ absolutely since it occurs entirely within a homogeneous phase, but only *changes* in $\varphi_s - \varphi^s$ can be determined. The point at which $\varphi_b - \varphi_s = 0$ represents the point of zero net charge in the space-charge layer of the semiconductor and is thus somewhat analogous to the electrocapillary maximum on mercury (*i.e.*, ${}^{\text{soln.}}g^{\text{s.c.}}_{\text{ion, free}} = 0$ at $\varphi_b - \varphi_s = 0$, but it is not necessarily true that ${}^{\text{soln.}}g^{\text{s.c.}}_{\text{ion, bound}} = 0$ under the same conditions).

Variations in $U$ at constant $\varphi_b - \varphi_s$ (not necessarily $\varphi_b - \varphi_s = 0$, however) are the primary source of information on interfacial structure, corresponding to the shift in the electrocapillary maximum of mercury. Since current density is also a variable (except for ZnO) it may be desirable in some cases to determine $\delta(\varphi_s - \varphi^s)$ at constant $i$ or even at constant $U$. The inter-relationship of these quantities is shown in Fig. 4 where hypothetical curves of $\varphi_b - \varphi^s$ *versus* $U$ for two different conditions of a semiconductor electrode (*e.g.*, change in concentration of some critical ion in solution) are plotted. As discussed in III(iii), the shape of such curves may be time-dependent.

Equation (61) may be applied to the situation in Fig. 4.

$$\delta U = \delta(\varphi_b - \varphi_s) + \delta(\varphi_s - \varphi^s) \tag{61}$$

$\delta(\varphi_s - \varphi^s)$ at constant $\varphi_b - \varphi_s$ is the horizontal separation $\delta U$ at any point, while $\delta(\varphi_s - \varphi^s)$ at constant $U$ is the vertical separation between the curves. In the general case shown in the figure, these quantities are not constant but vary with the position at which they are measured. This results from various phenomena occurring at different levels of polarization. The final quantity, $\delta(\varphi_s - \varphi^s)$ at constant $i$ may be derived by substituting the appropriate values in eqn. (61). Hypothetical points of equal current density are shown on the curves in Fig. 4. Use of eqn. (61) is equivalent

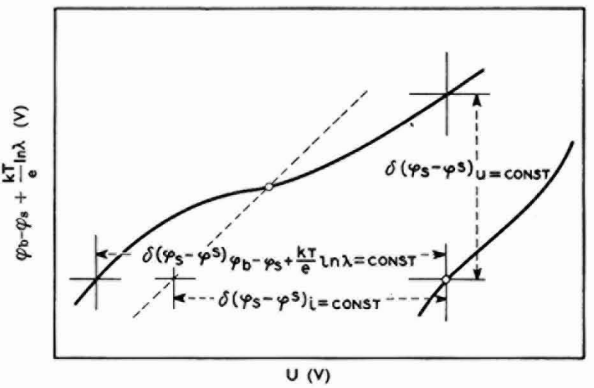


Fig. 4. Determination of $g(\varphi_s - \varphi^s)_{\varphi_b - \varphi_s + kT/e \ln \lambda = \text{const.}}$, $\delta(\varphi_s - \varphi^s)_{U = \text{const.}}$ and $\delta(\varphi_s - \varphi^s)_{i = \text{const.}}$

to drawing a line of unit slope through one of the points and measuring the horizontal or vertical distance of the other point from that line. Starting from some particular condition of the electrode, such lines of unit slope may often be obtained experimentally for rapidly applied polarization as discussed in III.

At high frequencies the charge storage phenomena at the interface are dominated by the properties of the semiconductor space-charge layer as discussed below. Although this is fortunate in one sense since it permits determination of $\varphi_b - \varphi_s$, the charging processes *per se* are of physical rather than electrochemical interest.

At lower frequencies, one can in principle see effects of changes in structure of, or charge distribution in, the Helmholtz region but the observations to date indicate a situation of considerable complexity (*e.g.* ref. 19) and until the simpler features of the interface including electrode kinetics are more clearly understood little progress can be expected in this direction.

## II. METHODS

There are three principal methods for determining the semiconductor space-charge p.d., namely measurements of surface conductance, photovoltage and capacitance. Of these the last is by far the most important in electrochemical experiments although the first two have found some limited use.

### (*i*) *Surface conductance*

When $\varphi_b - \varphi_s$ is equal to zero the densities of carriers are uniform from the bulk right up to the surface. At other values of $\varphi_b - \varphi_s$ this is not the case because of

the Boltzmann factor and in general the conductance of the space-charge region parallel with the surface is different from the value for the same volume of bulk material. By using very thin samples the surface conductance can be made an appreciable fraction of the whole and changes in the total conductance of the sample may be observed when $\varphi_b - \varphi_s$ is varied, either by external polarization or by changes in composition of the environment.

The additional surface conductance is given by

$$\Delta G = e\mu_n \Gamma_n + e\mu_p \Gamma_p \tag{66}$$

assuming that bulk mobilities apply in the space-charge region. Evaluation of the surface excess of holes and electrons as a function of $\varphi_b - \varphi_s$ shows that $\Delta G$ becomes large and positive as $|\varphi_b - \varphi_s|$ becomes large and has a minimum value when $\varphi_b - \varphi_s$ is equal to $-kT/e \ln(\lambda^2/b)$. An example is shown in Fig. 5. Measurements of $\Delta G$ con-

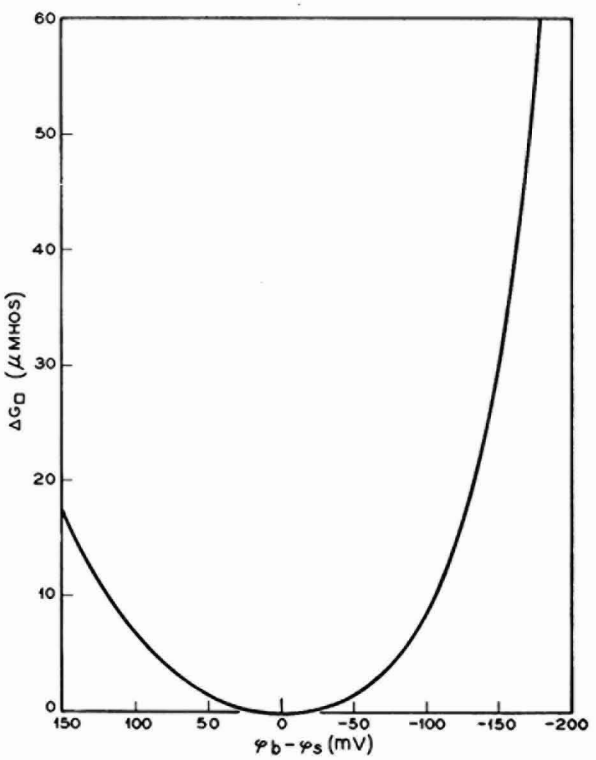


Fig. 5. Calc. conductance change ($\mu$ mho/square) *vs.* p.d. across the space-charge region for 41.7 Ω cm *p*-type Ge.

stitute a means of determining $\varphi_b - \varphi_s$, and have been extensively used for semiconductor–gas and semiconductor–vacuum interfaces[20].

One limitation is that quantitative use of the method generally requires that the minimum value be experimentally observable since the bulk conductance of the electrode cannot be calculated with sufficient precision. The usefulness of this method in an electrolyte also depends greatly on the polarizability of the interface. If current

flows between the electrode and the solution, any conductance measurement will contain a contribution from "leakage" current through the electrolyte.

In the limiting case of an ideally polarizable electrode there is no problem in making either a.c. or d.c. conductance measurements, with the exception that if, due to the presence of surface states or some other cause, the charge distributes in such a way as to produce changes in potential across the Helmholtz region, capacitative coupling effects may influence the a.c. measurements.

Of the system reported in the literature, zinc oxide[21], and silicon under circumstances where a thick stable oxide layer is formed[22], somewhat approach the ideal behavior. It has been shown that in some non-aqueous solutions, germanium also behaves in a relatively simple manner[23].

Germanium in aqueous solutions shows intermediate behavior. At small polarization, the differential resistance of the interface is relatively high in neutral non-oxidizing solutions and in this region measurements agree fairly well with theory[24]. At higher anodic polarization, the interfacial resistance decreases and the conductance through the solution increases. At very high anodic polarization, the additional conductance could, in principle, become limited by the conductivity of the solution, but this is not too helpful in solutions commonly used ($>M/10$) since at this point the conductance due to the germanium is a negligible fraction of the total.

A further problem arises when polarization of the interface results in considerable faradaic current flow. In traversing the thin sample an ohmic drop is generated and the surface is no longer equipotential. Since the electrode potential varies over the surface, so in general will $\varphi_b - \varphi_s$. This variation must be kept small or the simple theory can no longer be applied. Also if the configuration of the experiment is such that all of the polarizing current flows towards one end of the sample, the change in the ohmic drop along the sample when the polarizing current is changed may obscure the effect of the conductance change. This can be overcome by means of a suitably balanced arrangement[24].

Conductance measurements have been reported for silicon by HARTEN. It was shown that changes in electrode potential and in $\varphi_b - \varphi_s$ were equal over a range of $\sim$0.6 V when the electrode potential was varied by using solutions containing various concentrations of ceric ammonium sulfate[25]. Similar agreement with theory was found over a smaller range for external polarization[26].

BRATTAIN AND BODDY[27] report measurements on germanium using an electrode in which all arms of a bridge arrangement were cut in a continuous loop from a single crystal. This device has the advantage of being automatically temperature-compensated but is somewhat complicated to make and offers no other real advantages. The conductance was measured at 17 c/sec and showed evidence of considerable contribution from leakage through the electrolyte and hence did not agree well with the simple theory. The observed conductance was however reproducibly related to $\varphi_b - \varphi_s$ on surfaces contaminated by contact with solutions of cupric, argentic, and aurichloride ions[28].

The a.c. measurement was criticized by KROTOVA AND PLESKOV[29] as being invalidated by low frequency capacitance effects. However, the d.c. and a.c. measurements have been compared and turn out to be practically identical[24]. A minimum conductance was observed at the same electrode potential in each case. HARTEN AND MEMMING[14] have used a method whereby the polarization was automatically swept

over the desired range in about 20 sec and the conductance continuously observed on an oscilloscope. These authors also observed minimum values, in contrast to KROTOVA AND PLESKOV who claim that no minimum is observed in aqueous solutions.

The particular advantage of the conductance measurement is that it is not influenced by the presence of surface states as are the two methods described below.

*(ii) Photovoltage*

When the surface of a semiconductor is illuminated with light of energy greater than the band gap, hole-electron pairs are created and a change in $\varphi_b - \varphi_s$ occurs which may be observed as an instantaneous change in the electrode potential. The physical theory is discussed by GARRETT AND BRATTAIN[30], while more specific applications to electrochemical experiments are discussed by DEWALD[31] and by LAZORENKO-MANEVICH[32]. The change in $\varphi_b - \varphi_s$ on illumination is always in the direction of flat band (*i.e.*, $\varphi_b - \varphi_s = 0$) hence the photovoltage itself is positive when the bands are bent down, negative when the bands are bent up and zero at flat band. In addition, there is the Dember potential (analogous to a liquid-junction potential) caused by the fact that electrons diffuse from the illuminated region more rapidly than holes. If the rate of injection of carriers is constant, the Dember potential is also constant, and is independent of $\varphi_b - \varphi_s$. The observed photovoltage is the algebraic sum of these quantities.

There are four limitations to the determination of $\varphi_b - \varphi_s$ from this measurement.

1. It is generally necessary to know the surface recombination velocity over the experimental range unless this is either small or constant.

2. The absolute value of the number of added carriers produced by the illumination must be known or eliminated from the equations in some way.

3. The theory applies only to the "instantaneous" photovoltage, *i.e.*, the effect observed before any charge transfer occurs across the interface due to the change in potential distribution induced by illumination.

4. The presence of surface states modifies the theory, primarily by shifting the potential scale but also with small changes in the form of the relationship between $\varphi_b - \varphi_s$ and photovoltage.

From ref. 30 the change in $\varphi_b - \varphi_s$ in the absence of surface states due to a light intensity, $L$, is given by

$$\frac{\mathrm{d}(\varphi_b - \varphi_s)}{\mathrm{d}L} = -\frac{kT}{ei_s} \cdot \frac{1 - \exp(-e(\varphi_b - \varphi_s)/kT)}{1 + \lambda^{-2} \exp(-e(\varphi_b - \varphi_s)/kT)} \tag{67}$$

where $i_s$ is the minority carrier saturation current given for $n$-type by

$$i_s = q p_o \left[(D_P/\tau)^{\frac{1}{2}} + s\right] \tag{68}$$

and the Dember potential is

$$\frac{\mathrm{d}\varphi_D}{\mathrm{d}L} = -\frac{kT}{ei_s} \cdot \frac{b-1}{b} \cdot \frac{\lambda^2}{1 + (\lambda^2/b)[(b+1)(L/i_s)+1]}. \tag{69}$$

The above equations have been applied to the case of germanium in neutral aqueous solution[33] where $s$ is known to be sufficiently small[27,34] that it may be neglected, and fast surface states are absent. In the limiting small signal case, as $L \to 0$ the equations become

$$\frac{\mathrm{d}(\varphi_b-\varphi_s)}{\mathrm{d}\delta} = -\frac{kT}{e}\cdot\frac{1-\exp(-e(\varphi_b-\varphi_s)/kT)}{\lambda+\lambda^{-1}\exp(-e(\varphi_b-\varphi_s)/kT)} \tag{70}$$

and

$$\frac{\mathrm{d}\varphi_D}{\mathrm{d}\delta} = -\frac{kT}{e}\cdot\frac{b-1}{\lambda-\lambda^{-1}b} \tag{71}$$

where $\delta=(p^*-p_o)\,n_i^{-1}$ for $n$-type, $p^*$ being the hole concentration just inside the space-charge region under illumination. The form of the algebraic sum of eqns. (70) and (71) in a particular case is shown in Fig. 6. When $s$ is neither negligible nor constant the complete equations must be used.

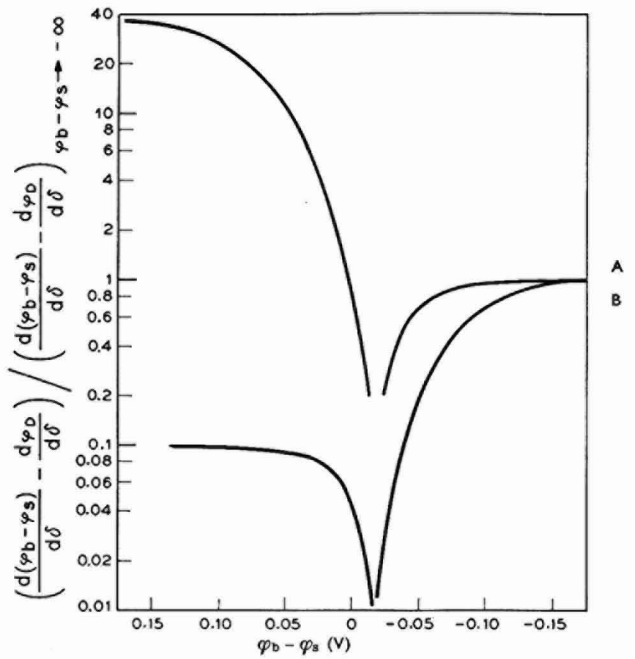


Fig. 6. Calc. relative photovoltage *vs.* p.d. across the space-charge region for (A), 16.5 Ω cm $n$-type; (B), 30 Ω cm $p$-type Ge. The discontinuity is a change of sign and the left-hand branch is negative in each case.

To determine $\varphi_b-\varphi_s$ it is necessary to know the value of $\delta$ or to have some means of eliminating it. This may be done by determining the limiting values of the photovoltage for large $|\varphi_b-\varphi_s|$. Actually only one value need be determined since

$$-\left(\frac{\mathrm{d}(\varphi_b-\varphi_s)}{\mathrm{d}\delta}-\frac{\mathrm{d}\varphi_D}{\mathrm{d}\delta}\right)_{\varphi_b-\varphi_s\to-\infty}\Big/\left(\frac{\mathrm{d}(\varphi_b-\varphi_s)}{\mathrm{d}\delta}-\frac{\mathrm{d}\varphi_D}{\mathrm{d}\delta}\right)_{\varphi_b-\varphi_s\to+\infty} = \lambda^2 \tag{72}$$

In practice the asymptotic values are closely approached for quite moderate values of $\varphi_b-\varphi_s$ as shown in Fig. 6.

The agreement between $\varphi_b-\varphi_s$ determined from these measurements and those of interfacial capacitance, provided confirmation of the absence of significant densities of fast states at the interface between germanium and neutral electrolytes[33].

The point of zero photovoltage can be determined with much less difficulty since it is not affected by changes in magnitude of surface recombination velocity. PLESKOV AND TYAGAI[35] have used this measurement on variously doped samples, in conjunction with determination of the potential of the maximum of surface recombination velocity, to investigate the potential distribution across the interface.

The third requirement noted above necessitates that the light pulse should have a fast rise-time. The actual rise-time necessary in any such experiment is determined by the rate of the "slow" equilibration that takes place after the surface becomes illuminated, which is itself dependent on the polarization. About 35 $\mu$sec was found adequate in ref. 33 although faster pulses have been used[35].

The final requirement of absence of surface states is the most severe limitation on the usefulness of the method, because such states are frequently present. Since the photovoltage can be calculated for any particular distribution of surface states it would seem that its widest use would be in the confirmation of data provided by capacitance measurements.

*(iii) Interfacial capacitance*

The charge in the semiconductor space-charge layer is given by eqn. (18). Differentiation with respect to $\varphi_b - \varphi_s$ yields the capacitance of this region

$$\frac{dq_{s.c.}}{d(\varphi_b-\varphi_s)} = \frac{e^2 n_i^2 \mathscr{L}^2}{2kT q_{s.c.}^{\frac{1}{2}}} \{\lambda[\exp(e(\varphi_b-\varphi_s)/kT)-1]+\lambda^{-1}[\exp(-e(\varphi_b-\varphi_s)/kT)-1]\} \quad (73)$$

Evaluation of this function shows a minimum value, the magnitude and position of which, for a given semiconductor are dependent on doping. The minimum value for intrinsic germanium is $\sim 2.04 \times 10^{-8}$ F cm$^{-2}$, while for semiconductors with larger band gaps, *e.g.* silicon, it is still smaller. The theoretical space-charge capacitance for a particular germanium sample is shown in Fig. 7.

The capacitance of the region between the electrode surface and the ohp may

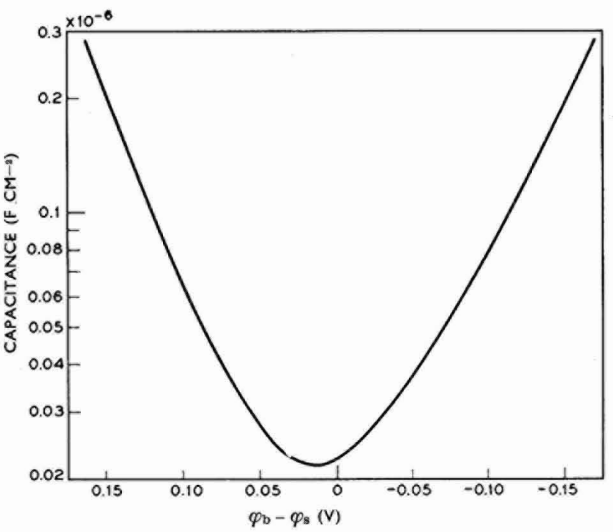


Fig. 7. Calc. capacitance *vs.* p.d. across the space-charge region for 16.5 Ω cm *n*-type Ge.

be assumed to be of similar magnitude to that at smooth, clean, metal electrodes ($\gtrsim 20 \cdot 10^{-6}$ F cm$^{-2}$) since the dimensions and dielectric constant should be essentially similar (although films may be a problem in some cases). This assumption is supported by a measured value of $\sim 23 \cdot 10^{-6}$ F cm$^{-2}$ for the (100) face of germanium[36].

Beyond the ohp, the capacitance will be determined in the usual way by the properties of the electrolyte, and can be made larger than the Helmholtz capacitance by working at sufficiently high electrolyte concentrations. Since

$$^{\text{soln.}}\Delta^{\text{s.c.}}\varphi = (\varphi_b - \varphi_s) + (\varphi_s - \varphi_2) + (\varphi_2 - \varphi^s) \tag{24}$$

then for a charge applied to the interface, neglecting faradaic effects and surface states

$$\frac{\delta\, ^{\text{soln.}}\Delta^{\text{s.c.}}\varphi}{\delta q} = \frac{\delta(\varphi_b - \varphi_s)}{\delta q} + \frac{\delta(\varphi_s - \varphi_2)}{\delta q} + \frac{\delta(\varphi_2 - \varphi^s)}{\delta q} \tag{74}$$

*i.e.*,

$$\frac{1}{C_{\text{meas.}}} = \frac{1}{C_{\text{s.c.}}} + \frac{1}{C_{\text{Helmholtz}}} + \frac{1}{C_{\text{Gouy}}} \tag{75}$$

and since for a moderately doped semiconductor at potentials not too far from the space-charge capacitance minimum

$$C_{\text{Helmholtz}} \gg C_{\text{s.c.}} \tag{76}$$

and

$$C_{\text{Gouy}} \gg C_{\text{s.c.}} \tag{77}$$

at moderate electrolyte concentrations, then

$$C_{\text{meas.}} \approx C_{\text{s.c.}} \tag{78}$$

which also follows from eqn. (56).

When surface states are present and provided that sufficient time is allowed that some of the charge on the semiconductor will be trapped in the states, then

$$\delta q = \delta q_{\text{s.c.}} + \delta q_{\text{s.s.}} \tag{79}$$

and

$$\frac{\delta q}{^{\text{soln.}}\Delta^{\text{s.c.}}\varphi} = \frac{\delta q_{\text{s.c.}} + \delta q_{\text{s.s.}}}{^{\text{soln.}}\Delta^{\text{s.c.}}\varphi} \tag{80}$$

or using eqn. (56) which will apply for densities of states sufficiently small that inequality (55) still holds, then,

$$\frac{\delta q}{^{\text{soln.}}\Delta^{\text{s.c.}}\varphi} \approx \frac{\delta q_{\text{s.c.}}}{\delta(\varphi_b - \varphi_s)} + \frac{\delta q_{\text{s.s.}}}{\delta(\varphi_b - \varphi_s)} \tag{81}$$

which is equivalent to

$$C_{\text{meas.}} \approx C_{\text{s.c.}} + C_{\text{s.s.}} \tag{82}$$

provided that eqns. (76) and (77) hold and also that

$$C_{\text{s.s.}} \ll C_{\text{Helmholtz}} \tag{83}$$

and

$$C_{\text{s.s.}} \ll C_{\text{Gouy}} . \tag{84}$$

These equations and eqn. (62) show that if impedance measurements are made at a sufficiently high frequency such that no charge is transferred to the surface states, and in the absence of faradaic processes, then the observed capacitance should approximate to that of the semiconductor space-charge region. At lower frequencies, where charge trapped in the states changes during the measuring time, the observed capacitance is the sum of that due to the space-charge and the surface states, subject of course to the various restrictions given above.

In general, impedance measurements give information on the distribution of charge across the interface, and through frequency effects, changes in the distribution with time. Semiconductor surfaces are generally sufficiently complicated that a full analysis over a wide range of frequencies, which would include effects of surface state charging, carrier recombination–generation in the space-charge and surface regions, faradaic processes and changes in adsorbed species, has not been made. In the case of zinc oxide where fast surface states and faradaic processes occur only to a negligible extent, good agreement has been found between theory and experiment over a wide range of frequencies, provided allowance is made for the presence of partially ionized donors[21]. Germanium is more complex since anodic dissolution (or cathodic hydrogen evolution) imposes a limit on the lowest useful frequency. In addition, the anodic dissolution reaction[37] involves a step which can be considered as the delayed charging of surface states[36], while germanium cathodes show behavior both in the bulk and at the surface which can be ascribed to additional energy levels introduced by the presence of hydrogen atoms[38].

At present, the most interesting aspect of impedance measurements lies in the higher frequency region where many of the complications are avoided and the effect of the space-charge capacitance is predominant. The simple space-charge capacitance has been observed both for zinc oxide[21] and germanium[27]. The value of this measurement is that $\varphi_b - \varphi_s$ may be readily determined from it. A.c. methods have been commonly used and almost certainly will ultimately provide the most detailed and accurate information. D.c. pulse methods however offer some advantages and can be taken up to quite high effective frequencies where a.c. methods are somewhat less suitable.

(*a*) *a.c. Methods.* Various bridges have been described, [*e.g.*, refs. 39, 13, 19] and are generally of conventional design. Except in the case of zinc oxide, the behavior with change in measuring frequency is quite complicated including, for instance, regions of apparent negative capacitance[19].

(*b*) *d.c. Pulse method.* This method has been successfully employed on germanium in a number of investigations[27,29,40] and also on silicon with somewhat less success[41]. The electrode potential is observed as a function of time in response to a (usually) square current pulse as shown in Fig. 8. If the observations can be made in a sufficiently short time such that only charging of the space-charge region occurs, then

$$C_{s.c.} = i \cdot \left(\frac{dt}{dU}\right) \tag{85}$$

and the capacitance is determined from the reciprocal of the slope of the charging curve (BC in Fig. 8). When this method is used for very short times ($\sim 1\ \mu$sec) practical problems may be encountered due to oscillations in the measuring circuit which may make it difficult to measure the slope. In this case it becomes more favorable to allow

the current to flow for a known length of time, $\delta t$, and measure the voltage response, $\delta U$, then

$$C_{s.c.} = \frac{i \cdot \delta t}{\delta U} \tag{86}$$

The quantities $\delta U_1$ and $\delta U_2$ in Fig. 8 are actually identical, but $\delta U_2$ is much easier to measure since it is the vertical separation between the horizontal base-line AA′ and the (on a 1-$\mu$sec scale) almost horizontal line DE, which is the decay of overvoltage on open circuit. Oscillations at B and rounding of the pulse at C make $\delta U_1$ much

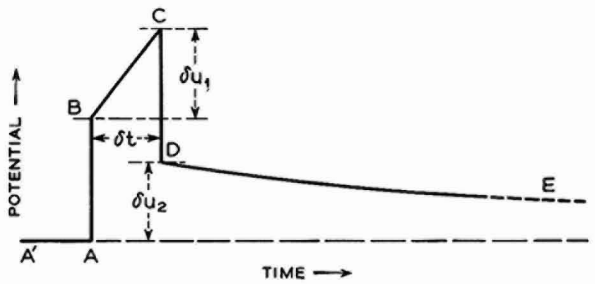


Fig. 8. Response of the semiconductor–electrolyte interface to a rectangular current pulse.

harder to measure. When oscillations occur at B they generally also occur at D of course, but DE can be extrapolated more easily than can the relatively short and sharply-sloping line, BC. The potential jumps shown as AB and CD are also equal to one another and represent, principally, ohmic drop in the system as the pulse turns on and then off.

Analysis of the data is considerably simplified if the pulse width is short compared with the time constant for decay of the overvoltage (as is the case in the figure). This is easily achieved on germanium where the time constant is many milliseconds at small polarization and reduces to a few tens of microseconds at an anodic polarization of $\sim$1 mA cm$^{-2}$.

The decay of overvoltage is reasonably close to being exponential on all three low-index planes except at the very lowest currents when roughly 10% of the total signal may have a somewhat faster decay. This situation is not much changed between temperatures of 0° and 80°, although at higher temperature the over-all decay at low polarization is faster. The magnitude of the decay-time constant is approximately equal to the product of the capacitance of the space-charge region and the "differential resistance", $d\eta/di$, obtained from the current voltage characteristic[27].

An estimate of the Helmholtz capacitance on germanium electrodes has been made by a double pulse technique[36]. Large-signal charging experiments have also been reported[29].

(c) *Equivalent circuit.* Numerous proposals for the equivalent circuit of the interface have been made[13,19,21,27,42,43] which approximate the behavior in the moderately high frequency ($\sim$1 Mc) region. Figure 9 (a–d) shows the synthesis of increasingly more realistic representations, although the real situation must be much more complex than 9(d). It is customary to work at sufficiently high frequency that 9(a) applies, although there are conditions, *e.g.* high anodic polarization of germanium

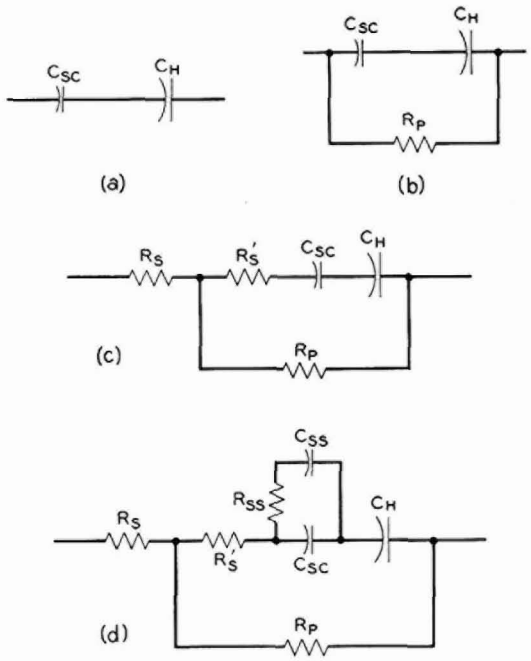


Fig. 9. Equivalent circuits. (a), At high frequency (no loss of charge by faradaic processes) and in the absence of fast surface states. Normally $C_H \gg C_{SC}$ and hence $C_H$ may be neglected. (b), Similar to (a) but with the addition of faradaic current flow. This introduces a time constant ($\tau = R_P(C_{SC}^{-1} + C_H^{-1})^{-1}$) into the system and hence limits the frequency range over which useful measurements can be made. (c), The inclusion of series resistance in the bulk of the sample and in the space-charge layer was found to be adequate to describe small signal d.c. charging experiments on Ge in neutral solns.[27]. (d), Surface states add a parallel capacitance. The product $R_{SS} \cdot C_{SS}$ describes the equilibration time of the states with the space-charge layer.

electrodes, where $R_P$ becomes very small and the time constant, $R_P \cdot (C_{SC}^{-1} + C_H^{-1})^{-1}$, becomes of the order of microseconds. Some pulse data have been corrected for this effect[27].

## III. EXPERIMENTAL RESULTS

Since eqns. (58) and (62) are of primary importance in establishing the physical validity of the measurements, their experimental justification will be dealt with first.

$$(i)\ \delta U \approx \delta(\varphi_b - \varphi_s) \tag{62}$$

Confirmation of this equation comes directly from capacitance measurements, since only if it holds will the experimentally-measured value be equal to that calculated for the space-charge layer. Early a.c. measurements[39] on germanium in acid and alkaline solutions showed that the capacitance minimum did not agree with the theoretical value, although it approached it at the highest frequency ($10^6$ c/sec). Subsequently, measurements were reported on zinc oxide in neutral solution[21], which indicated that the observed capacitance was, within experimental error, entirely that due to the semiconductor space-charge layer. The analysis was a little complex

since partially-ionized donors had to be considered. Also no minimum value was observed since *p*-type inversion layers are not produced on zinc oxide, which occurs only as an *n*-type semiconductor. However good agreement between experiment and theory was obtained for several differently doped crystals which could only be so if eqn. (62) were correct.

Differential capacitance measurements on germanium in neutral solution by the d.c. pulse method[27] also confirm eqn. (62). In this case, as shown in Fig. 10, a minimum value was observed which simplified the analysis. This value, which is a unique reference point, agreed with theory assuming that the surface roughness factor (real area/apparent area) had the value 1.3, this being consistent with the value

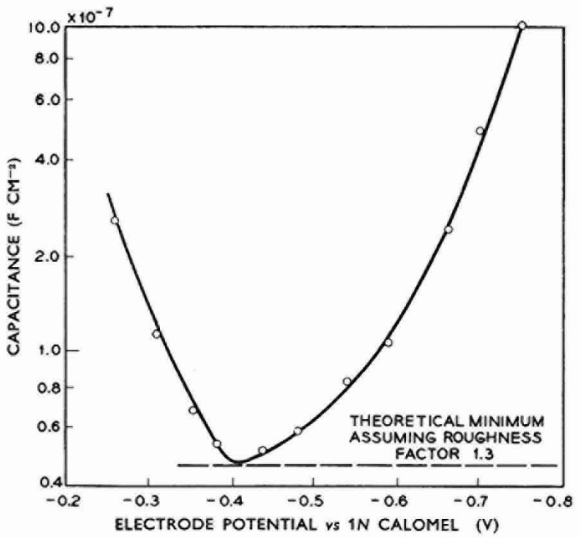


Fig. 10. Measured capacitance for Ge electrode in neutral $K_2SO_4$ solution (42.2 Ω cm, *n*-type, (100) orientation)[27].

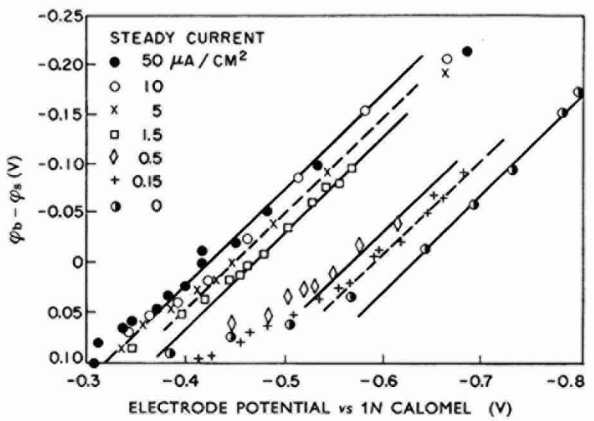


Fig. 11. Comparison between change in electrode potential and change in space-charge p.d. (deduced from capacitance data). Rapid polarization superimposed on various steady currents. Ge 22 Ω cm, *n*-type (100) orientation in neutral $K_2SO_4$ soln.[27].

experimentally determined for germanium surfaces etched in a similar way[44]. In addition, these data could be used to determine $\varphi_b - \varphi_s$, assuming that the observed capacitance was solely that of the space-charge region over the whole range of polarization. It was found, starting from any electrode potential in this range, that if a small range of polarization ($\sim \pm 50$ mV) was rapidly swept through, then $\delta U$ was equal to $\delta(\varphi_b - \varphi_s)$ deduced from the capacitance (Fig. 11). This simple result indicates quite strongly that the assumption that eqn. (62) holds in the small signal case is valid, particularly since the experiment was carried out on various electrodes, both $n$- and $p$-type, with similar conclusions. No fixed distribution of surface states near the middle of the gap of sufficient density to contribute significantly to the measured capacitance could lead to such a result. Thus, eqn. (62) applies both to differential ($< 10$ mV) and large signal ($\sim 50$ mV) cases. At longer times after the application of polarization, relaxation occurred and changes in $\varphi_s - \varphi^s$ were inferred from eqn. (61).

Figure 12 shows capacitance data for more highly doped electrodes obtained by MEMMING[45] using an a.c. method at high frequency ($\sim 50$ kc). The agreement with theory over part of the range indicates that eqn. (62) is obeyed. The departure from agreement is thought to be due primarily to depletion of minority carriers by electrochemical reactions.

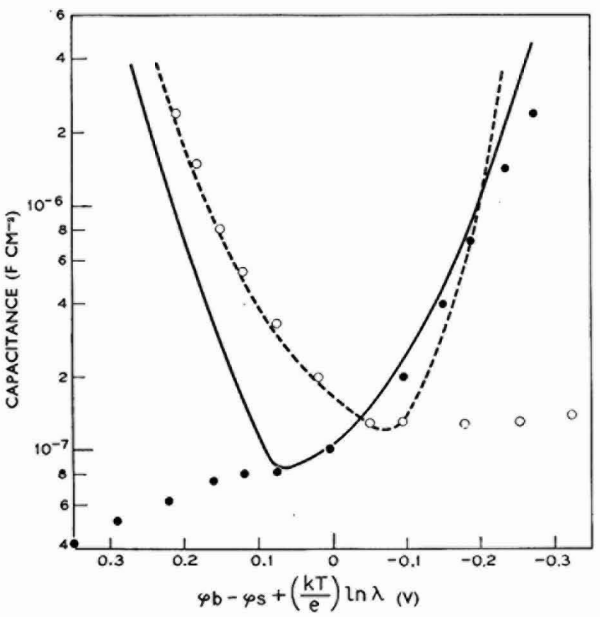


Fig. 12. Capacitance data for Ge electrodes: ○, 0.1 Ω cm $p$-type; ●, 0.1 Ω cm $n$-type[45]. Theoretical curves (– – –), $p$-type; (———), $n$-type.

HOFFMAN-PEREZ AND GERISCHER[13] reported minimum values of somewhat greater magnitude over the whole pH-range and concluded that surface states were present. However, the effect of quite small traces ($< 10^{-7}$ $M$) of particular impurity ions in the solution has been found to exert a marked influence on interfacial capacitance measurements[28,46].

Measurements of differential capacitance on silicon electrodes by both a.c.[47] and d.c.[41] methods show minima considerably larger than those predicted by theory, presumably due to surface states and hence eqn. (62) cannot be checked. HARTEN has demonstrated by another method[25] that eqn. (62) holds for silicon. The electrode potential was varied by taking different concentrations of ceric ammonium sulfate in 1 $N$ sulfuric acid and the change in conductance of the electrode (thin slice) was measured. There was excellent agreement between the measured and theoretical values of conductance change assuming eqn. (62) to hold. In this context, the great sensitivity of capacitance measurements in detecting surface states is to be noted. For instance, the space-charge capacitance minimum for 440 Ω-cm $n$-type silicon is $\sim 2 \cdot 10^{-9}$ F cm$^{-2}$ while $10^{10}$ cm$^{-2}$ surface states (a relatively small density) have a maximum capacitance of $\sim 1.5 \times 10^{-8}$ F cm$^{-2}$ and hence can, if occurring at an appropriate energy near the space-charge minimum, completely dominate the observed capacitance. This same density of surface states on changing its charge by one unit per state produces a change in surface charge of $\sim 1.6 \times 10^{-9}$ C. This charge acting across the Helmholtz layer, assuming a capacitance of 20 $\mu$F cm$^{-2}$, produces a change in $\varphi_s - \varphi^s$ (and hence also in the electrode potential) of less than 0.1 mV and is experimentally undetectable.

$$(ii)\ \delta\left\{\varphi_b - \varphi_s + \frac{kT}{e} \ln \lambda\right\} = 0 \tag{58}$$

This equation was derived for a semiconductor in electrochemical equilibrium but few simple cases exist (*e.g.*, redox couples in neutral solution on zinc oxide[31]) and have been insufficiently investigated.

The equation can be modified for a non-equilibrium electrode like germanium by including the electrode potential as a variable thus:

$$\varphi_b - \varphi_s + \frac{kT}{e} \ln \lambda = U + \text{const.} \tag{87}$$

If various differently-doped electrodes are compared at the same value of $U$, then $\varphi_b - \varphi_s + (kT/e) \ln \lambda$ should remain constant throughout. Experimentally, as shown in Figs. 13(a) and (b), it is found that the equation applies to rapidly polarized germanium anodes up to the point where time effects (*q.v.*) on the potential distribution occur[27,33]. It will be shown in the next section that the constant in eqn. (87) is dependent on the current density but that it does not change instantaneously on changing the current density. This conclusion already arises from the data shown in Fig. 11.

The essential requirement for eqn. (87) to hold, is that $\varphi_s - \varphi^s$ should be independent of the Fermi level. It follows from this that at constant $U$, the sum of $\varphi_b - \varphi_s$ and ${}^{sc}\Delta^{m}\varphi$ must be constant since no other regions are affected by change in semiconductor Fermi level. Consequently $\varphi_b - \varphi_s$ must vary in such a way as to compensate exactly for the electron activity term, $(kT/e) \ln \lambda$, at the metal–semiconductor interface.

The data in Fig. 13 then indicate two things. First that $\varphi_s - \varphi^s$ is in fact constant (in principle it varies minutely because the contribution to $\varphi_s - \varphi^s$ of ${}^{\text{soln.}}g^{\text{s.c.}}_{\text{ion,free}}$ varies with $\varphi_b - \varphi_s$, but this is negligible). Further, the fact that the data fit the theoretical model over a range of doping provides further evidence that the values of $\varphi_b - \varphi_s$ determined from capacitance must be correct.

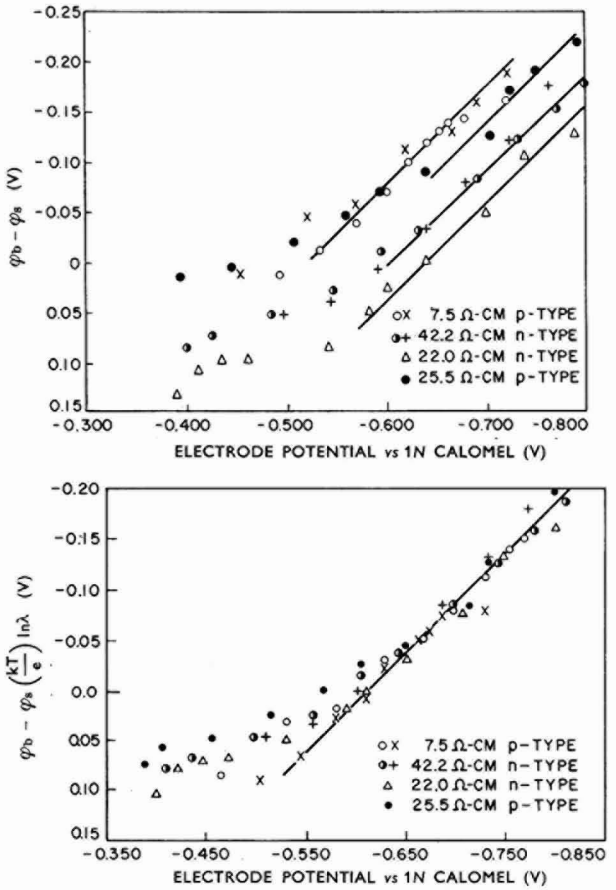


Fig. 13. (a) Variation of inner p.d. for various Ge electrodes of (100) orientation. (b) Same data, but considering the p.d. between the Fermi level and the intrinsic level at the surface. Rapid polarization in neutral $K_2SO_4$ soln.[27].

Sections III (i) and (ii) clearly indicate that the simple physical model of the interface is adequate both for zinc oxide and germanium. The capacitance may be used to deduce $\varphi_b - \varphi_s$ and hence the behavior of $\varphi_s - \varphi^s$ may be investigated using eqn. (61).

*(iii) Time effects in polarization behavior*

Capacitance measurements on zinc oxide can be fitted to theory over a wide range of polarization on the assumption that $\delta(\varphi_s - \varphi^s)$ is zero[21] at all times, provided that the electrode was initially allowed to equilibrate with the solution for several hours.

On germanium, the situation is complicated by time effects. If polarization over a particular range is carried out rapidly, it can also be shown that $\delta(\varphi_s - \varphi^s)$ is zero, *i.e.*, $\delta U \approx \delta(\varphi_b - \varphi_s)$[27] which is demonstrated for limited ranges of polarization in Figs. 11 and 13. By using a technique in which the polarizing current is swept over a

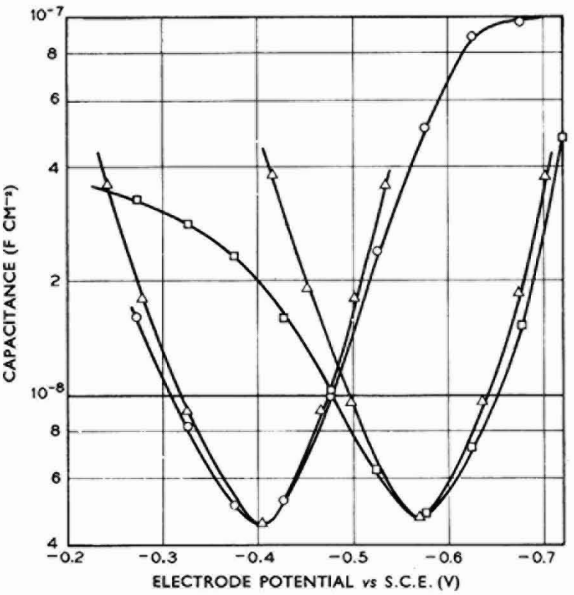


Fig. 14. Comparison between measured and theoretical capacitance, Ge 30 Ω cm, *p*-type, (110) orientation. □, 0–200 μA; ○, 200–0 μA; sweep time 5 sec; △, calc. values[50].

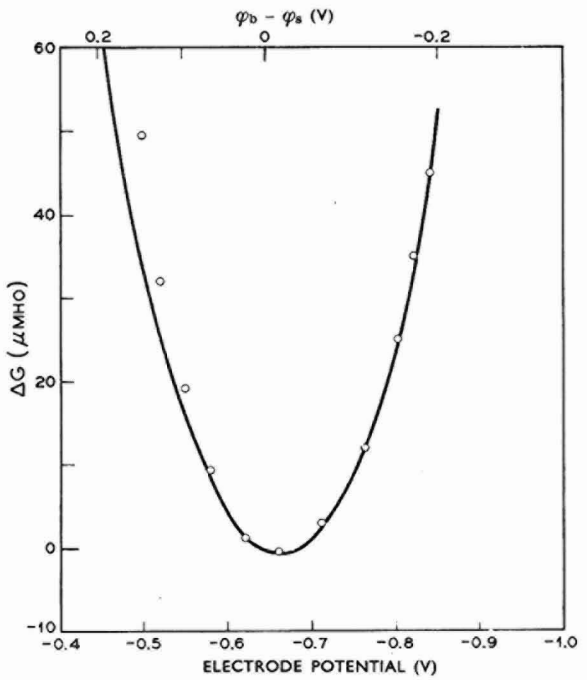


Fig. 15. Comparison between measured and theoretical conductance change for intrinsic Ge. The potential scales have been arbitrarily matched to fit the curves[4].

desired range, combined with rapid photographic determination of the capacitance as a function of electrode potential, this has been shown by the data in Fig. 14 to hold over a wider range of polarization[50]. A similar result using conductance measurements[14] is shown in Fig. 15. This is the simple behavior predicted by eqn. (62).

If a longer time is allowed to elapse between the application of polarization and measurement of the capacitance (or any other method for determining $\varphi_b - \varphi_s$) it is concluded from eqn. (61) that $\varphi_s - \varphi^s$ has changed. The ultimate magnitude of $\delta(\varphi_s - \varphi^s)$ increases with current density and comprises, very approximately, 50% of $\delta U$[27,40,51]. Some data are shown in Fig. 16 from which it is clear that $\delta U \neq \delta(\varphi_b - \varphi_s)$.

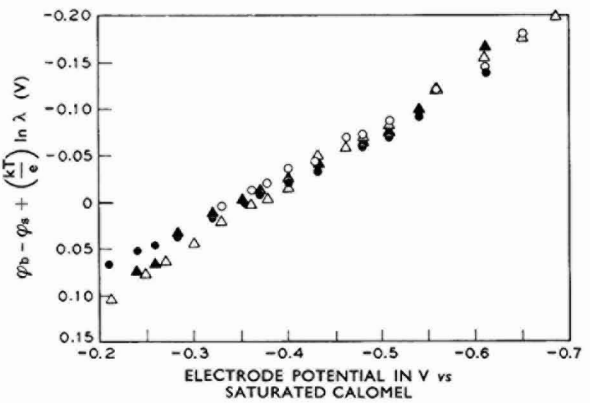


Fig. 16. Effect of relaxation on potential distribution. 30 Ω cm *p*-type: ○, photovoltage; △, capacity. 16.5 Ω cm *n*-type: ●, photovoltage; ▲, capacity.

Also apparent from this figure, is the fact that eqn. (58) still holds when the polarization is allowed to relax to a steady state, *i.e.*, the data are independent of Fermi level and that capacitance and photo-voltage measurements are in good agreement. This relaxation phenomenon was tentatively suggested to be due to the desorption of oriented water molecules[15,33]. An alternative explanation has recently been suggested[36] which involves the mechanism for anodic dissolution of germanium proposed by BECK AND GERISCHER[37]. The rate-determining step in this mechanism is the breaking of a bond between neighboring germanium atoms in the surface and sub-surface planes after a hole has become trapped there resulting in a one-electron bond ($Ge^+Ge$). The equilibrium determining the concentration of the positively charged species ($Ge^+Ge$) is of first order in the surface concentration of holes and hence [$Ge^+Ge$] increases with anodic polarization. The species ($Ge^+Ge$) can be considered as a surface state, the density of which increases exponentially with energy since its concentration is proportional to the surface hole concentration which in turn depends exponentially on $\varphi_b - \varphi_s$.

Since the rate-determining step is dependent on [$Ge^+Ge$], then the concentration of this species must, in the steady state, attain a value appropriate to the current density, thus

$$i_{\text{anod.}} \propto [Ge^+Ge] - [Ge^+Ge]_o \,. \tag{88}$$

where $[Ge^+Ge]_o$ is the concentration on open circuit. The additional surface charge

$e\delta$[Ge$^+$Ge] produces a field at the surface and hence produces changes in p.d. between the surface and the bulk of the solution. As will be pointed out in III(v), $\varphi_1-\varphi^s$ is maintained constant by an electrochemical equilibrium between hydrogen ions at the ihp and in the bulk of the solution. However $\varphi_s-\varphi_1$ is not thus restricted and changes in it may be observed as $\delta U-\delta(\varphi_b-\varphi_s)$. The p.d. change, $\delta(\varphi_s-\varphi_1)$, and the extra charge, $e\delta$[Ge$^+$Ge], are related through the capacitance between the surface and the ihp

$$\delta(\varphi_s-\varphi_1) = \frac{e\delta[\mathrm{Ge^+Ge}]}{C_{s-1}} \tag{89}$$

If $C_{s-1}$ is constant, eqns. (88) and (89) suggest that $\delta(\varphi_s-\varphi_1)$ should be linearly dependent on $i_{\mathrm{anod}}$. Actually, as found experimentally, it is more nearly proportional to ln $i_{\mathrm{anod}}$[40] indicating that $C_{s-1}$ may be dependent on the field.

An experiment based on this model has been used to determine the Helmholtz capacitance of a germanium electrode[36]. A known charge, $(\delta q)$, was put on to the interface and a sufficiently long time allowed to elapse that some of it was transferred from the space-charge layer to the "surface states", but sufficiently short that there was negligible faradaic current. Since $\delta U$ may be directly observed and $\delta(\varphi_b-\varphi_s)$ deduced from the capacitance changes, then from

$$\delta U = \delta(\varphi_b-\varphi_s)+\delta(\varphi_s-\varphi^s) \tag{61}$$

and applying eqn. (89) in the limit of short times and small values of $\delta(\varphi_s-\varphi_1)$ (assuming $\delta(\varphi_1-\varphi^s)$ to be zero because of the ionization equilibrium)

$$C_{s-1} = \frac{\delta q}{\delta(\varphi_s-\varphi^1)} \tag{90}$$

For the germanium (100) surface, the observed value was $23\pm3$ $\mu$F cm$^{-2}$.

In the case of silicon[26], it was found from conductance measurements that when the surface was polarized in the usual way rather than by changing the solution composition, agreement with theory, *i.e.*, $\delta(\varphi_s-\varphi^s)=0$, was obtained over a limited region. No minimum conductance was observed, possibly due to depletion of minority carriers by the electrochemical reaction, so the result is not entirely unambiguous. Moreover, when the electrode potential of germanium is varied by using various concentrations of ferricyanide and measurements of capacity are made, it is found that the data are very similar to those obtained with conventional polarization after relaxation, *i.e.*, $\delta(\varphi_s-\varphi^s)$ is considerable[53].

*(iv) Effect of some anions and cations*

The effect of a variety of ions on germanium electrodes in aqueous solutions has been studied. Corrosion by oxidizing agents[52] and spontaneous deposition of heavy metal ions to form surface states[28,45,46] do not come within the province of this review. The halide ions and hydrogen ion will be discussed in later sections. Many other ions are inactive, by which is meant that their presence in solution has no effect on the electrode potential of the point of zero charge (*i.e.*, $\delta U_{\varphi_b-\varphi_s=0}=0$) nor on any other observed quantity. Figure 17 illustrates the effect of some anions[53] on capacitance data taken for a (111)-oriented germanium electrode in various solutions, all buffered to the same pH value. $M/10$ solutions of $K_2SO_4$, $NaClO_4$ and $KNO_3$ buffered with $\sim M/20$ $KH_2PO_4$/KOH mixtures, (or the appropriate sodium salts in the case

of $NaClO_4$) gave data which were identical within experimental error. Variation of the phosphate concentration by a factor of ten had no effect. ($M/10$ $K_2SO_4$ was added to the solution of lowest phosphate concentration to maintain the ionic strength.) Since it is most unlikely that sodium ion and perchlorate ion have exactly compensating effects, they are assumed to be inactive. There was negligible difference between the data for phosphate- or phthalate-buffered solutions at a pH value of 5.9.

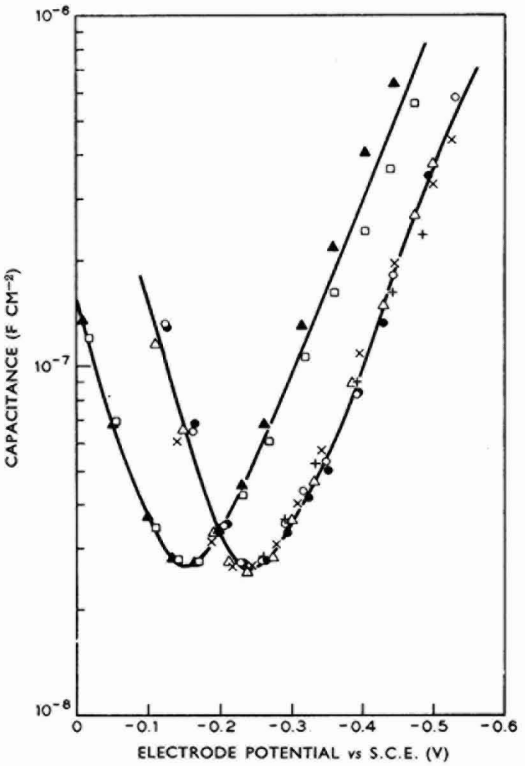


Fig. 17. Capacitance data for various anions:
pH. 7.45
●, $K_2SO_4$ $M/10$, $KH_2PO_4$ $M/20$; ○, $NaClO_4$ $M/10$, $NaH_2PO_4$ $M/20$; △, $KNO_3$ $M/10$, $KH_2PO_4$ $M/20$; ×, $KH_2PO_4$ $M/5$; +, $K_2SO_4$ $M/10$, $KH_2PO_4$ $M/50$.
pH 5.9
▲, $K_2SO_4$, $M/10$, phosphate buffer; □, $K_2SO_4$ $M/10$, phthalate buffer.
Ge 52.7 Ω cm, $p$-type, (111) orientation.

The effect of a number of cations[53] is shown in Fig. 18. $M/10$ $LiNO_3$ and $CsNO_3$ were buffered with mixtures of phosphoric acid and LiOH, or CsOH solutions, respectively. $M/10$ $NH_4H_2PO_4$ was adjusted to the same pH by addition of $NH_4OH$ solution. The potassium and sodium ion solutions were similar to those shown in Fig. 17.

The data are identical near the capacity minimum; and in particular the minimum itself, which represents a constant value of $\varphi_b - \varphi_s$ in these experiments, occurs at the same electrode potential in each case showing that $\varphi_s - \varphi^s$ is constant at

that particular value of electrode potential independent of the nature of the ions present. This indicates no "specific adsorption" of sulfate, perchlorate, nitrate, or phosphate, also sodium, potassium, lithium, cesium or ammonium ions.

The moderate disagreement at more positive potentials is due to the approach

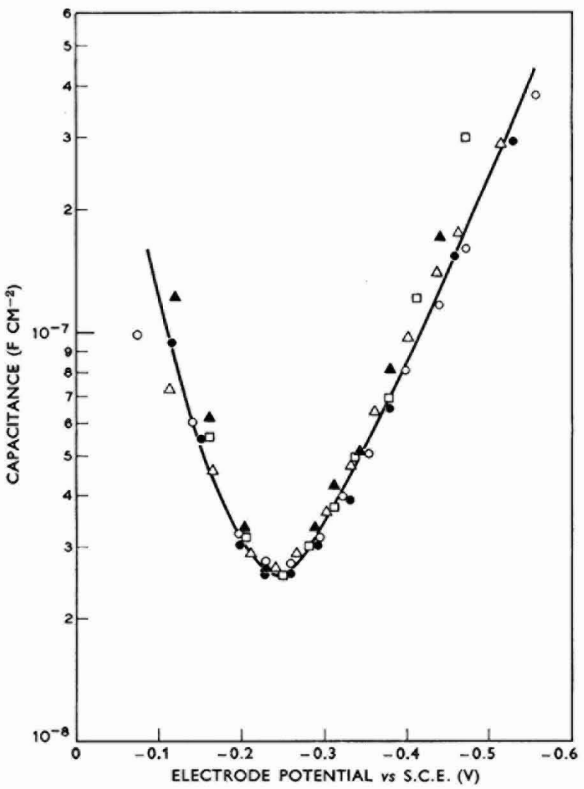


Fig. 18. Capacitance data for various cations. ○, $K_2SO_4$; ●, $LiNO_3$; △, $NH_4H_2PO_4$; ▲, $NaClO_4$; □, $CsNO_3$; buffered to pH 7.45 with phosphate; all solns. ~ $M/6$; same electrode as in Fig. 7.

to saturation at higher current densities (the electrode was nearly intrinsic, 52.7 Ω cm *p*-type), and at more negative potentials to the typically somewhat erratic behavior of germanium at very low current densities.

*(v) Effect of hydrogen ion concentration*

In their early experiments, BOHNENKAMP AND ENGELL[39] observed that change in the pH value caused a marked displacement of the capacitance curves along the electrode potential axis. HOFFMAN-PEREZ AND GERISCHER[13] made similar measurements and interpreted the data in terms of the pH-dependent ionization of hydroxyl groups covalently bonded to the surface. This establishes a "dissociation double-layer" between the plane of the bound hydroxyl groups, which we now identify as the ihp mentioned in the earlier description of the model, and the excess positive charge at the ohp:

$$Ge—OH + H_2O \rightleftarrows Ge—O^- + H_3O^+ \tag{91}$$

Following the argument given in ref. 12, it can be shown that since there is equilibrium between hydrogen ion at the ihp and in the bulk of the solution

$$\frac{d(\varphi_1 - \varphi^s)}{dpH} = -\frac{2.303\,kT}{e}\left(1 - d\log\left(\frac{a_{GeO^-}}{a_{GeOH}\cdot a_{H_2O}}\right)\Big/ dpH\right) \tag{92}$$

where $a_{H_2O}$ is usually a constant and may be neglected. At constant $\varphi_b - \varphi_s$

$$\delta U = \delta(\varphi_s - \varphi^s) \tag{93}$$

which may be expressed as

$$\delta U = \delta(\varphi_s - \varphi_1) + \delta(\varphi_1 - \varphi^s) \tag{94}$$

The electrode potential of the capacitance minimum was assumed to represent a condition of constant, but unknown $\varphi_b - \varphi_s$. It was found experimentally that

$$dU_{cap,min}/dpH \approx -2.3\,kT/e \tag{95}$$

This suggests either that d log $(a_{GeO^-}/a_{GeOH})$/dpH is negligible and there is no change in $\varphi_s - \varphi_1$ (the p.d. between the surface and the ihp) with change of pH or that the effect of these two quantities exactly cancels out over a wide range of pH. The latter seems unlikely although not impossible. If the former is true it raises an interesting question of the reason for the absence of a discreteness of charge effect[54] in this case. It has been suggested that rapid exchange of protons between the —OH and $—O^-$ groups in the ihp and between these groups and hydrogen ions in the ohp, has the effect of "smearing out" the charge in the ihp[15] and hence causes a more effective shielding of the region between the surface and the ihp. Hence it also seems likely that, at a given pH value, $\varphi_1 - \varphi_s$ has a fixed value which cannot be changed by moderate polarization except possibly at high frequency where the ionization equilibrium cannot respond or when the solution composition near the electrode surface changes due to faradaic processes.

Similar results to the above have been found by a number of other workers. BODDY AND BRATTAIN[15] made differential capacitance measurements on germanium electrodes and found that between pH values of ~4.5 and ~11.5 the data were consistent with eqns. (58) and (62) and hence could be used to determine $\varphi_b - \varphi_s$ directly. From eqn. (61), $d(\varphi_s - \varphi^s)$/dpH was found to be close to $-2.3\,kT/e$. HARTEN AND MEMMING[14] made measurements of surface conductance on germanium under conditions of rapid polarization and by observing the minimum, which was assumed to represent a fixed value of $\varphi_b - \varphi_s$, they showed behavior of $dU_{cond.min}$/dpH similar to the above. A qualitatively similar result has been obtained from observations of the point of zero photovoltage ($dU_{p.v.=0}$/dpH ≈ 46 mV) by PLESKOV AND TYAGAI[35]. All three low index planes behave similarly[14,15]. Figure 19 summarizes some data from various sources.

It may be appropriate to comment on the reasons for assuming covalently-bonded hydroxyl groups rather than specific adsorption of hydroxyl ions, which would in principle give the same value of $d(\varphi_1 - \varphi^s)$/dpH. The following points are relevant:

(a) Germanium is known to go into solution in the 4+ oxidation state as a complex anion (*e.g.*, germanate). It seems unlikely that this would go through $Ge^{4+}$ as an intermediate which is subsequently complexed in solution.

(b) It has been observed that germanium surfaces are readily oxidized by water at room temperature[55].

(c) $\varphi_b - \varphi^s$ is much more sensitive to hydrogen ion than to iodide ion (*q.v.*) in contrast to the behavior of mercury. This indicates a phenomenon differing somewhat from specific adsorption as observed on mercury electrodes, where the highly polarizable iodide ion has the most marked effect.

(d) The absence of a discreteness of charge effect can more easily be accounted for on the basis of covalently-bonded groups.

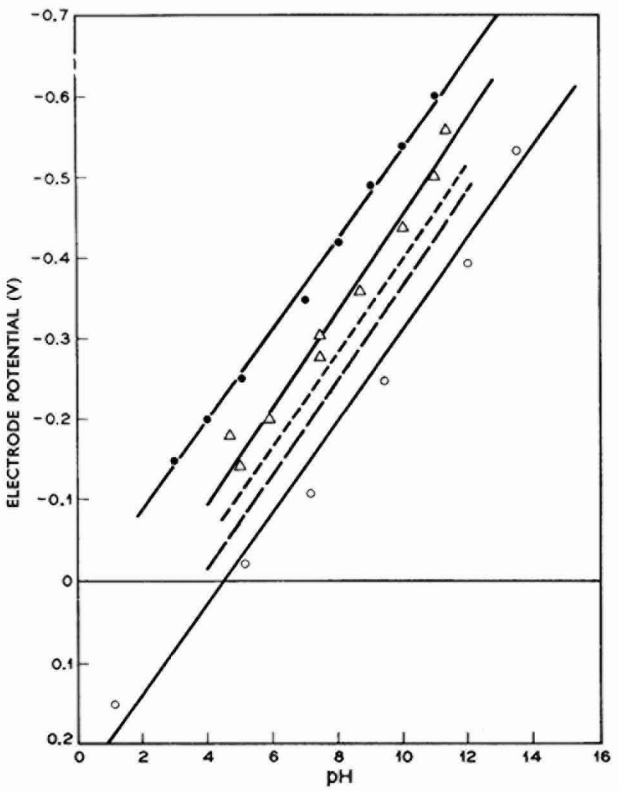


Fig. 19. Effect of pH on the potential distribution for Ge electrodes. ● Potential of conductance minimum (*vs.* calomel) for intrinsic semiconductor, (111) orientation[14]; ○, potential of capacitance minimum (*vs.* N.H.E.) for intrinsic semiconductor, (100) orientation[13]; △, potential for $\varphi_b - \varphi_s + (kT/e) \ln \lambda = 0$ (*vs.* N.H.E.), (100) orientation; – – –, (*vs.* N.H.E.), (110) orientation; — —, (*vs.* N.H.E.), (111) orientation[15].

Capacitance measurements made on silicon are not susceptible to analysis for $\varphi_b - \varphi_s$, due to contributions from surface states. However, measurements have been made at various values of pH[41] and the curves for passivated electrodes are similar in shape over the whole range. If it is assumed that the minimum in the capacitance represents a constant, but unknown, value of $\varphi_b - \varphi_s$, as was found to be the case for germanium[13], then it appears from Fig. 20, taking the pH values 0 and 14 that

$$\mathrm{d}U_{\mathrm{cap.min}}/\mathrm{dpH} = \mathrm{d}(\varphi_s - \varphi^s)_{\varphi_b - \varphi_s = \mathrm{const.}}/\mathrm{dpH} \approx 60\ \mathrm{mV} \tag{96}$$

although it must be conceded that the data points do not lie on a particularly good straight line. However it does seem that a process similar to that for germanium may apply.

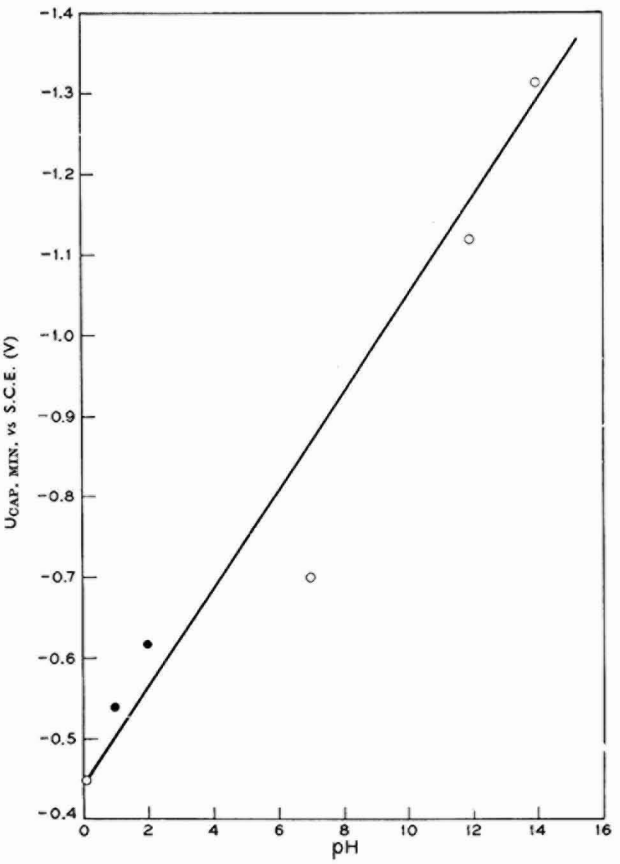


Fig. 20. Variation of the electrode potential of the capacitance minimum on Si electrodes (measured at 10 Kc) with pH value. ○, 7 Ω cm *n*-type; ●, 8 Ω cm *n*-type[41].

PLESKOV[18] found that the Tafel curves for anodic dissolution of GaAs were shifted by about 0.75 V for a pH change of 14 units ($\mathrm{d}U/\mathrm{dpH} = 54$ mV). This is similar to the behavior of germanium where practically all of the change in electrode potential at constant c.d. occurs in $\varphi_s - \varphi^s$ and suggests that the above concepts also apply to GaAs.

In his work with zinc oxide, DEWALD[21] found differences in $U_{\varphi_b - \varphi_s = 0}$ depending on whether the samples were etched in acid or alkali prior to the measurements which were made in nearly neutral solution. The effect took several hours to relax and was interpreted in terms of adsorption of hydrogen ions during the etching.

*(vi) Effect of crystal orientation*

The surface atoms in semiconductor crystals generally have relatively small numbers of nearest neighbors and are prevented from migrating by strongly directional bonds of more or less covalent character depending on the particular material, in contrast to the case at metal electrodes where the number of nearest neighbors is large and surface diffusion occurs relatively easily. This situation is particularly marked for the Group IV elements and one anticipates that the orientation of the crystal will strongly influence the properties of the Helmholtz layer through differences in the interfacial structure. Such effects have not been widely observed on solid metals in electrochemical experiments, partly due to insensitivity of the methods for determining the point of zero charge on solid metals and partly to the relative ease with which the surfaces can attain an equilibrium configuration due to surface migration.

Differences in potential distribution have been observed on differently oriented germanium electrodes using both capacitance and photovoltage measurements[56] and

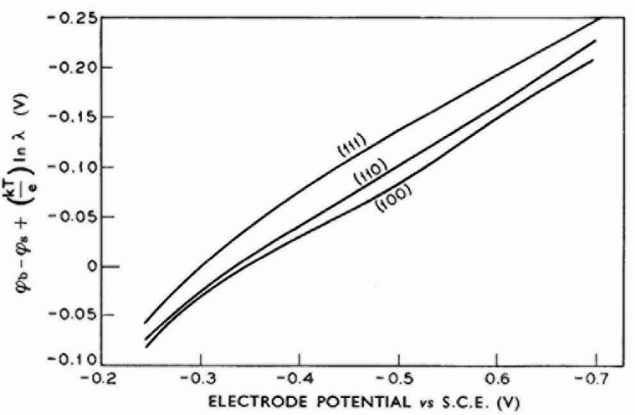


Fig. 21. Effect of orientation on the distribution of potential for Ge electrodes. Steady polarization in neutral $K_2SO_4$ solution[56].

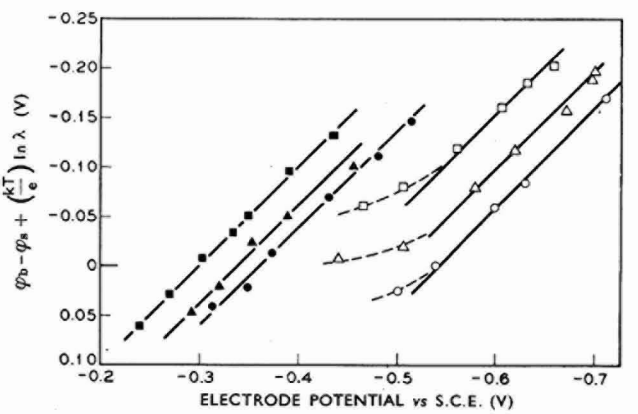


Fig. 22. Effect of orientation on the distribution of potential for Ge electrodes. Rapid polarization superimposed on a steady current of 45 $\mu$A cm$^{-2}$ (filled points) and on zero initial current (open points). ○, (100); △, (110); □, (111)[56].

a qualitatively similar effect observed by conductance measurements[14]. Figure 21 shows the effect of crystal face when the polarization is allowed to relax to a steady state, while Fig. 22 shows the effect of rapid polarization imposed on two different original states of steady polarization of the electrode. Those properties which are fundamental to the physics of the space-charge region, *e.g.*, eqns. (58) and (62), are not changed, but properties which are sensitive to the structure of the Helmholtz region are influenced, notably in this case $(\varphi_s - \varphi^s)_{\varphi_b - \varphi_s + (kT/e) \ln \lambda = \text{const.}}$ as shown by the horizontal shift between the data for different orientation in Figs. 21 and 22.

There are a number of possible contributions to the difference between crystal faces:

(a) Different densities and arrangements of surface hydroxyl groups (Fig. 23).

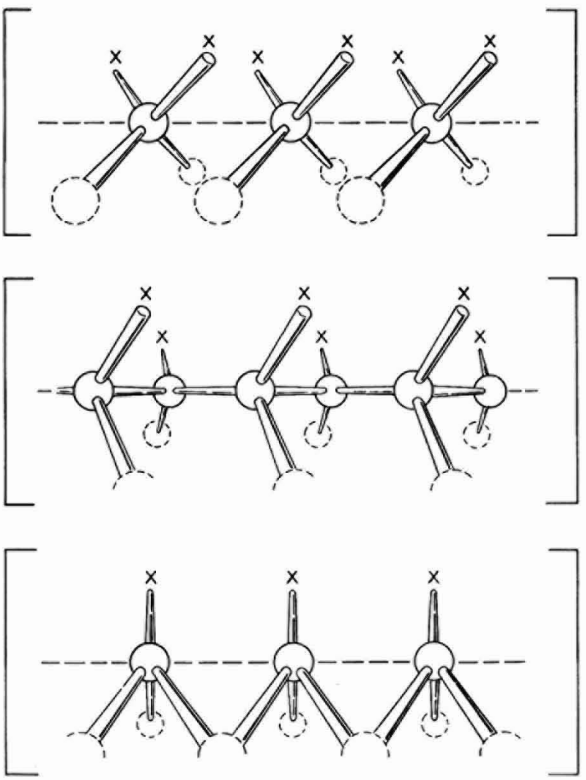

Fig. 23. Configuration of the low-index planes of a diamond-type crystal. The dashed line represents the surface plane. × is a monovalent species covalently bonded to the surface atoms.

(b) Different magnitudes of charge in the ihp due to ionization of hydroxyl groups, because of either differences in the density of the groups or differences in their degree of dissociation.

(c) Different densities of the species (Ge+Ge) at the same current density.

Of these, (a) affects $^{\text{soln.}}g^{\text{s.c.}}_{\text{dipole}}$ while (b) and (c) affect $^{\text{soln.}}g^{\text{s.c.}}_{\text{ion, bound}}$. There has been no successful attempt at distinguishing these possibilities, and of course there

may be others, particularly involving the orientation of solvent molecules within the region between the ihp and the ohp.

*(vii) Effect of ionic strength*

A few hitherto unpublished data have been obtained on the effect of ionic strength on the potential distribution at germanium anodes[57]. Solutions with ionic strengths in the range ~ 3.0–0.003 $M$ were made containing $NaClO_4$ and $NaH_2PO_4$/NaOH buffer to maintain the pH value at 7.5. At ionic strengths below 0.1 $M$ the solutions contained only the buffer.

It should be noted that even at an ionic strength of 0.003 $M$ the minimum capacitance of the space-charge layer in the solution is ~ 16 $\mu$F cm$^{-2}$, much larger than that of the semiconductor space-charge layer, and hence eqn. (62) still applies for rapid polarization.

Decrease of the ionic strength had very little effect on the open-circuit electrode potential or on the Tafel curves but the capacity minimum moved progressively to more negative electrode potentials (Fig. 24). From the usual analysis of the capaci-

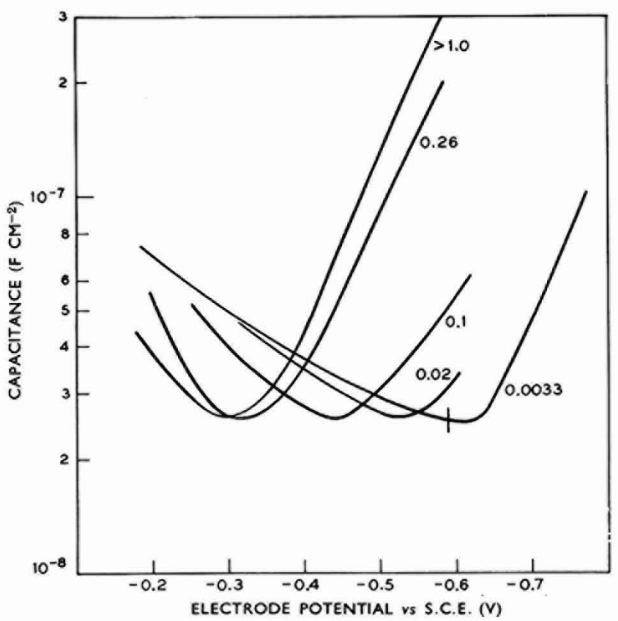


Fig. 24. Effect of ionic strength on capacitance data for Ge 32 Ω cm, $p$-type, (110) orientation[57]. The vertical line on the 0.0033 $M$ curve marks the open-circuit electrode potential.

tance data, $\delta(\varphi_s - \varphi^s)_{i=0}$ was obtained as a function of the ionic strength and is shown in Fig. 25. These data are only semi-quantitative (there has been no allowance for liquid junction potential for instance, although changes in this are quite small in the low concentration range where the largest effects are observed) and will be discussed only briefly.

Note first that change in ionic strength is not likely to promote any change in

potential between the electrode surface and the ihp ($\delta(\varphi_s - \varphi_1) = 0$), while $\delta(\varphi_b - \varphi_s)$ is already accounted for in the data in Fig. 25.

This leaves only the region between the ihp and the bulk of the solution. Since hydrogen-ion equilibrium is thought to exist between these locations it seems at first sight that $\varphi_1 - \varphi^s$ is thermodynamically determined and hence independent of the extent of the space-charge region in the solution (*i.e.*, independent of the ionic strength).

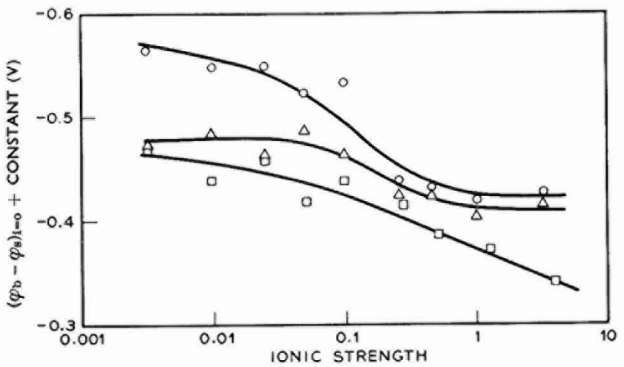


Fig. 25. Variation of the p.d. from a point just inside a Ge (100) surface to the bulk of an electrolyte solution as a function of ionic strength, deduced from Fig. 24 and similar data. ○, (100); △, (110); □, (111).

However the magnitudes of some relevant quantities should be considered. It was found in ref. 15 that $d(\varphi_1 - \varphi^s)/dpH$ was $\sim -60$ mV over a range of about 400 mV. The data of HOFFMAN-PEREZ AND GERISCHER[13] extend over about 700 mV but show some curvature particularly in acid solutions. This seems to indicate that d log $(a_{GeO^-}/a_{GeOH})/dpH$ is negligible over a range of $\sim$400 mV centered around a pH value of 8 but may become significant beyond this range. Noting that, due to the negative charge in the ihp, cations are likely to predominate at the ohp, we will assume the capacitance between the ihp and the bulk of the solution at high ionic strength to be $\sim 20\ \mu F\ cm^{-2}$ [58]. Hence $\sim 1.6 \cdot 10^{-5}$ C cm$^{-2}$ are necessary to produce a 400-mV change across this region. This charge can be produced by the ionization of $\sim 10^{14}$ cm$^{-2}$ hydroxyl groups. On a (100) surface there are $\sim 6 \cdot 10^{14}$ cm$^{-2}$ germanium atoms and hence $\sim 12 \cdot 10^{14}$ cm$^{-2}$ hydroxyl groups. Thus apparently there can be a change in the number of ionized groups amounting to about 10% of the total number available before changes in log $(a_{GeO^-}/a_{GeOH})$ become appreciable.

A change in the ionic strength will alter the integral capacitance between the ihp and bulk of the solution, and in order to maintain the potential at the value determined by the thermodynamics of the ionization equilibrium there must be a change in charge, given by

$$\delta Q = \delta C(\varphi_1 - \varphi^s)\ . \tag{97}$$

The extra charge is seen to be dependent both on the magnitude of the capacitance change between the ihp and the bulk of the solution and on the total potential across this region. Neither quantity is known; however, a suitable combination could give values of $\delta Q$ sufficiently large (*i.e.*, $>10\%$ of the total OH-groups) that there

might be an appreciable change in log ($a_{GeO^-}/a_{GeOH}$) since the change in charge must arise by changes in the concentrations of these species. Changes in $\varphi_1 - \varphi^s$ with ionic strength may be qualitatively understood on this basis. The important point to note is that experiments which investigate the effect of other variables should be carried out at constant ionic strength to eliminate this source of change in potential distribution.

(*viii*) *Effect of halide ions*

The halide ions cause pronounced changes in potential distribution at germanium electrodes. The effect is not simple but it shows several salient features which will be described. Final data are in course of publication[53]. Figure 26 shows the effect of various concentrations of iodide ion on the capacitance-electrode potential relationship for (110)-oriented electrodes. Both the pH value and the ionic strength were

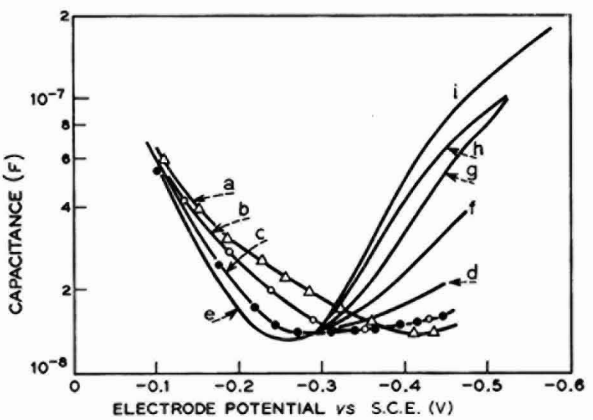


Fig. 26. Capacitance data for a Ge electrode (32 Ω cm, *p*-type, (110) orientation) in solns. of const. pH (7.45) and const. ionic strength (3.1 *M*) but with various iodide ion concns[53]. (a), 3; (b), 1; (c), $3 \cdot 10^{-1}$; (d), $10^{-1}$; (e), o–$10^{-1}$; (f), $3 \cdot 10^{-2}$; (g), $10^{-2}$; (h), $3 \cdot 10^{-3}$; (i), $10^{-3}$ *M*.

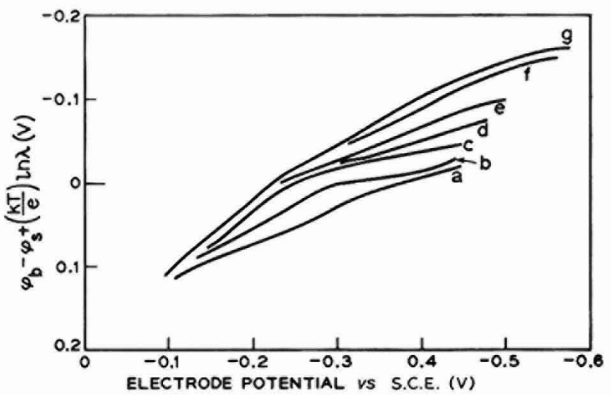


Fig. 27. Variation of the p.d. between a point just inside a Ge (110) surface and the bulk of an electrolyte soln. as a function of iodide ion concn. and current density, deduced from the data in Fig. 26. (a), 3; (b), 1; (c), $3 \cdot 10^{-1}$; (d), $10^{-1}$; (e), $3 \cdot 10^{-2}$; (f), $10^{-2}$; (g), $< 10^{-2}$ *M*.

maintained constant. Since the magnitude of the capacitance minimum remains essentially constant throughout the iodide concentration range, this provides evidence that, at least at that point, there are no fast surface states produced by the presence of iodide ion. The analysis of capacitance measurements made under conditions of rapid polarization superimposed on various initial conditions of steady anodic polarization shows that $\delta U \approx \delta(\varphi_b - \varphi_s)$ over a limited range and is consistent with the absence of a significant density of fast surface states over the whole range of the measurements. In this case the measured capacitance may be used to compute $\varphi_b - \varphi_s + (kT/e) \ln \lambda$ which is plotted *versus* electrode potential in Fig. 27.

Two features of the experiments are of particular interest:

(a) The effect of iodide ion is diminished as the solution becomes more alkaline[53].

(b) The effect becomes smaller with higher anodic polarization (Fig. 27).

The first of these points seems to indicate that the following competitive process is involved

$$\mathrm{Ge{-}OH} + \mathrm{I^-} \rightleftarrows \mathrm{Ge{-}I} + \mathrm{OH^-} \tag{98}$$

and that the halide ions may, like the hydroxyl ion, become covalently bonded to the surface. The fact that the germanium–halide bond is known to be covalent and that it tends to be a stable configuration in solutions where the ratio of concentrations of halide ion to hydroxyl ion is high, lends some support to this[59]. The only alternative would seem to be the unnecessarily complex postulate of another region at which hydroxyl and halide ions were competing for "specific adsorption" sites, located presumably between the plane of the covalently-bonded hydroxyl groups and the ohp, *i.e.*, that there are two distinct ihp's.

The decrease in $\delta(\varphi_s - \varphi^s)$ at higher anodic polarization is believed to be an effect of the current density rather than the field at the interface. This arises from Step I of the scheme for anodic dissolution of germanium, (100), proposed by BECK AND GERISCHER[31]:

$$\mathrm{Ge:} \quad +2\,\mathrm{H_2O} \rightarrow \mathrm{Ge}\begin{matrix}\diagup\mathrm{OH}\\ \diagdown\mathrm{OH}\end{matrix} + 2\,\mathrm{H^+} + (2-\lambda_1)e^- - \lambda_1 e^+ \tag{99}$$

or alternatively as given in a later review[3]:

$$\mathrm{Ge:} \quad +2\,\mathrm{OH^-} + \lambda_2 e^+ \rightarrow \mathrm{Ge}\begin{matrix}\diagup\mathrm{OH}\\ \diagdown\mathrm{OH}\end{matrix} + (2-\lambda_2)e^- \tag{100}$$

If it is assumed that

$$\mathrm{Ge:} \quad +2\,\mathrm{I^-} + \lambda_3 e^+ \rightarrow \mathrm{Ge}\begin{matrix}\diagup\mathrm{I}\\ \diagdown\mathrm{I}\end{matrix} + (2-\lambda_3)e^- \tag{101}$$

is slow compared to the other two reactions above, particularly the first (since the second probably does not apply at a pH value of 6.2), and also that the equilibrium in eqn. (98) is established relatively slowly, then at high anodic c.d. the surface would be mostly Ge—OH but at lower c.d. would tend to the equilibrium composition described by eqn. (98).

A quantitative description cannot be made at present since it is not known how $\delta(\varphi_s - \varphi^s)$ is divided between $\delta({}^{\mathrm{soln.}}g^{\mathrm{s.c.}}_{\mathrm{dipole}})$, and $\delta({}^{\mathrm{soln.}}g^{\mathrm{s.c.}}_{\mathrm{ion,bound}})$. The first of these

terms will obviously be affected by substitution of —I for —OH, whereas the second term may be affected in several ways:

(a) The inductive effect of the covalently-bonded iodide radical may change the degree of ionization of neighboring hydroxyl groups and hence change $\varphi_1 - \varphi^s$, the p.d. established by the ionization equilibrium.

(b) The density of bound charges on the *surface* may change (*e.g.* the positively-charged intermediate in the anodic dissolution reaction) due to the different atomic arrangement.

(c) Even if the density of bound charge remains constant, the capacitance between the surface and the ihp may change and the existing charge could produce a different value of $\varphi_s - \varphi_1$.

It will be clear that the situation is somewhat more complex than that on mercury electrodes where neither effects of current nor of "surface states" need be considered.

Qualitatively similar effects of smaller magnitude are observed for the other halides[57].

*(ix) Non-aqueous solutions*

The only work in non-aqueous solutions which appears to be of significance in the present context is that of KROTOVA AND PLESKOV[29] who investigated germanium in N-methyl formamide solutions of KBr. Surface conductance measurements are more reliable in this system than in aqueous solutions due to the much smaller

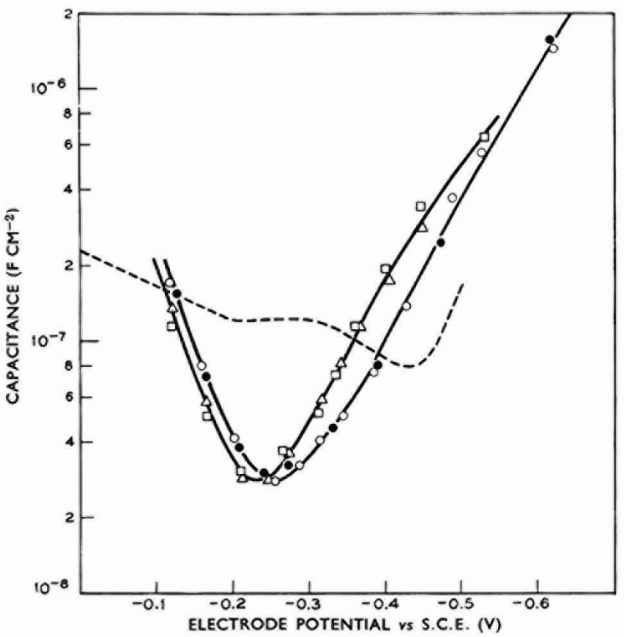


Fig. 28. Capacitance data for Ge (52.7 Ω cm, *p*-type, (111) orientation) in various solutions: ○, *M*/10 $K_2SO_4$; △, 1:1 methanol–water containing *M*/10 $NaClO_4$; □, 1:1 ethanol–water containing *M*/10 $NaClO_4$; ●, *M*/10 $NaClO_4$ aq. containing 10% triethylamine. All the above buffered to pH 7.45 with phosphate. — — —, *M*/10 $NaClO_4$ in methanol[57].

faradaic current over a considerable range of polarization. Analysis of the conductance measurements showed that, for the case in which the polarization was allowed to relax, both $\varphi_b - \varphi_s$ and $\varphi_s - \varphi^s$ changed by approximately equal amounts in a manner not very different from that observed in aqueous solutions. This suggests that $\delta(\varphi_s - \varphi^s)$ caused by polarization is related to the semiconductor surface *per se*, *i.e.*, surface states, as suggested in the literature[29,36] rather than changes in configuration of a layer of adsorbed, oriented solvent molecules[15,56].

It was reported, also, that the differential capacitance was close to the value expected for that of the semiconductor space-charge layer. This would seem to be a system meriting further study.

A few results with mixed solvents and with methanol have been obtained[57] and are summarized in Fig. 28. In all cases but one the solutions contained $M/10$ $NaClO_4$ and were buffered to pH 7.45 with phosphate. In the case of methanol alone, the buffer was omitted.

These data were exploratory and were not pursued in detail. The main features were the following:

(a) Addition of 10% triethylamine to the solution had no observable effect on the capacitance data, in contrast to the behavior of mercury electrodes.

This is not surprising since even if adsorption did occur the hydrogen-ion equilibrium would shift just sufficiently that $\varphi_1 - \varphi^s$ was maintained constant. Evidence of adsorption might be obtained from measurements of the Helmholtz capacitance. Such measurements have not been made on this system, but in the case of solutions saturated with octyl alcohol a very definite effect on Helmholtz capacitance was observed even though the data for space-charge capacitance *versus* electrode potential were not affected[36].

(b) 1/1 mixtures of methanol or ethanol with water had a small, apparently identical effect. At potentials more positive than $-0.25$ V the curve was shifted $\sim 20$ mV more positive.

This is only marginally more than the reproducibility of the experiments but, if a real effect, would be consistent with a decrease of $a_{H_2O}$ by about a factor of two, and a consequent redistribution of the hydroxyl ionization equilibrium expressed in eqn. (91). At potentials between $-0.25$ and 0.45 the discrepancy between the curves was larger ($\sim 50$ mV) but the reason is not known.

(c) The methanol solution gave quite dissimilar results from the methanol–water mixture. The measured capacitance was obviously no longer simply that of the space-charge region and could not be analyzed to determine $\varphi_b - \varphi_s$.

Methanol is known to oxidize germanium surfaces[55] so that possibly the problem is due to formation of an oxide film which is insoluble in methanol. Oxide films grown on germanium in air or in nitric acid are found to have surface states associated with them[53].

## SUMMARY

Generalizations are probably unjustifiable at the present stage, but a number of interesting features seem to be well established.

Both zinc oxide and germanium, and to a lesser extent silicon, have been found to behave consistently with the simple physical model of a system with properties

dominated by the semiconductor space-charge layer. Germanium shows complicated time effects whereas zinc oxide does not.

The effect of hydrogen ion on $\varphi_s - \varphi^s$ (the p.d. between a point just inside the semiconductor surface and the bulk of the solution) is very marked in all cases. The absence of a discreteness of charge effect on germanium suggests a rapid exchange of charge between bound hydroxyl groups and hydrogen ion in solution. This further suggests that $\varphi_1 - \varphi^s$ may be independent of polarization at constant pH.

On germanium electrodes, variations in $\varphi_s - \varphi^s$ due to changes in crystal orientation, ionic strength and concentration of halide ion have been observed. Since polarization of the electrode also produces variations in $\varphi_s - \varphi^s$, it is frequently advantageous to work under conditions where the effect due to polarization is minimized, *i.e.*, by making comparisons at constant current.

## REFERENCES


1 J. F. DEWALD, *Semiconductors*, edited by N. B. HANNAY, A. C. S. Monograph, #140, Reinhold, New York, 1959.
2 M. GREEN, *Modern Aspects of Electrochemistry*, Vol. II, edited by J. O'M. BOCKRIS, Butterworths, London, 1959.
3 H. GERISCHER, *Advances in Electrochemistry and Electrochemical Engineering*, Vol. I, edited by P. DELAHAY, Interscience, New York, 1961.
4 H. U. HARTEN, *Festkorperprobleme*, 3 (1964) 81.
5 V. A. MIAMLIN AND YU. V. PLESKOV, *Usp. Khim.*, 32 (1963) 470.
6 H. F. GÖHR, *The Electrochemistry of Semiconductors*, edited by P. J. HOLMES, Academic Press, New York, 1962.
7 D. R. TURNER, *The Electrochemistry of Semiconductors*, edited by P. J. HOLMES, Academic Press, New York, 1962.
8 E. A. EFIMOV AND I. G. ERUSALIMCHIK, *Electrochemistry of Germanium and Silicon*, The Sigma Press, 1963.
9 R. PARSONS, *Modern Aspects of Electrochemistry*, Vol. I, edited by J. O'M. BOCKRIS, Butterworths, London, 1954.
10 M. GREEN, *Solid State Physics in Electronics and Telecommunications*, Academic Press, New York, 1960, p. 619.
11 S. I. PEKAR, *J. Exptl. Theoret. Phys. (USSR)*, 31 (1956) 351.
12 M. J. SPARNAAY, *Rec. Trav. Chim.*, 79 (1960) 950.
13 M. HOFFMAN–PEREZ AND H. GERISCHER, *Z. Elektrochem.*, 65 (1961) 771.
14 H. U. HARTEN AND R. MEMMING, *Phys. Lett.*, 3 (1962) 95.
15 P. J. BODDY AND W. H. BRATTAIN, *J. Electrochem. Soc.*, 110 (1963) 570.
16 W. ERIKSEN AND R. CAINES, *J. Phys. Chem. Solids*, 14 (1960) 87.
17 D. R. TURNER, *J. Electrochem. Soc.*, 105 (1958) 402.
18 YU. V. PLESKOV, *Dokl. Akad. Nauk SSSR*, 143 (1962) 1399.
19 H. GOBRECHT AND O. MEINHARDT, *Berichte Bunsenges. Physikalische Chemie*, 67 (1963) 151.
20 W. SHOCKLEY AND G. L. PEARSON, *Phys. Rev.*, 74 (1948) 232. E. N. CLARK, *Phys. Rev.*, 91 (1953) 756.
21 J. F. DEWALD, *Bell System. Tech. J.*, 39 (1960) 615.
22 A. UHLIR, *Bell System Tech. J.*, 35 (1956) 333.
23 M. D. KROTOVA AND YU. V. PLESKOV, *Physica Status Solidi*, 2 (1962) 411.
24 P. J. BODDY AND W. H. BRATTAIN, to be published in *Surface Science*, 3 (1965).
25 H. U. HARTEN, *Z. Naturforsch.*, 16a (1961) 1401.
26 H. U. HARTEN, *Z. Naturforsch.*, 16a (1961) 459.
27 W. H. BRATTAIN AND P. J. BODDY, *J. Electrochem. Soc.*, 109 (1962) 574.
28 P. J. BODDY AND W. H. BRATTAIN, *J. Electrochem. Soc.*, 109 (1962) 812.
29 M. D. KROTOVA AND YU. V. PLESKOV, paper presented at 17th meeting of CITCE, Moscow, 1963.
30 C. G. B. GARRETT AND W. H. BRATTAIN, *Phys. Rev.*, 99 (1955) 376.
31 J. F. DEWALD, *The Surface Chemistry of Metals and Semiconductors*, edited by H. C. GATOS, Wiley, London, 1960.
32 R. M. LAZORENKO–MANEVICH, *Zh. Fiz. Khim.*, 36 (1962) 2066.
33 P. J. BODDY AND W. H. BRATTAIN, *Ann. N. Y. Acad. Sci.*, 101 (1963) 683.

34 P. J. BODDY AND W. H. BRATTAIN, submitted to *J. Electrochem. Soc.*
35 YU. V. PLESKOV AND V. TYAGAI, *Dokl. Akad. Nauk SSSR*, 141 (1961) 1135.
36 P. J. BODDY, Extended Abstracts of the Electrochemical Society Meeting, San Francisco, 1965.
37 F. BECK AND H. GERISCHER, *Z. Elektrochem.*, 63 (1959) 500.
38 H. GERISCHER, *Anales de Fisica y Quimica*, 56 (1960) 535.
39 K. BOHNENKAMP AND H. J. ENGELL, *Z. Elektrochem.*, 61 (1957) 1184.
40 P. J. BODDY, *J. Electrochem. Soc.*, 111 (1964) 1136.
41 R. M. HURD AND P. T. WROTENBERY, *Ann. N. Y. Acad. Sci.*, 101 (1964) 876.
42 R. MEMMING, *Phillips Res. Rep.*, 19 (1964) 323.
43 R. M. LAZARENKO–MANEVICH, *Dokl. Akad. Nauk SSSR*, 144 (1962) 1094.
44 J. T. LAW, *J. Phys. Chem.*, 59 (1955) 543.
45 R. MEMMING, *Phys. Lett.*, 4 (1963) 89.
46 W. H. BRATTAIN AND P. J. BODDY, Report of the International Conference on the Physics of Semiconductors, Exeter, 1962, p. 797.
47 H. GOBRECHT AND O. MEINHARDT, *Berichte Bunsenges. Physikalische Chemie*, 67 (1963) 142.
48 V. A. TYAGAI AND YU. V. PLESKOV, *Soviet Phys.-Solid State English Transl.*, 4 (1962) 246.
49 S. J. ELLIS; *J. Appl. Phys.*, 28 (1957) 1262.
50 P. J. BODDY AND W. J. SUNDBURG, *J. Electrochem. Soc.*, 110 (1963) 1170.
51 A. A. IAKOVLEVA, T. L. BORISOVA AND V. I. VESELOVSKII, *Dokl. Akad. Nauk SSSR*, 145 (1962) 598.
52 H. GERISCHER AND F. BECK, *Z. Physik. Chem. NF*, 23 (1960) 8.
53 P. J. BODDY AND W. H. BRATTAIN, to be published.
54 O. ESIN AND B. MARKOV, *Acta Physicochem.*, 10 (1939) 353.
55 M. J. SPARNAAY, *Ann. N. Y. Acad. Sci.*, 101 (1963) 973.
56 W. H. BRATTAIN AND P. J. BODDY, *Proc. Nat. Acad. Sci. U. S.*, 48 (1962) 2005.
57 W. H. BRATTAIN AND P. J. BODDY, unpublished data.
58 A. N. FRUMKIN, *Trans. Faraday Soc.*, 36 (1940) 117.
59 L. M. DENNIS AND F. E. HANCE, *J. Am. Chem. Soc.*, 44 (1922) 2854.

# SHORT COMMUNICATIONS

## The impedance of the quinhydrone electrode

We have recently published[1] measurements of the rates of a number of unsubstituted quinone redox reactions at mercury electrodes using the polarographic technique. In view of the probable participation of one or more adsorbed intermediates we considered that measurements by a relaxation method would provide additional information on the mechanism. Here we report results for the benzoquinone system at 25° in 1 *M* aqueous $KNO_3$ containing 0.1 *M* acetic acid–1 *M* sodium acetate buffer of pH = 5.6. The dropping-mercury electrode had a drop time of about 15 sec and its impedance was measured using an equal ratio a.c. bridge described elsewhere[2]. The mean potential of the D.M.E. was measured with respect to a saturated calomel electrode using a Pye Universal potentiometer.

Measurements of the impedance at constant frequency and varying imposed mean potential were analysed by the impedance plane diagram method[3]. Figure 1

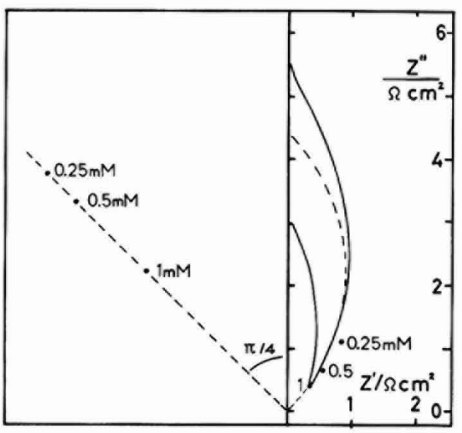


Fig. 1. Polar polarogram for 1 m*M* quinhydrone soln. in 1 *M* $KNO_3$ containing acetic acid–acetate buffer of pH 5.6 at 25°. $Z^{11}$ is the imaginary component of the electrode impedance and $Z^1$ the real component. The measurements were made at 1 Kc/sec. Similar measurements at lower quinhydrone concns. are indicated by points representing the peak of the polarogram and the centre of the circle through the origin and the peak point.

shows the complete polarogram for a 1 m*M* quinhydrone solution and the peak points for 0.5 and 0.25 m*M* solutions. The centres of circles passing through the origin and the peak point are shown at the left-hand side of the diagram and it can be seen that they lie on the line passing through the origin at an angle of $\pi/4$ to the vertical. This is the limiting line corresponding to the case of a diffusion-controlled reaction. It is also evident that a single circle cannot be drawn passing through the origin of the peaks at different concentrations and the capacity point for the base electrolyte. This behaviour is similar to that observed for the thallium-amalgam electrode[4]. As a

further test for the apparent diffusion-controlled nature of this reaction we have calculated the product $q/\omega$ which should be a constant if this assumption is correct. Using the nomenclature of SLUYTERS *et al.*[3,4] we write

$$q=\theta+\sigma/\sqrt{\omega}+\frac{(\sigma^2/\omega)}{\theta+(\sigma/\sqrt{\omega})} \tag{1}$$

where $\theta$ is the polarisation resistance, $\sigma$ the coefficient of the Warburg impedance and $\omega$ the angular velocity of the a.c.; $q$ was calculated from the equation

$$(q/2)^2=[(Z^1-R_c)-q/2]^2+[Z^{11}]^2 \tag{2}$$

where $Z^1$ and $Z^{11}$ are the real and imaginary components of the cell impedance and $R_c$ is the resistance of the base solution. Values of $q/\omega$ at 14 frequencies between 500 and 5000 c/sec yield a mean of $67.6\pm0.3$ $\Omega$ cm$^2$ sec$^{-\frac{1}{2}}$ at a mean potential corresponding to the minimum value of $\sigma$ which tends to confirm the assumption of diffusion control.

Correspondingly, the experimental values of the components of the electrode impedance at the reversible potential plotted according to RANDLES[5] and ERSHLER[6] yield straight lines which are not parallel; further, the line for the real component cuts the origin, while that for the imaginary component has a positive intercept. This suggests that adsorption of the reactants is causing a change of the double-layer capacity which would also be consistent with the plot in Fig. 1. We have therefore used the latter results (*i.e.*, constant frequency, variable mean potential) to calculate the double-layer capacity in the presence of the reaction. If the reaction is diffusion-controlled then the impedance is given by[3]

$$\left[(Z^1-R_c)-\frac{1}{2\omega C_{dl}}\right]^2+\left[Z^{11}-\frac{1}{2\omega C_{dl}}\right]^2=\frac{1}{4\omega^2 C_{dl}^2} \tag{3}$$

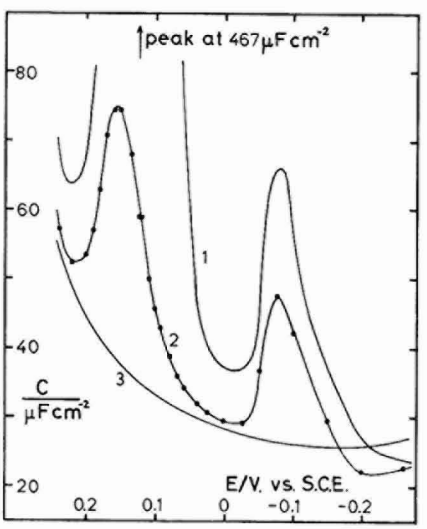


Fig. 2. Values of the experimental and double-layer capacities for 1 m$M$ quinhydrone in 1 $M$ $KNO_3$ containing acetic acid–acetate buffer, pH 5.6 at 25°. (1), Experimental capacity; (2), double-layer capacity calc. from eqn. (3), base electrolyte capacity.

and the value of $C_{dl}$ obtained from this equation is shown in Fig. 2. It is evident that the double-layer capacity is considerably altered by the presence of quinhydrone as would be expected from the adsorption properties of aromatic molecules. The significance of the small peak at the more negative potential is not known at present; it was also found using the solutions containing quinone only. Recalculation of the Randles–Ershler plot using the double-layer capacity at the reversible potential from Fig. 2 (58.8 $\mu$F cm$^{-2}$) yields a common line for the real and imaginary components which passes through the origin. The slope of this line corresponds to a mean diffusion coefficient of $9.5 \times 10^{-6}$ cm$^2$ sec$^{-1}$ assuming a two-electron reaction. This is in satisfactory agreement with the mean value of $1.00 \times 10^{-5}$ cm$^2$ sec$^{-1}$ calculated from results[7] in 2 *M* KCl at 21°.

The present results appear to contradict the earlier polarographic measurements in that they suggest that the rate constant of this reaction is more than $10^3$ greater than that calculated previously[1]. While these results could be accounted for, approximately, by assuming a rate-controlling step occurring between the two electron transfers, it seems more probable that the presence of adsorbed intermediates produces values of rate constants which are misleading as a result of over-simplified analysis. We expect that further work will throw some light on this problem.

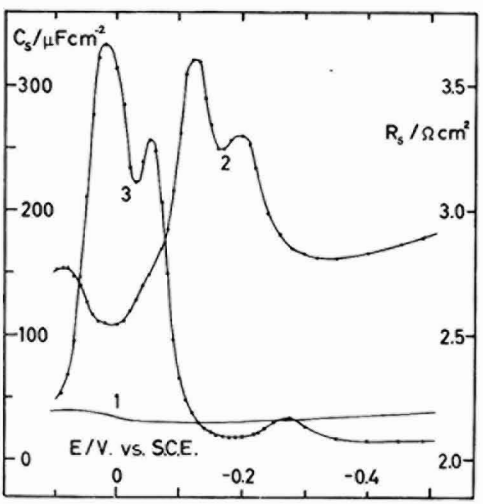


Fig. 3. Components of cell impedance for 1 m*M* 1,4-naphthoquinone in 1 *M* $KNO_3$ containing acetic acid–acetate buffer, pH 4.6. (1), Capacity of the base electrolyte; (2), resistance in the presence of reactant; (3), capacity in the presence of reactant.

Finally we report that similar measurements on 1,4-naphthoquinone in aqueous buffers (pH = 4.6 and 5.6) give results which cannot be analysed by any methods so far proposed, since the resistance and capacity peaks occur at different potentials (Fig. 3)

*Acknowledgements*

We acknowledge gratefully the receipt of scholarships from the Consejo Nacional de Investigaciones Cientificas y Tecnicas (Republica Argentina) and from

the Department of Technical Co-operation (U.K.) which enabled J.R.G. to carry out the work described here.

*Department of Physical Chemistry,* J. R. GALLI
*University of Bristol (England)* ROGER PARSONS

1 J. M. HALE AND R. PARSONS, *Trans. Faraday Soc.*, 59 (1963) 1429.
2 R. PARSONS AND P. C. SYMONS, in course of publication.
3 M. SLUYTERS-REHBACH AND J. H. SLUYTERS, *Rec. Trav. Chim.*, 82 (1963) 525.
4 M. SLUYTERS-REHBACH, B. TIMMER AND J. H. SLUYTERS, *Rec. Trav. Chim.*, 82 (1963) 557.
5 J. E. B. RANDLES, *Discussions Faraday Soc.*, 1 (1947) 11.
6 B. V. ERSHLER, *Zh. Fiz. Khim.*, 22 (1948) 683.
7 E. A. AIKAZYAN AND YU. V. PLESKOV, *Zh. Fiz. Khim.*, 31 (1957) 205.

Received April 24th, 1965

*J. Electroanal. Chem.*, 10 (1965) 245–248

## Characteristics of glow-discharge electrolysis in aqueous, non-aqueous and molten systems*

In glow-discharge electrolysis one of the electrodes is withdrawn from the solution and kept in the gas phase while the other is immersed in the solution; relatively higher voltages at reduced pressure have to be applied for the current to cross the gas–solution boundary. The glow discharge is similar to that in gases with metal electrodes and the cathode fall is very near the solution when the vapour-phase electrode is made the anode. That the large energy concentration in the cathode drop can be so effectively employed for bringing about chemical reactions is due to a favourable combination of several factors. The cathode drop is also a point of particularly high temperature. The phase boundaries, metal–gas and liquid–gas behave in exactly the same way regarding the passage of the electric current; this behaviour is unexpected.

*Experimental*

The cell consisted of an H-shaped glass vessel with the anolyte and catholyte in the two limbs separated by a filter-paper plug. A thick platinum wire, fitted to a stainless-steel holder, served as the vapour-phase electrode. The tip of the platinum electrode was kept 0.5 cm above the liquid surface and a spiral of platinum wire dipping into the solution in the other limb was the auxiliary electrode. The anode and cathode chambers were separately connected to the vacuum line and pressure was maintained constant at 50 mm mercury during the electrolysis, by means of a float manostat. The required high d.c. voltage was obtained from a rectifier assembly comprising 872 A diodes and a centre-tapped transformer 3750-0-3750 V. The circuit included a suitable condenser, choke and rheostat to regulate and maintain a steady discharge at constant current.

* This paper was presented at the V Seminar in Electrochemistry, held at the Central Electrochemical Research Institute, Karaikudi, in January 1965.

All aqueous solutions were prepared from pure chemicals and distilled water, 125 ml of 1 *N* solutions of sodium chloride, sodium bromide, sodium iodide, barium chloride, strontium nitrate and chromic acid and saturated copper sulphate were tried out as electrolytes in glow-discharge electrolysis. Characteristic results are given in Table 1.

TABLE 1

| *Electrolyte* | *Striking voltage* ± 20 *V* | *Remarks* |
|---|---|---|
| 1. Sodium chloride | 1050 | (a) Initially usual glow, but after a few minutes bright yellow sodium glow appeared at the tip of the anode and disappeared after some time. Stirring increased the duration of the sodium glow.<br>(b) Sodium glow round the glow-discharge cathode and the electrode became red hot. |
| 2. Sodium bromide | 900 | (a) As above.<br>(b) As above. |
| 3. Sodium iodide | 675 | (a) As above but the entire space round the electrode was full of yellow glow.<br>(b) Glow round the cathode. |
| The glow was examined with a constant deviation spectrograph and the lines corresponded to those of sodium. | | |
| 4. Barium chloride | 750 | (a) Pale green colour round the anode sometimes filling the entire chamber.<br>(b) Pale green glow round the cathode which became red hot. |
| 5. Strontium nitrate | 750 | (a) Glow normal lilac, but after some time the colour became deeper with crimson. |
| 6. Copper sulphate (satd.) | 675 | (a) Very impressive blue-green colour with lilac cone; fine reddish-brown deposit on the electrode and also on the walls of the vessel. On cooling the deposit became black. |
| 7. Copper sulphate (satd.) and sodium chloride (9 g) | 675 | (a) Yellow glow near the tip of the g.d. anode, lilac glow cone and blue-green cloud filling the entire chamber. |
| 8. Chromic acid | 1800 | (a) No glow.<br>(b) No glow. |

(a) Anode in vapour.
(b) Cathode in vapour.

Metal ions like sodium, barium, strontium and copper impart their characteristic colours to the usual glow of the low-pressure electrolysis; the glow occurs round the electrode and sometimes fills the entire cell. This effect might be due to (i) the vaporisation taking place readily under the low pressures obtained in glow-discharge electrolysis and (ii) the vapour coming under the influence of the electric field and the very high temperature obtaining in the cathode drop. The values of the striking voltages for the sodium halides are consistent with the ionisation potentials of the anions (12.952 V for Cl, 11.8 V for Br and 10.6 V for I). A discharge could not be initiated in the case of chromic acid because of its poor conductance. COUCH AND BRENNER[1] could not obtain the characteristic glow with salt solutions other than

those of copper and indium, perhaps because of the large volume (2–3 l) of solution used and because the glow-discharge anode was kept 1 in. above the solution.

The study of non-aqueous systems is of interest in assessing the role of water in glow-discharge electrolysis, but very little work on glow-discharge electrolysis in non-aqueous solvents has been reported. The formation of hydrazine[2,3] in liquid ammonia has been studied. CADY, EMELÉUS AND TITTLE[4] studied the liquid sulphur dioxide system. Various non-aqueous solvents were tried under glow-discharge electrolysis and several of them (dioxane, aniline, glacial acetic acid and glycerol) do not initiate any glow discharge below 1500 V d.c. The discharge characteristics are not improved by the addition of salts but the addition of water alone or with the salt does initiate the discharge. This is supported by the observation of CADY, EMELÉUS AND TITTLE[4] that addition of water improves the conductivity of liquid sulphur dioxide. Phenol and ethylene glycol gave a very pale bluish glow at 900 and 675 V d.c., respectively. The few hydroxyl radicals present in the vapour and accelerated to the solvent surface may be responsible for the feeble glow; whereas with glycerol, because of its high viscosity, vaporisation does not readily take place to initiate the discharge. In most of the non-aqueous systems there is no gas evolution and as the vapour pressure is low, the glow discharge can be maintained for some time even after switching off the vacuum pump; this is impossible in aqueous systems.

Sodium chloride, lithium chloride, stannous chloride, sodium dihydrogen phosphate and urea were heated to molten liquids and glow-discharge electrolysis was tried on each, but no glow discharge could be initiated below 1950 V d.c. It is, therefore, essentially the radicals from the water vapour, accelerated by the cathode fall near the solution, bombarding the substrate that are responsible for the phenomena in glow-discharge electrolysis.

*Acknowledgements*

The author expresses his sincere thanks to Dr. C. V. SURYANARAYANA, for his kind encouragement and Prof. K. S. G. DOSS, Director Central Electrochemical Research Institute, Karaikudi, for his keen interest in this investigation.

*Central Electrochemical Research Institute,*
*Karaikudi (India)*

B. S. R. SASTRY

1 D. E. COUCH AND A. BRENNER, *J. Electrochem. Soc.*, 106 (1959) 628.
2 A. HICKLING AND G. R. NEWNS, *Proc. Chem. Soc.*, (1959) 272.
3 B. S. R. SASTRY, *Proc. Indian Sci. Congr., 47th, 1960.*
4 G. H. CADY, H. J. EMELÉUS AND B. TITTLE, *J. Chem. Soc.*, (1960) 4138.

Received March 24th, 1965

*J. Electroanal. Chem.*, 10 (1965) 248–250

## BOOK REVIEW

*Quantitative Chemistry* by JÜRG WASER, W.A. Benjamin Inc., New York, 1964, 432 pages, cloth $6.60, paper $4.35.

This is a well-written introduction to quantitative analysis emphasizing the physical principles involved and uniting clear, illustrative experiments with their theoretical basis. Although written for American undergraduates meeting chemistry for the first time, it is by no means limited in application. The teaching of British students in their final two years at school (A-level syllabus) could gain considerably from the attitude encouraged by Professor WASER which emphasizes both the practical virtues and the importance of understanding why every step is carried out, the very antithesis of old "cook-book" analytical chemistry.

From the analytical balance, Professor WASER leads on to gravimetric, volumetric and gas analysis, ion-exchange resins, coulometric analysis and finally, determination of the formula of a complex ion by colorimetry and the method of continuous variation. The particular value of the approach is clearly illustrated by the section on acid–base titrations which is firmly rooted in the Brønsted–Lowry definition. This is very well explained and is applied to polyprotic acids as well as to non-aqueous solutions. The use of a direct-reading pH meter to plot titration curves must be a great help to a beginner, who in the past has been left to study the theory of indicators in a purely abstract way. Similarly the redox titration is accompanied by a lucid explanation of electrode potentials—a remarkable feat since no thermodynamics is assumed. One of the four appendices gives a little, but this is of doubtful assistance at this level.

The book is well laid out and printed; the summaries of each chapter being a thoughtful aid to the student. The writing is so clear and direct that it is quite a shock to run up against "comformance" for "conformity". It is to be hoped that more students will get their introduction to quantitative chemistry by the route mapped out in this excellent introduction.

ROGER PARSONS
University of Bristol

# ANNOUNCEMENT

## NINTH CONFERENCE ON ANALYTICAL CHEMISTRY IN NUCLEAR TECHNOLOGY

The Ninth Conference on Analytical Chemistry in Nuclear Technology will be held in Gatlinburg, Tennessee, on October 12, 13 and 14, 1965, under the sponsorship of the Analytical Chemistry Division of the Oak Ridge National Laboratory. The Laboratory is operated by the Union Carbide Corporation for the U. S. Atomic Energy Commission.

The conferences will be held in the Huff House of the Mountain View Hotel. Registration will begin on October 11 at 4.00 p.m. in the hotel lobby and continue each day for the duration of the Conference. The sessions will begin at 9.00 a.m. daily.

The Conference will be composed of six sessions embracing the following subjects:

1. Analytical Chemistry of the Transuranium Elements.
2. Symposium on the Role of Analytical Chemistry in Pure Materials Research.
3. Selected Papers on Bio-Analytical Techniques.
4. Miscellaneous Subjects.

Participation in the Conference will be on the basis of invited contributions; however, a limited number of papers, up to 25 minutes in length, are solicited and will be accepted provided the subject matter of such contributions is in accord with the over-all objectives of the Conference and meets with the approval of the program committee. In any case, review papers are discouraged.

1. *Analytical Chemistry of the Transuranium Elements*

Papers should describe original, unpublished work that makes a real contribution to the analytical chemistry of the transuranium elements. Although the subject matter is not necessarily intended to be restrictive, papers on the following subjects of transuranium chemistry are solicited: ionic methods of analysis; radiochemical methods of analysis; new areas or techniques potentially useful to analytical chemists, such as improved nuclear measurements, separation methods, and other useful processes; special facilities and equipment that have been developed and tested in actual "hot" operations.

2. *Symposium on the Role of Analytical Chemistry in Pure Materials Research*

As part of this Conference, a symposium on the role of analytical chemistry in pure materials research is being arranged. It is anticipated that the discussions in this symposium will cover the broad aspects of this work, such as: the analytical requirements as viewed by the pure materials researcher; the standards program with emphasis on the standards currently available and what the future standards program entails; the use of the spark source mass spectrograph, the potential usefulness of particle accelerators, and the role of electrical test methods; what facilities are necessary and the problems of a general analytical laboratory; and, finally, some of the more illustrative examples of accurate and precise methods of analysis of pure materials.

3. *Selected Papers on Bio-Analytical Techniques*

Selected papers will be presented on bio-analytical techniques of direct application to biological macro-molecular separations technology. Emphasis will be given to those techniques that are appropriate for automated analytical methods.

4. *Miscellaneous Subjects*

A limited number of papers will be accepted under the general heading of miscellaneous subjects for presentation in one or more sessions, provided such papers have some direct bearing on the general subject of the Conference, *i.e.*, analytical chemistry in nuclear technology.

*Exhibition of Modern Analytical Instruments and Laboratory Equipment*

Facilities will be available to manufacturers and dealers in laboratory supplies for the installation of 14 exhibits on modern developments in analytical instrumentation, equipment and supplies. Information concerning the availability of and rental charges for exhibit space may be secured by writing directly to R. B. DAVENPORT, Oak Ridge National Laboratory, P. O. Box X, Oak Ridge, Tennessee 37831.

*General information*

Abstracts of papers and any inquiries concerning the Conference, including requests for the program and copies of the printed abstracts, should be directed to the Oak Ridge National Laboratory, P. O. Box X, Oak Ridge, Tennessee 37831, attention: C. D. SUSANO, Chairman.

The registration fee, except for full-time students, is $5.00 per person. Proceedings of the Conference will *not* be published; however, abstracts of all papers will be published and made available to all persons attending the Conference.

Reservations for lodging should be made by direct communication with: The Mountain View Hotel, Gatlinburg, Tennessee 37738.

# CONTENTS




Printed in The Netherlands

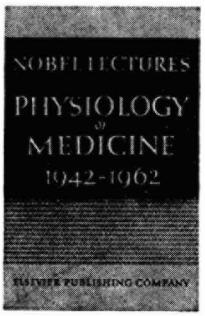


# NOBEL PRIZE LECTURES

## CHEMISTRY

## PHYSIOLOGY OR MEDICINE

## PHYSICS

each category to be contained in three volumes

1901–1921/1922–1941/1942–1962

In the world of science, the history of research and progress in the last sixty years is largely a history of the accomplishments of the Nobel Prize winners. Annually these achievements are placed in perspective at the Nobel Prize ceremonies held each December in Stockholm. Published for the Nobel Foundation, the collected Nobel Lectures are being issued, for the first time in English, by Elsevier. The lectures have been arranged in chronological order according to subject, beginning in 1901 and continuing through 1962. Each lecture is preceded by the presentation address to the prizewinner and followed by his or her biography. Initially, the Nobel Prize Lectures in CHEMISTRY, in PHYSICS, and in PHYSIOLOGY or MEDICINE will be issued, each in three volumes (not separately available), to be completed in about one year.

now published

### NOBEL LECTURES CHEMISTRY 1942–1962

Alder – Calvin – Diels – Giauque – Hahn – Hevesy – Heyrovsky – Hinshelwood – Kendrew – Libby – McMillan – Martin – Northrop – Pauling – Perutz – Robinson – Sanger – Seaborg – Semenov – Stanley – Staudinger – Sumner – Synge – Tiselius – Todd – Vigneaud – Virtanen

xiv + 712 pages, 41 tables, 228 illustrations, 481 lit. references, 1964
*price per set of three volumes: £ 24.0.0 or Dfl. 240,—*

### NOBEL LECTURES PHYSIOLOGY OR MEDICINE 1942–1962

Beadle – Békésy – Bovet – Burnet – Chain - Cori, C. F. – Cori, G. T. – Cournand – Crick – Dam – Doisy – Enders – Erlanger – Fleming – Florey – Forsmann – Gasser – Hench – Hess – Houssay – Kendall – Kornberg – Krebs – Lederberg – Lipmann – Medawar – Moniz – Müller – Muller – Ochoa – Reichstein – Richards – Robbins – Tatum – Theiler – Theorell – Weller – Wilkins – Waksman – Watson

xiv + 839 pages, 33 tables, 200 illustrations, 844 lit. references, 1964
*price per set of three volumes: £ 24.0.0 or Dfl. 240,—*

### NOBEL LECTURES PHYSICS 1942–1962

Appleton – Bardeen – Blackett – Bloch – Born – Bothe – Brattain – Bridgman – Cerenkov – Chamberlain – Cockcroft – Frank – Glaser – Hofstadter – Kusch – Lamb – Landau – Lee – Mössbauer – Pauli – Powell – Purcell – Rabi – Segrè – Shockley – Stern – Tamm – Walton – Yang – Yukawa – Zernike

xiii + 621 pages, 183 illustrations, 376 lit. references, 1964
*price per set of three volumes: £ 24.0.0 or Dfl. 240,—*

ELSEVIER PUBLISHING COMPANY
AMSTERDAM LONDON NEW YORK

2728